TOMBOLA GOLD

ASX Announcement

4 May 2022

"Report by Ken Collerson Improves Targeting of Mineralisation by Burra, South Australia"

Tombola Gold Ltd, ACN 148 860 299 ("**the Company**"), refers to the above Announcement, released on 29 March 2022, which contained a link to a Report by Dr. Ken Collerson titled "*Review of Exploration Data from Burra, S.A. to Improve Targeting Copper, Copper-Gold and REE Mineralisation*" dated 24 March 2022. Dr. Collerson prepared this Report for the Company as an Independent Expert.

The data in Dr. Collerson's Report at Item 12.1 on Page 56 of his Report was extracted from an ASX Announcement released by Investigator Resources Limited (ASX:IVR) on 22 January 2018 titled "*High Cobalt and REEs Upgrade Potential at Historic Copper Mine in South Australia*"

The Company further advises that it is not aware of any new information or data that materially affects the information included in the Investigator Resources Limited ASX Announcement referred to above and that all material assumptions and technical parameters underpinning the estimates in this market announcement continue to apply and have not materially changed.

For ease of reference, the full text of the Dr. Collerson's Report is now included with this Announcement.

This Release has been approved by the Board of Directors.

For further enquiries:

Byron Miles
Managing Director
bmiles@tombolagold.com.au

Jane Morgan
Investor and Media Relations
jm@janemorganmanagement.com.au
+ 61 (0) 405 555 618

Review of Exploration Data from Burra, S.A. to Improve Targeting Copper, Copper-Gold, and REE Mineralisation

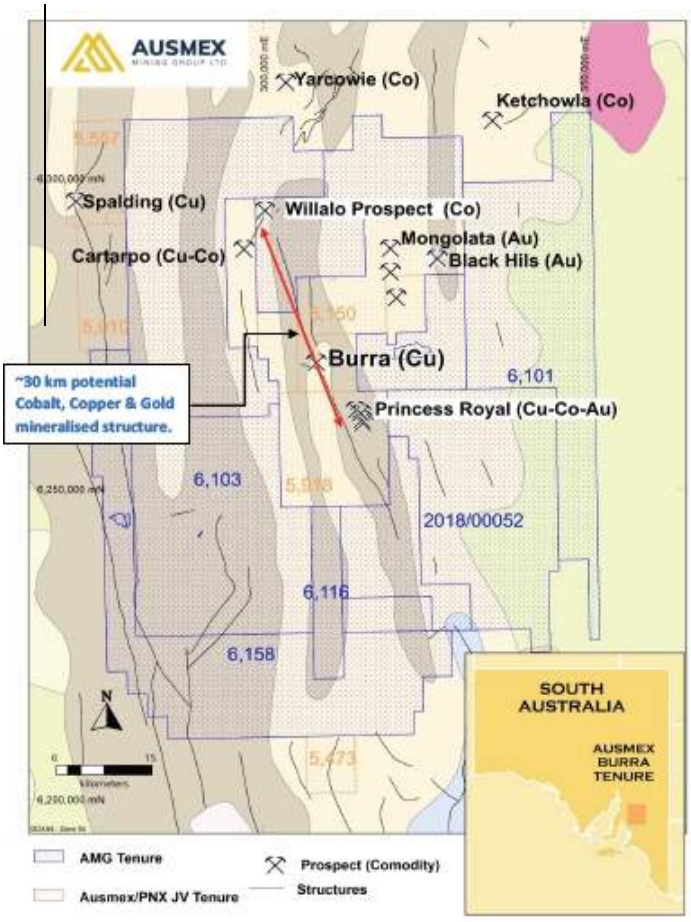

TOMBOLA GOLD

Report for Tombola Gold Limited

Emeritus Professor Ken Collerson PhD, FAusIMM KDC Consulting

March 24th 2022

Contents

1 Executive Summary

This report reviews historic exploration data that includes field observations, assay data and geophysical models obtained by AusMex, Phoenix Copper Ltd. and other explorers in the Burra area.

The review was commissioned to provide constraints on the origin of Cu-Au-Ni-Co-REE mineralisation in the district.

In addition, the regional context of the projected boundary of the Delamerian Orogen is also discussed in order to provide information regarding the petrochemical affinity of basement drill holes.

Lithological, geochemical and geophysical data are reviewed for the following:

- The region immediately east of Tomoba's Burra tenure which contains numerous Delamerian mafic to granitic intrusions:
- The basement east of the Fleurieu Arc, east of the southern Mount Lofty Ranges that is obscured by a venieer Murray Basin sediments.
- The Konnenberry Arc that flanks the Curnamona Craton and represents the northern extension of the Delamerian Orogen.

It is concluded that mineralisation in the Burra area evolved in two stages.

The first metallogenic event occurred during break-up of the Neoproterozoic supercontinent Rodinia. This allowed formation the Cu-Au-REE-Co mineralisation at Burra e.g., the Princess Royal Deposit.

Based on Cu-Ni-Co-HREE systematics, the metal source is interpreted to be associated with plume generated mafic to ultramafic intrusions. Geophysical surveys including MT, magnetics, gravity and radiometric data indicate that such an intrusion possibly underlies the Cartarpo - Willalo- Mullaby area.

The second metallogenic event occurred in the early Palaeozoic, in response to Delamerian magmatism. The gold mineralisation at Mongolata which is characterised by elevated Se, Te, Bi and Hg, as well as by a log normal distribution of Ag/Au, is clearly epithermal in character. Radiometric data indicate that the source of the Mongolata system lies to the east, in a magmatic zone that flanks the western edge of the Delamerian Orogen.

Comparatively little is known about the composition of the Delamerian intrusive suite east of Burra. Although outcrops of Bendigo granite have been mapped, no modern geochemical data is available. Nevertheless, t earlier studies, based on alteration style, suggested that the Bendigo granite could host a Cu-Au-Mo porphyry system.

A review of available chemical data for Delamerian intrusions in the Fleurieu Arc east of the southern Mount Lofty Ranges and outcropping volcanics in the Konnenberry Arc indicates the presence of metallogenically significant potassic alkaline lithologies. Importantly, compositions resemble members of the shoshonite suite and as well as plume generated ocean island basalts.

This is an important observation, as shoshonite suite lithologies represent a unique class of alkaline potassic igneous rocks, because they host world-class epithermal gold-silver and porphyry copper-gold deposits. For example, in the circum-Pacific region e.g., gold deposits such as the 2520 t Grasberg Mine in West Papua and the 1190 t Ladolam-Lihir deposit in Papua New Guinea. The giant

(660 t) Porgera deposit in Papua New Guinea is also hosted by medium-to-high potassium-bearing gabbro and mafic porphyry with compositions that trend towards shoshonites.

In view of the evidence for potassic alkaline magmatism in the Delamerian Orogen, it is recommended that basement cores be sampled for lithogeochemical study to establish if these potassic alkaline lithologies extend north from Truro north into the Burra area.

The area clearly has high potential for discovery of Cu-Au porphyry style systems similar to the Cu-Au porphyry mineralisation recently discovered in western Victoria by Staverly Minerals (e.g., Staverly Minerals ASX Announcement Nov. 2, 2020 and more recent announcements). Thus it possibly represents some of the most prospective, yet least explored tenure, in Australia.

2 Scope of Report

This report was commissioned by Tombola Gold Limited- to improve understanding of the geochemical, geophysical and geodynamic controls on Cu-Ni-Co-REE±Au mineralisation in the vicinity of Burra, South Australia.

The review provides a scientific rationale to improve Tombola's targeting and hence exploration success in the Burra area of the Narkara Arc in the Southern Flinders Ranges.

The review includes:

(1) An assessment of historic assay data obtained by Phoenix Copper Ltd. and other explorers in the Burra area

(2) Integration of these interpretations with geophysical data, especially with the closely spaced MT grid in the area to the west of the historic workings at Princess Royal

(3) Enhancement of these data sets via discovery of open file geophysical data sets (IP, gravity, magnetic and radiometric surveys) that improve understanding of the conductive structures identified by recent MT surveys.

(4) Identification of tenure acquisition opportunities, where mapping and geochemical data, combined with metallogenic models indicate enhanced prospectivity.

(5) Advice for subsequent geophysical surveys

(6) Documentation of targets to be tested by extending RC drill holes with diamond tails and suggestions regarding the best approach to take to drill below the historic workings at Princess Royal

(7) Improved understanding geodynamic controls on metallogenesis during the Neoproterozoic fragmentation of the supercontinent Rodinia and subsequent arc magmatism associated by the development of the early Palaeozoic Delamerian orogenic belt. Importantly, subduction zone/slab tear magmatism is an ideal geotectonic environment for epithermal and porphyry style mineralisation.

(8) An assessment the geological, geodynamic and metallogenic context of Neoproterozic and possible Delamerian age mineralisation the southern Finders Ranges and the western extension of the Curnamona Craton.

(9) Identification of possible igneous lithologies that may have been metal sources in Burra mineralisation.

(10) A review of data from MT Target 2 which lies NE of Mullaby. This anomaly is overlain by Murray Basin sediments to the north east Burra and is oblique to the main structural trend in district. Furthermore the MT target appears to underlie the Mongolata and the Black Hills gold fields. This could indicate that it is imaging an epithermal system above a deeper porphyry.

(11) Suggestions are given on the best array of vector elements to test this hypothesis.

(12) The recent discovery of Cu-Au Butte porphyry style mineralisation buried beneath the sediments of the Murray Basin in western Victoria by Staverly Minerals (e.g., Staverly Minerals ASX Announcement Nov. 2 2020), is particularly relevant to Tombola's exploration strategies. This relevance is enhanced by the presence of partially exposed Delamerian granitic plutons and buried mafic intrusions east and south east of Burra.

(13) Thus, advice is provided regarding the possible mineral system responsible for anomaly 2 beneath the Mongolata - Black Hills area. It is interpreted to a belt of Delamerian felsic and mafic intrusions that form part of a prominent plutonic belt beneath the Murray Basin east of Burra. Importantly, this poorly exposed plutonic complex, appears to extend below the Murray Basin south and east of the Kanmantoo trough and as far north as the Koonenberry Belt to the east of the Curnamona Craton.

3. Introduction

Success in exploration by resource companies requires a comprehensive understanding of the target mineral system in the region where exploration is being undertaken. Importantly, such knowledge evolves as a multi-faceted matrix that necessitates an appreciation of the regional geodynamic and metallogenetic evolution of the exploration area.

Important parameters in this matrix include:
1. Deposit styles
2. An appreciation of metal source or sources
3. The availability and ligand chemistry of transporting fluids
4. The presence of structural or chemical traps for mineral deposition
5. Knowledge of chemical and geophysical vectors that provide critical targeting information for drilling.

Tombola's tenure extends over a highly prospective but poorly explored, but group of contiguous tenements centered on the historic copper mine at Burra, South Australia. These tenements were acquired through a joint venture with Phoenix Copper Ltd.

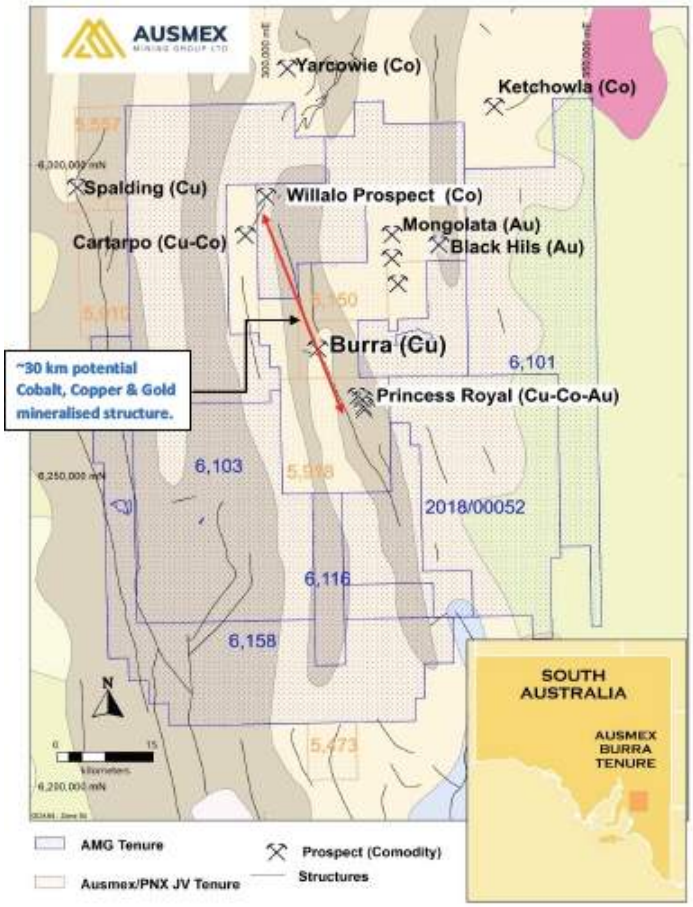

Figure 1: Tombola's tenements in the Burra area

4. Burra Mineral Deposit

4.1 Background

The rich copper deposits in the district were discovered in 1843 and were initially worked by the S.A. Mining Association, who obtained some 234,600 tons of ore containing approximately 22 % Cu. The mine finally closed in 1877 due a drop in the price of copper. Copper mineralisation consists of mesothermal veins of chalcopyrite, bornite and pyrite in a gangue of calcite, quartz with occasional barite is common throughout the area. These veins commonly occur in reverse strike faults. According to Brett (1956) supergene carbonate ore derived from the primary mineralisation, that is common in the area, is believed to have formed by the precipitation of downward percolating acid copper solutions with carbonate wall-rock. At the Princess Royal Mine, low grade veins occur in a brecciated and shattered zone at the axis of a dome structure, while at the Burra Mine, low grade veins occur in breccia between two strike faults.

Location of the Princess Royal and other Cu deposits in the Burra district are shown in Figure 1. Structurally the Burra deposit is situated on the eastern limb of regional shallow north plunging anticline. The lodes are bounded by two steep east dipping fault zones, the Kingston's Fault to the west and the Tinline's Fault to the east, both of which strike approximately north-south. The faults are interpreted to be fault splays off the regional Kooringa Fault.

Figure 2 shows their relationship to MT defined conductive crustal structures

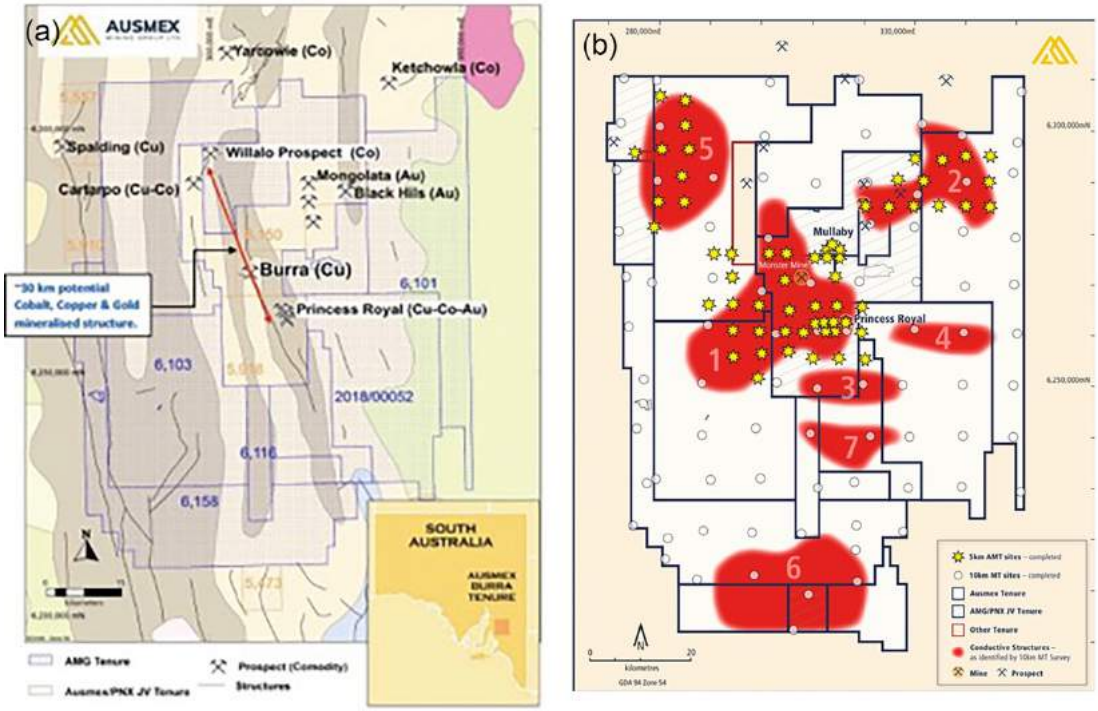

Figure 2 (a) locations of Black Hill, Willalo and Princess Royal in Tombola's tenure in the Burra Area. Aso shown is the location of the prospective Cartarpo tenement west of Willalo (b) Conductive structures identified in the MT survey of the Burra area.

According to Brett (1956) the host rocks comprise a sequence of marbles, limestone, dolomites, fluvioglacials, quartzites and shales of Sturtian and Torrensian age. They are folded into a series of gently north-pitching folds. Folding is intense in the vicinity of both the Burra Mine and the Princess Royal Mine, closed to a domal structure. Strike faulting along the axes of anticlines in the area has also been reported.

4.2 Deposit Style

Despite its extensive mining history, the origin of the mineral system in the district has been the subject of much debate. This is reviewed in detail by George (2017). Mineralisation was interpreted by Thomson (1963) and Johnson (1965) either as remobilised syngenetic or as epigenetic related to igneous activity (Wright, 1975) due to the occurrence of minor igneous rocks in the Burra are. Igneous rocks include a feldspar porphyry ~600 m southwest of the Burra Mine open cut (Dickinson, 1942). However, this unit was subsequently interpreted as a volcaniclastic siltstone containing feldspar phenocrysts (Preiss et al., 2009). Nixon et al. (1965) mapped five sub-parallel porphyry dyke like bodies in the Burra pit which Scriven (1977) reinterpreted as units of welded tuff, based on eutaxitic textures and rhyolitic compositions. A rock resembling an agglomerate was also recognized within the open pit by Lambert et al., (1987).

The syenitic porphyry in the open pit was mineralised with copper sulphides, mostly chalcocite and bornite, and was extracted during the second phase of mining between 1970-1981. As the mineralisation appeared unmetamorphosed, the igneous rocks were considered to have been emplaced towards the end of the Delamerian.

A large number of samples from the Burra open pit next to the porphyry appear to be tuffaceous or volcaniclastic in origin (Drexel and McCallum, 1986; Drexel, 2008). This evidence provided further support to the view that Burra mineralisation may have had an igneous source which may even have played a role in the formation of the lower Skillogalee Dolomite.

This is based on the observation that the Kooringa Member of the Skillogalee Dolomite contains significant, shattered or splintered fragments of fresh microcline feldspar and quartz rather than abrasion caused by fluvial transport. This, together with the presence of high K and Ba indicated a volcaniclastic ash-fall origin for the matrix. Minerals identified in some samples include feldspar (sometimes >80 %), plagioclase, kaolinite, sericitic mica and sulphides (mostly pyrite and trace chalcocite).

As these volcaniclastic units occur within the Kooringa Member, they were considered contemporaneous with deposition. Subsequent U-Pb zircon geochronology (Drexel 2008) yielded an age for the porphyry of 797 ± 5 Ma. This was confirmed with U-Pb geochronology of 792 ± 6 Ma and 797 ± 7 Ma for two porphyry samples (Preiss et al., 2009). Zircons were also separated from volcaniclastic layers in unit 2 of the Kooringa Member. This population of zircons was also interpreted to be of volcanic origin gave an age of 788 ± 7 Ma (Preiss et al., 2009).

Based on this information, Drexel (2008) suggested that volcanic activity occurred during and immediately after deposition of the Kooringa Member and that the porphyry and volcaniclastics

within the member were genetically related. Thus it was suggested that the porphyry intruded sediments in near horizonal sill like lenses soon after Kooringa deposition. Cu-bearing hydraulic breccias caused by the passage of magmatic fluids have been reported in the Kooringa Member. The porphyry sill was subsequently folded to its current near vertical orientation with the host sediment during the Delamerian Orogeny.

Furthermore, this could indicate that the porphyry magma was emplaced from an undiscovered volcanic vent. As the breccias comprise angular dolomitic clasts derived from the Kooringa Member, Drexel (2008) concluded that this unit had lithified prior to magmatic brecciation.

In view of the close association between the porphyry and volcaniclastics of the Kooringa Member, George (2017) suggested that future exploration should focus on the identification of volcanic vents within the extensive Kooringa Member, rather than on syn- or post-Delamerian age intrusions. It is recommended that this should be tested.

In this regard, it is important to note a copper mineralised agglomerate containing brecciated volcanic fragments was also recognised in the Burra Pit. Both volcanic and sedimentary are present , some of which are interpreted to have had a distal not local origins. Volcanic glass, often with flamme or spherulitic structures, interpreted as a probable welded tuff. Thus, the agglomerate may represent a shallow side vent from an erupting volcano that produced the ash falls within the Kooringa Member and thus, may be contemporaneous with this member. In addition, possible volcaniclastic tuffs have been identified within the Kooringa Member ~1.5 km south-southeast and thus distal from of the Burra pit by Preiss, (2002). Indications of alkaline magmatism are preserved in a 'fenitised?-carbonatised? chert' ~200 m south of the pit (Whittle, 1973). A possible syenitic rock has also been reported from the small 'Grove quarry' next to the Barrier Highway 5 km north-northwest of Burra in a unit interpreted as a northern exposure of the Kooringa Member (Elliott et al., 2003).

4.3 Evidence for Igneous Activity in the Skillogalee Dolomite

The Skillogalee Dolomites in the northern part of the Burra pit have been subdivided into dolomites, limestones and non- carbonates based on acid testing, Drexel, 2008; Preiss et al., 2009). Dolomitic units were identified as containing a significant quartz and feldspar silt component based on thin-section petrography. Facies changes are present such that limestone units may grade laterally to dolomite. Some limestone units consist of fine regular rhythmic laminations interpreted as chemical precipitates from a lacustrine setting (Drexel, 2008).

However, in the southern third of the pit Drexel (2008) noted that the 14 well-defined lithologies had been highly altered due to potash metasomatism, silicification and hydraulic brecciation. In addition, lithologies also showed evidence of acid leaching/bleaching of original carbonates and siltstones due to the breakdown of primary sulphides. Furthermore, the southern section of the pit is reported to contain contained more volcaniclastic sediments than the north, suggesting it is proximal to a volcanic vent.

Of the 14 units identified in the Burra pit by Drexel (2008), the Kooringa Member was represented by units 2-14. Unit 1 is a comparatively pure dolomite lacking silt and is therefore classified within the lower Skillogalee Dolomite directly beneath the Kooringa Member. The

purer dolomite of the lower Skillogalee Dolomite is again exposed east of the Burra pit and unit 14. Importantly some units contain muscovite and phlogopite as alteration phases.

A unit of white dolomitic marble containing secondary copper sulphides, oxides and carbonates (e.g., chalcocite, covellite, cuprite, azurite, malachite) has been reported from the bottom of the Burra open pit in close contact with the Kingston shear and diapiric breccia. It is reported that the dolomitic marble was largely left unmined since it could not be extracted by excavator, nor processed via the ammonia leaching used in the processing plant. The marble is exposed over a maximum width of 45 m and length of 130 m. Its southern end is located at the southern wall of the open pit. Additional smaller marble bodies are found adjacent to the porphyry and further north within units 1 and 2.

A small exposure of light grey dolomite in the pit containing significant malachite-azurite veining with lesser chalcocite appears to have escaped significant recrystallization.

According to Drexel (2008) the exposure may be dolomitised (which would destroy former crystalline structure), or alternatively could be part of unit 1 (or lower) that escaped recrystallisation caused by intrusion of the porphyry. Drexel (2008) suggested that the unit could have crystallised from hydrothermal fluids originating from the parent porphyry. Another explanation suggests that the dolomitic marble may be a more recrystallized section of the lower Skillogalee Dolomite that occurs directly beneath the sequence observed in the pit wall as well as to the west of the Kingston shear. A third explanation is that the dolomitic marble is a carbonatite possibly associated with the diapir.

Drexel's (2008) description of the marble is quite informative. Specifically that:
"An unusual variant of the marble that can still be accessed in the open cut is at sample site B264/80. The outcrop here is a layered, copper-mineralised recrystallised dolomitic breccia containing clasts and layers of potash feldspar. The feldspar was probably derived from, or associated with, the quartz-feldspar metasomatites common in and around the main orebody. To its immediate east is a dolomite breccia (grey, angular dolomite clasts in a yellow-brown dolomite matrix) containing a possible dolomitic sandstone dyke (sample site B288/80); this breccia is un-mineralised, despite being in contact with the heavily copper stained recrystallised dolomitic breccia. A detailed study of this outcrop may provide information relevant to the understanding of potash metasomatism and mineralisation in the Burra orebody."

This model should be tested geochemically because Sr, Ba, Nb, REEs and Y are typically enriched in carbonatite magma.

Reports of potash metasomatism and silicification at lower levels in the pit by Drexel (2008), is also significant, as K-metasomatism is a common feature fenites, resulting from fluids emanating from carbonatite intrusions (Elliot et al., 2018).

The following important observations were made by Drexel (2008):

1. The unit contains up to 77% K-feldspar and 20% quartz which was absent at higher levels

2. K metasomatized rocks also occur as breccia clasts, indicating the metasomatism occurred early in the mineralising process.
3. K metasomatism was possibly associated with intrusion of the porphyry.
4. This is supported by the proximal association between the porphyry and extensive alteration in the southern part of the pit where the intusion was emplaced at least to the level of unit 6 of the Kooringa Member.
5. K-feldspar was also present within the dolomitic marble.

Tourmaline, a boron-bearing phase, was identified by Drexel (2008) in the alteration zones close to the porphyry and the agglomerate at the base of the pit. As tourmaline replaced quartz, feldspar and kaolinite(?), tourmalinisation likely occurred after potash metasomatism and silicification. Traces of tourmaline have also been reported from the porphyry. The presence of tourmaline indicates that the syn-mineralisation fluids were boron-bearing.

4.4 Burra Mineralisation

According to Drexel (2008) igneous units in the Burra pit (including the porphyry and an agglomerate) intrude tuffaceous siltstones and dolomites of the Kooringa Member towards the base and southwestern side of the open pit. Copper mineralised jigsaw and crackle (granular) breccia occurs in the Skillogalee Dolomite due to hydraulic brecciation caused by pressurised volcanic fluids (Nixon et al., 1965; Drexel, 2008). Approximately vertical ferruginous pipes, as well as larger areas of ferruginisation, occur within and around copper mineralisation, inferred to be previous iron-(copper)-sulphide ores. These sometimes contain coarse limonite pseudomorphs after pyrite.

Three copper mineralisation events have been proposed at Burra. The first mineralisation was likely chalcopyrite dominant, though little chalcopyrite is still preserved. Euhedral chalcopyrite crystals including bornite blebs have been observed in the porphyry but these have mostly been altered to chalcocite (Nixon and Townend, 1966). However, at greater depth in the pit, cubes of chalcocite (up to 5 cm in size) appear to pseudomorph pyrite, are the dominant sulphide in the porphyry. This suggests that pyrite may have been the primary sulphide in the porphyry. In this case, pyrite may have acted as a reducing agent that aided chalcopyrite deposition from deep magmatic fluids (Drexel 2008).

The second mineralisation event involved epigenetic enrichment of chalcopyrite to chalcocite and lesser covellite.

This was followed by supergene enrichment of sulphides with formation of the copper carbonates and oxides malachite, azurite, chrysocolla and cuprite during weathering.

5. Tomoba's Exploration Strategy in Burra Area

Exploration in the Burra region has previously focused on secondary copper mineralization associated with the numerous outcropping sediment-hosted stratiform copper deposits located in the Neoproterozoic and Cambrian sediments of the Adelaide Geosyncline, including the Monster Mine.

Tombola has taken a different approach and is using modern geophysics (MT) to explore for deeper magmatic mineral systems as well as using geochemical vectors to identify possible metal source lithologies and also to map out fluid pathways of metalliferous fluids.

A feature of these deposits is structural control at a range of scales. Deposit-scale features include fault control of individual orebodies, through to fault bounded basement features that control sedimentation. Regional scale controls include major geodynamic features such as the shape of the Delemarian orogen and crustal lineaments (G2 Corridor) that appear to control the location of deposits.

In view of the combination of the mafic and felsic intrusives in the region, combined with hydrothermal alteration, metal zonation (copper, copper-gold, base metals, REE), the G2 corridor and more recently the large AusLAMP defined conductive feature beneath, Ausmex has taken take a different exploration approach by investigating mineral system development associated with the Neoproterozoic break-up of Rodina and the effect of the early Palaeozoic Delamerian Orogeny.

Ausmex, (now Tombola Gold Limited) in collaboration with the University of Adelaide U (Prof. Heinson), undertook a gridded MT/AMT over the entire region of the Tombola controlled tenements at a 10km spacing with follow up at a 5km spaced grids in areas of conductivity. The recent AusLAMP (**Aus**tralian **L**ithospheric **A**rchitecture **M**agnetotelluric **P**roject) survey conducted for AusMex (ASX Market Releases 13 March, 2018; 5 July 2018) has identified a large conductive "MT flare" (~ 100 km in diameter) within the mid-to-lower crust directly beneath AusMex's/Tombola's tenure at Burra. This MT anomaly is shown in Figure 2.

Inversion modelling has allowed identification of seven anomalous conductive zones within the region (Figure 2b). One of these anomalies lies below the Princess Royal Deposit. A second conductive anomaly (designated Anomaly 2) lying to the NE and is associated with gold and base metal mineralization, proximal to felsic intrusives that were emplaced during the Delamerian Orogeny. These granites, which are interpreted to have played a major role in regional mineralisation, are not well understood because they are overlain by Murray Basin sediments and only minor outcrops have been mapped. The metallogenic implications of these intrusions is discussed below.

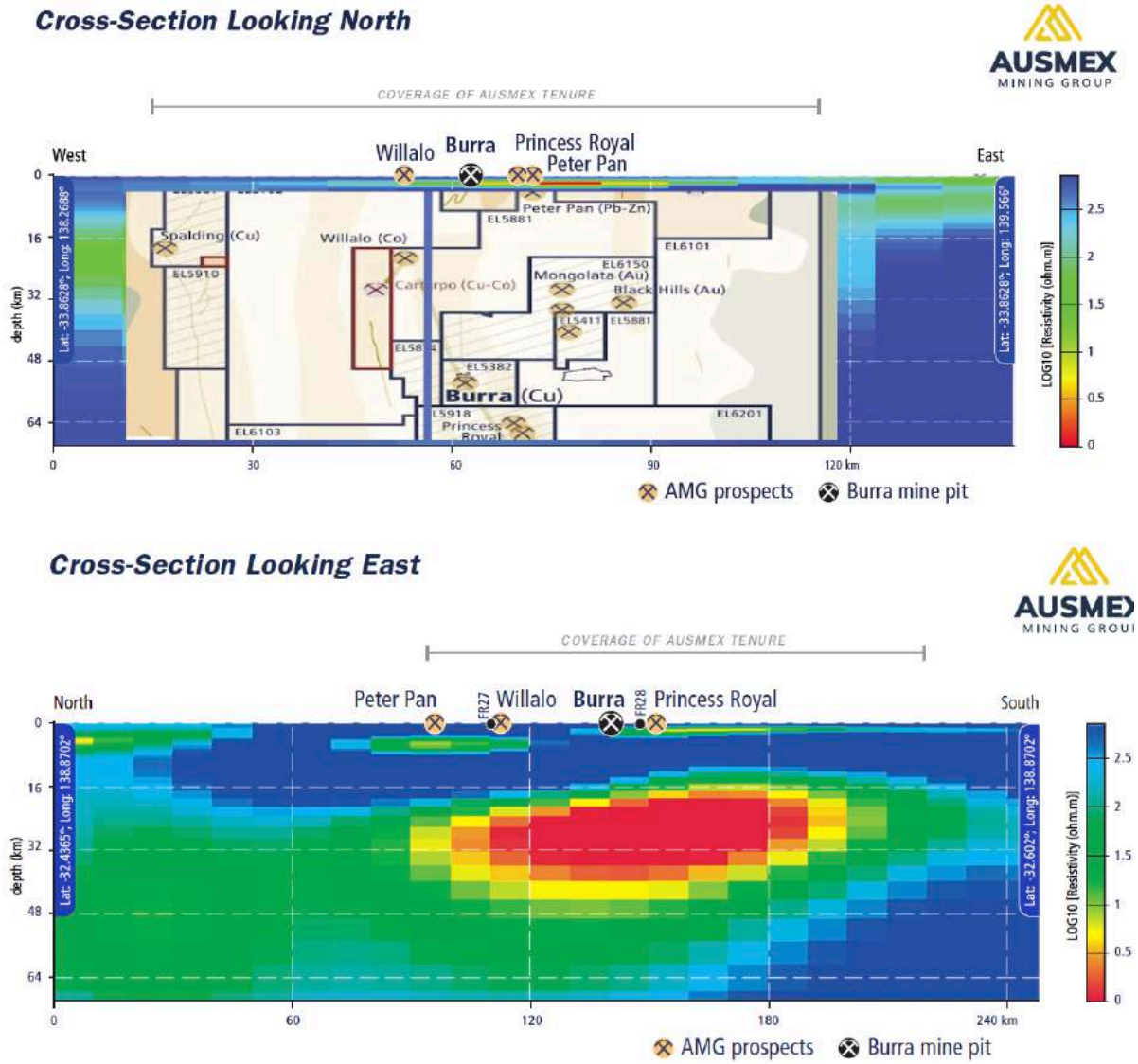

Figure 3: Large conductive MT flare (~ 100 km in diameter) within the mid-to-lower crust directly beneath AusMex's tenure at Burra.

6 Geochemical and Geodynamic Constraints on the Burra Mineral System

6.1 Neoproterozoic Burra Mineral System

Cu-Co-Au-REE mineralisation in the Burra area is hosted by Neoproterozoic Kooringa Member of the Skillogalee Dolomite. It has a magmatic source (Collerson 2018) and appears to be contemporaneous with intrusion of syenite porphyry dykes and eruption of tuffaceous units. These contain zircons which constrain the age of mineralisation to be 797 ± 5 Ma; U-Pb geochronology of two porphyry samples yielded ages of 792 ± 6 Ma and 797 ± 7 Ma for (Preiss et al., 2009) and zircons from volcaniclastic (tuffs) layers in unit 2 of the Kooringa Member interpreted to be of volcanic origin gave an age of 788 ± 7 Ma (Preiss et al., 2009).

The following key findings regarding the Princess Royal minerals system (Collerson, 2018) demonstrate the significant discovery potential of the region:

(1) The Co-Cu-Ni- Zn-REE-Au mineralisation at Burra is **hydrothermal** in origin.

(2) Hydrothermal fluids in the Princes Royal mineral system were fluorine-rich and oxidizing, similar to compositions of fluids inferred for the nearby world class Olympic Dam IOCG.

(3) The conductivity domain identified below Burra is similar in scale and character to the large MT conductive anomaly below Olympic Dam, ~380 km to the northwest.

(4) Like at Olympic Dam, the Burra conductivity anomaly is interpreted to image the metal migration regime involved in formation of the mineral system.

(5) **As the ~790 Ma Burra mineralisation) is ~800 Ma younger than the ~1590 Ma Olympic Dam deposit , it is likely that Burra mineral system formed in a younger mantle plume magmatic event than the event responsible for the IOCG deposit at Olympic Dam.**

(6) The metal enrichment of the lithosphere below Burra, is therefore interpreted to have been caused by the plume magmatic event associated with breakup of the supercontinent Rodina, between 820 Ma and 830 Ma, forming the Gairdner **L**arge **I**gneous **P**rovince **(LIP).**

(7) The Burra area has significant prospectivity because of its position in Rodinia. The terrane lying between the Gawler and Curnamona Cratons represents the most proximal region of non-Chinese lithosphere to have experienced plume induced magmatism associated with the breakup of Rodinia at ~820 Ma. This is confirmed by the plume geochemical signatures shown by the Gairdner dykes.

(8) The conductive regions seen in the AusLAMP images of lower to mid crust below Burra may reflect the presence of intrusions, similar to the Jinchuan and Lengshuiqing intrusions in SW China, that occur in a transported terrane that was previously juxtaposed against this part of Rodinia.

(9) Similar elemental covariations between Ni-Cu-Co at Princess Royal Black Hills, Peter Pan and Willalo show that they are likely to be genetically related.

(10) The metal association at Burra, dominated by Cu, Co and Ni together with Zn, Au and REEs indicates that metals were derived from a mafic alkaline igneous source.

(11) Princess Royal samples have non-chondritic Y/Ho and both negative and positive Ce/*Ce anomalies. The non-chondritic Y/Ho ratios indicate that the hydrothermal system at Princess Royal was halogen-rich (fluorine-rich). The negative and positive Ce/*Ce anomalies indicate that the fluids were oxidising.

(12) Willalo rock chip samples display significant coherent enrichment in Co, Cu and Ni. This is interpreted to indicate proximity to the mafic and ultramafic source of metals in the Burra mineral system. It is recommended that magnetic, gravity and radiometric data be investigated to identify accessible anomalies for drilling to target Jinchuan and Lengshuiqing style ore deposits as discussed below.

(13) **Potential targets in the Burra area include deposits simiar to the giant~830 Ma Jinchuan deposit (>500 Mt @ 1.2% Ni, 0.7% Cu, Cu/Ni 0.58, ~0.4g/t PGE) which is the largest single magmatic sulphide deposit on Earth.**

(14) Importantly, Willalo rock chip samples have mean Cu/Ni ratios (0.52±0.12) similar to the Jinchuan and Lengshuiqing deposits in China, e.g., 0.53±0.39 and 0.46±0.51 respectively. The Willalo area it therefore interpreted to be a high priority target for Co, Ni, Cu, Au as well as the PGE's.

6.2 Early Palaeozoic Mongolata Mineral System

The Mongalata goldfield is situated approximately 15km northeast of Burra. The goldfield extends northwards from Mongalata for some 12km. The host to the gold mineralisation is the Cox Sandstone, which is recognised as a widespread host to gold mineralisation in other parts of the Nackara Arc. The host to the gold mineralisation at the Bird-In-Hand Mine on the Woodside goldfield may also be a correlative of the Cox Sandstone (Preiss and Robertson, 2006). The Cox Sandstone Member is actually a feldspathic sandy siltstone, which forms part of the Tarcowie Siltstone Formation, which overlies the Tapley Hill Formation (Preiss, 1987). Some gold mineralisation also occurs in the underlying Tapley Hill Formation. Both the Tarcowie Siltstone and the Tapley Hill Formations belong to the Umberantana Group.

The Mongolata goldfield is underexplored and underdeveloped, with opportunities for discoveries along the 12km line of old surface workings and at depth into primary mineralisation.

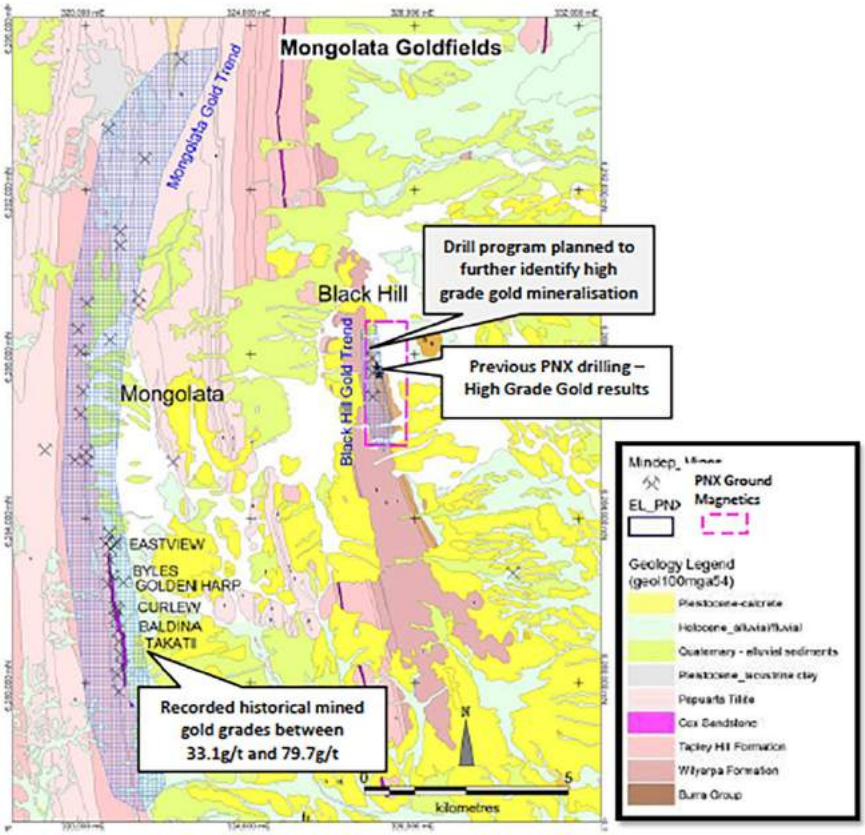

Figure 4: Geology of the Mongolata

The Mongolata goldfields are wholly within EL4233 and EL4970 and are defined by several historic mines and a number of small workings extending in a north-south strike orientation for approximately 12km

(Figures 2 and 4). Gold was discovered at Mongolata in 1930, and since that time small tonnages of high grade ore have been mined (Mongolata state battery production - 11,129 oz. from 7,684 tonnes, average: 45g/t Au).

Detailed mapping and sampling in the area by DMITRE in the 1980s and more recently by Phoenix Copper indicates that the gold mineralisation occurs within auriferous quartz-limonitic breccia lodes and veins associated with the thrust faulted contact between the Cox Sandstone and the underlying Tapley Hill Formation. Mongalata lithologies were deformed and metamorphosed to greenschist grade during the Delamerian Orogeny.

Previous exploration and mining in the Mongolata Goldfield have shown the presence of high-grade coarse-grained gold ln the oxidised zone occurring in cross cutting quartz-limonite-hematite-manganese-carbonate-pyrite veins. Breccia zones and faults are also reported to contain minor amounts of gold also occur within the footwall and hanging-wall sediments (Plimer, 1997). The gold grade, grainsize and distribution is highly irregular. Estimates based on battery records, production records, vein density and stope volumes suggest that the grade in the oxide zone from selective mining was > ~34 g/t Au and the minimum bulk grade in the oxide zone is 2 ± 0.5 g/t Au.

Redfire Resources (Simpson, 1997; Plimer, 1997) recognized the potential of the north plunging anticlinal structure beneath the masking cover sequence east of the northern extension of the Mongalata goldfield. They concluded the anticlinal fold closure defined by the trace of the Cox Sandstone would be favorable for dilation and the development of saddle reefs. Certainly the recognition of mineralisation at Mongalata in association with strike slip dilational jogs within the brittle Cox Sandstone by Redfire Resources (Plimer, 1997) supports this model. However, MIM sampling was restricted to the area directly east of the northern extension of the Mongalata field (Figure 9), and no systematic soil sampling was undertaken over the actual inferred position of the fold closure.

Trace element and stable (O, C and S) isotopic data for samples from the Mongolata goldfield were reported by Griessmann (2011) who concluded that the central Nackara Arc gold deposits were similar to Telfer Style systems. The Telfer deposits formed from metal-bearing magmatic fluids sourced from composite granitic plutons that underlie the district (Schindler et al., 2016).

Based on geochemistry and geophysical signature in the current review, Au mineralisation in the Mongolata - Black Hills area, is interpreted to be epithermal in origin and is likely associated with a younger and different source than the Burra mineral system. For example, log Ag/Au ratios calculated for Mongolata mineralisation define a log normal distribution (Figure 5).

According to Cole and Drummond (1986), deposits with Ag/Au ratios of one or less are dominated by native gold, electrum, tellurides, and argentite, regional propylitic alteration and may be associated with fluorite or minor alunite, adularia, quartz or calcite in veins. By contrast, deposits with log Ag/Au ratios greater than one are characterized by argentite, base-metal sulfides and sulfosalts, silver sulfosalts, electrum, and native silver, regional propylitic alteration, and quartz-rich veins. Native gold is usually subordinate to all other precious metal phases when the Ag/Au ratio is greater than one.

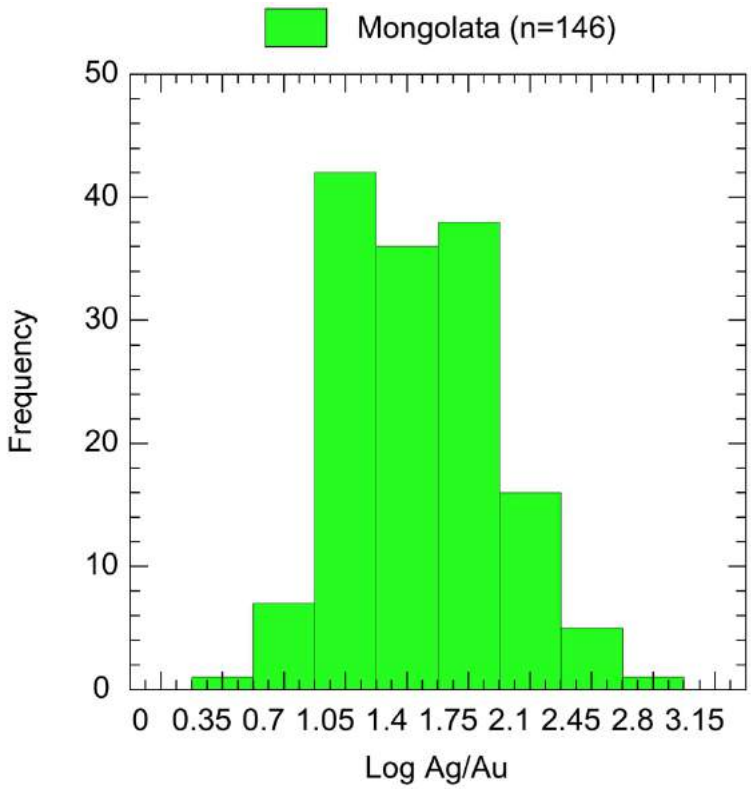

Figure 5: Histogram showing log Ag/Au distribution exhibited by Mongolata vein gold mineralisation

These mineralogic trends, the range in Ag/Au ratios, and the spatial distribution of minerals in a given deposit are commonly attributed to the complex relationships between source rock type, fluid flow velocities and flow patterns, transport properties (e.g., temperature, pH, salinity, total sulfur, etc.), and depositional mechanisms (e.g., boiling, mixing, cooling, etc.). They therefore reflect the transport and deposition of gold and silver in and from boiling hydrothermal solutions that have maintained a two-phase liquid--vapor fluid. The most significant effect of boiling on the chemistry of a hydrothermal solution is associated with the exsolution of CO_2 and H_2S. The loss of CO_2 causes significant changes in pH whereas H_2S exsolution destabilizes sulfides and perturbs the oxidation state. As a result of exsolution of CO_2 and H_2S, many boiling systems may undergo extensive acid alteration in high level epithermal environments.

Tellurium and other chalcophile elements can be used as a tracer of processes of metal extraction from their source, as well as transport, fractionation and deposition (Holwell et al., 2019). Tellurium has a crustal abundance of only ~5 ppb, but is notably enriched in volcanogenic massive sulfides and deep marine sediments, such as Fe–Mn nodules and crusts, limestone and shale (~1–200 ppm Te). When subducted, these lithologies may undergo devolatilisation and/or partial melting with metasomatic mass transfer of constituent elements like Te (and Au) into the mantle wedge. Te is particularly useful as like Au, it partitions into the metasomatising fluids/ melts that modify the composition of the lithospheric mantle during subduction and form localised Te- (and other metal)-rich domains. It is thus not surprising that magmas and mineral deposits that tap this enriched source have some of the highest Te contents of any magmatic systems. Due to its paucity in the continental crust, the Te signature of mafic magmas ascending through the crust is only minimally affected by crustal assimilation. As a result, the Te-enriched signature in post-subduction alkaline melts reflects the primary, subduction-modified mantle source.
The variable geochemical behaviour of Te at different P–T conditions provides the key constraint to support this hypothesis. At magmatic temperatures (> 1000 °C), Te behaves as a chalcophile element,

like Au, Cu and the PGE. Therefore, it is readily concentrated into sulfide melts, which cool and fractionate, generally forming Pt–Pd-telluride melts at ~900 °C and then Pt–Pd-telluride minerals at <400 °C. In hydrothermal environments, Te can be mobilised as chloride complexes at ~300 °C, as polytellurides in S- and CO2-rich fluids, and as telluride–bismuthide melts.

The combination of these aspects of Te behaviour enhances its applicability to understanding mantle-to-crust fluxes of metals, as it is an ideal tracer of both magmatic and hydrothermal processes.

Although Te is not generally included in routine analyses, limited data was reported by Griessmann (2011) for Mongolata and Black Hills (Table 1). These data plotted in Figure 6 show that Mongolata and Black Hills have a significant epithermal chatacter.

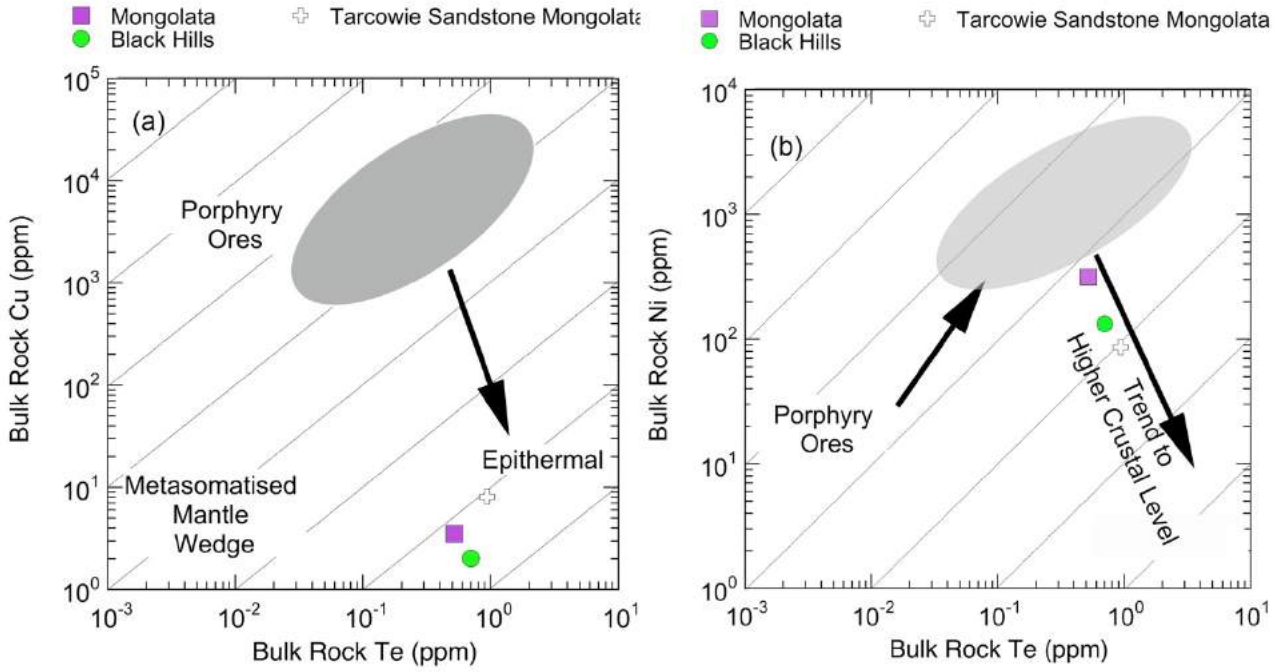

Figure 6: Tellurium/nickel and copper ratios through the lithosphere. (a) Plot of Te vs. Cu and (b) Te vs. Ni showing increase in Te/Ni up through the lithosphere with fractionation. Te vs. Cu showing divergent behaviour of Te in hydrothermal environments

Other elements listed in Table 1 that are enriched in epithermal systems include Hg, Bi, Sb and Se.

Table 1: Selected trace element compositions for samples from Mongolata and Black Hills. From Griessmann (2011)

	Mongolata	Tarcowie Sandstone	Black Hill
Te ppm	0.52	0.94	0.7
Hg ppm	0.55	0.78	0.48
Bi ppm	0.53	14.63	1.32
Sb ppm	0.24	2.57	0.23
Se ppm	14.59	42.58	6.16
Cu ppm	3.52	8.1	2.02
Ni ppm	314	85.62	133
Au ppm		0.18	
Ag ppm	0.08	0.08	0.1
Cu/Ni	0.1	1.13	4.93

All samples are significantly eniched in Ni, ranging from 86 to 311 ppm (Table 1). By contrast, the average Ni content of granite and in weathered upper crust are 15 and ppm 31 respectively (Kamber et al.,2005). Thus, the hydrothermal fluids responsible for mineralisation in the Mongolata field were most likely derived from mafic members of the Delamerian age magmatic-plutonic belt that occurs to the east of the Burra-Mongolata area. These intrusions define a prominent magnetically distinctive N-S trending belt that is mostly obscured by Murray Basin sediments (Figure. 4). Drill cores into this belt have compositions ranging from gabbro to diorite, monzonite and granite (Table 2).

One of these Delamerian plutons, the Bendigo Granite crops out north east of the Burra and overlies one of these circular magnetic features which has demagnetized cores or demagnetized rims characteristic of porphyry copper systems (Fig. 4 - blue dots). Although little data is available for the Bendigo Granite Langsford (1972) and Morrison (1989) provide some petrographic information. Morrisson (1989) commented that the Bendigo Granite was similar to the Anabama Granite.

The Bendigo granite is sericitised and highly altered with biotite being replaced by epidote and chlorite. The most strongly altered lithologies also are reported to contain calcite and dolomite. Langsford (1972) concluded that mineralisation in the Bendigo granite is copper-molybdenum porphyry style, based on the zonal distribution of a quartz-sericite-pyrite (phyllic zone) surrounding an inner propylitic zone of sericite-carbonate-epidote.

Marlow (2008) was of the opinion that the deeper potential for copper sulphide and precious metals along strike north of Burra had not been tested and that high potential existed for discovery of new deposits in untested areas underlain by alluvial cover along strike from known mineralisation.

Gold targets tarets include flexural slip dilational jogs and saddle reefs developed in fold closures of the host Cox Sandstone below alluvial cover. Specific structural targets mentioned by Marlow (2008) are shallow north plunging tight upright fold hinges that could host mineralisation.

These specific structural targets remain untested by systematic soil sampling. Thus the widespread occurrence of old gold workings within the tenement (historical grade up to 28g/t Au), as well as anomalous soil and rock chip sampling by previous explorers confirms the exploration potential of the region.

In this regard have previous explorers (CRAE, 1980; Petra Search 1997) noted that calcrete sampling over known mineralisation yielded anomalous results. This could be explained by the presence of gold in leaf litter. KDC's experience in the central Gawler Craton has indicated that the preferable way of sampling in calcrete is with auger drilling to obtain a depth profile. Using this technique in a consultancy for Tyranna Resources in 2016 to improved understanding of calcrete gold geochemistry near the Challenger Gold Mine in the western Gawler Craton. This allowed discrimination between true and false calcrete Au anomalies with great success identifying numerous targets that were confirmed by deep RC drilling and assays.

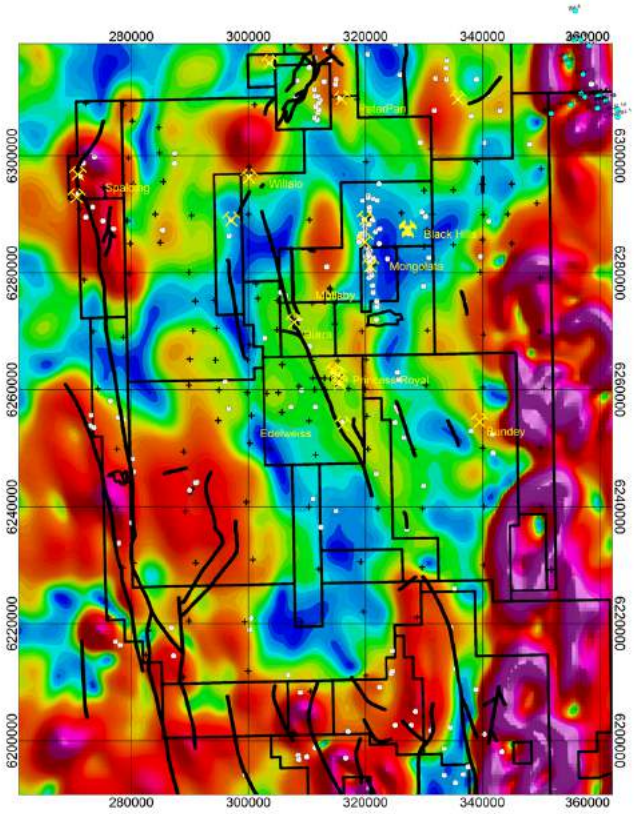

Figure 7: Depth Slices through the 3D Magnetic Vector Inversion (MVI) model output. Input data was regional magnetic compilation (Sarig and Gadds) gridded at 80m cell size. Geophysical Model produced by Kate Nelson - Geodiscovery Group. The pale blue circles in the top right hand corner show locations of samples of Bendigo granite.

Figures 8 and 9 show discrete zones of elevated K (Fig. 8a, 9a), high U (Fig. 8b) and high Th (Fig. 9b) extending from Mongolata through Black Hills towards the belt of Delamerian Intrusions east of Burra. Patterns reflect the concentration of potassium minerals (adularia and illite) in high-temperature alteration assemblages. These radiometric signatures are commonly associated with hydrothermal alteration in epithermal systems (Kwan et al., 2016).

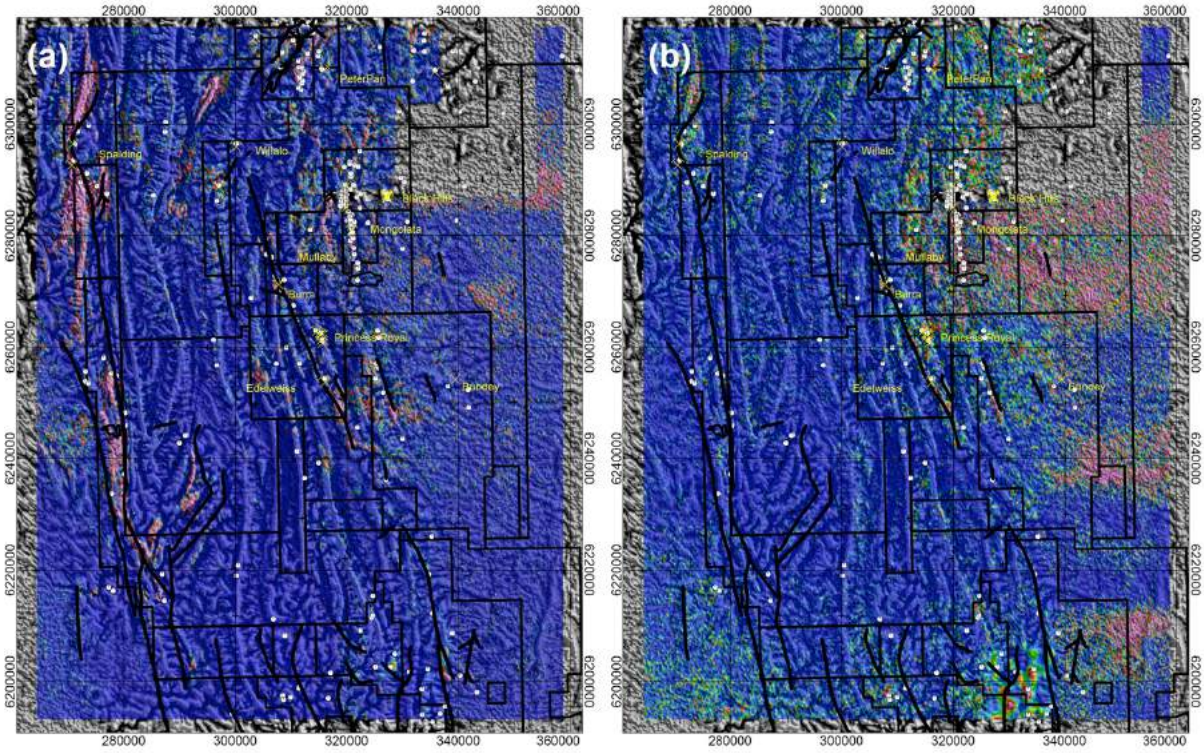

Figure 8: (a) Plot of K/Th and (b) U^2/Th showing data for the Burra area. Radiometric compilation 2019 (available on Gadds) gridded at 80m cell size. (a) Shows discrete zones of elevated K/Th ratio extending from Mongolata through Black Hills towards the belt of Delamerian Intrusions east of Burra. This shows the concentration of potassium minerals (adularia and illite) in high-temperature alteration assemblages. (b) Shows more prominently these zones of high U^2/Th in the vicinity of the Delamerian Intrusions east of Burra. Such features are commonly associated with hydrothermal alteration in epithermal systems (Kwan et al., 2016).

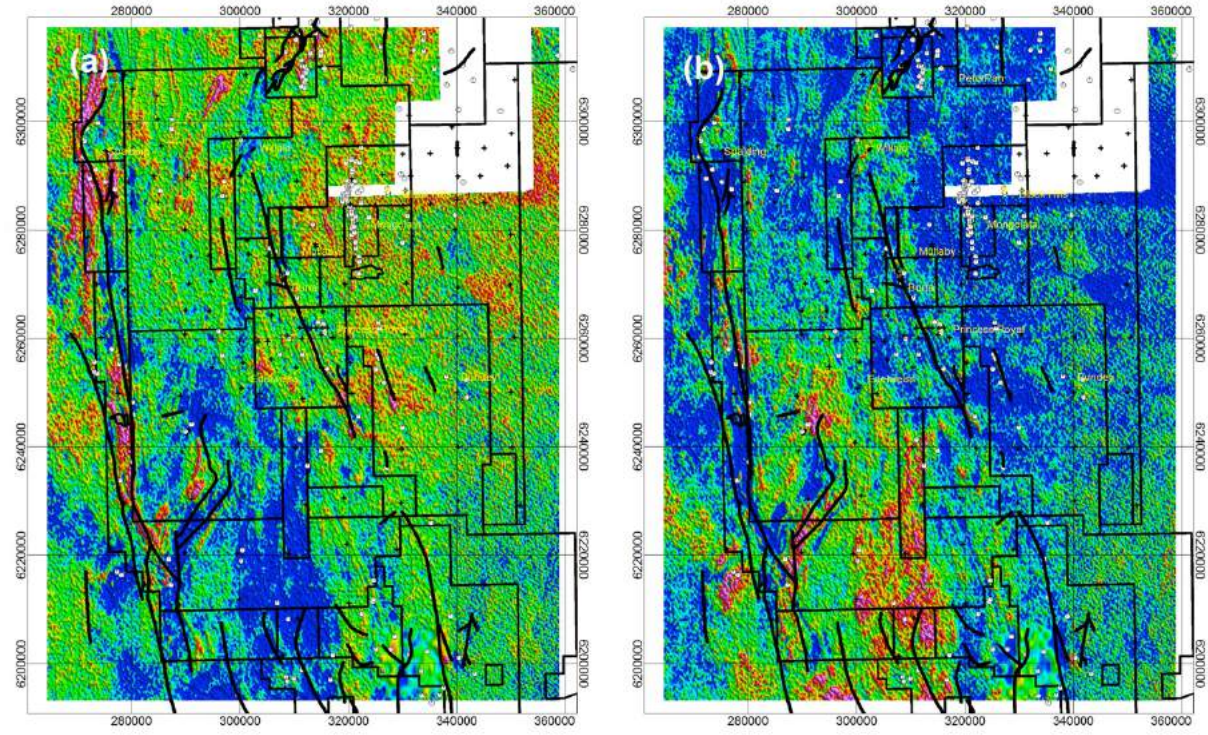

Figure 9: (a) Plot of K/Th and (b) Th/K showing data for the Burra area. Radiometric compilation 2019 (available on Gadds) gridded at 80m cell size. (a) Shows discrete zones of elevated K extending from Mongolata through Black Hills towards the belt of Delamerian Intrusions east of Burra. This shows the concentration of potassium minerals (adularia and illite) in high-temperature alteration assemblages. (b) Shows more prominently these zones of high Th relative to K in Delamerian Intrusions east of Burra. Such features are commonly associated with hydrothermal alteration in epithermal systems (Kwan et al., 2016)

Figure 7 clearly shows that the demagnetized zone containing the epithermal mineralisation at Mongolata extends northeast into the Bendigo granite. This zone of magnetic destruction also coincides with the conductive structure identified in the MT survey shown in Figure 2b. Thus, the prospectivity potential of this area is clearly quite high and should be explored by drilling.

7. Regional Tectonic Setting

The belt of Delamerian intrusions shown in Figure 10, is regionally significant continental magmatic arc. The belt extends from the Burra area, south to the Fleurieu Arc (Fig. 8) and north, flanking the Curnamona Cration, to the Koonenberry Belt in western N.S.W..

Tectonically the region represents the Neoproterozoic East Gondwana margin of southeastern Australia. This passive margin formed after the break-up of Rodinia (Scheibner, 1992). The margin is characterised by a series of salients and re-entrants that reflect modification by later geodynamic processes (Direen and Crawford, 2003a, Williams et al., 2009).

Debate about the polarity of the Delamerian convergence has continued between proponents of broadly east-dipping subduction below volcanic arcs facing towards the Gondwanan continent (Direen and Crawford, 2003b). However, other researchers favour west-dipping subduction below arcs facing away from Gondwana (e.g., Crawford and Keays, 1978, Flöttmann et al., 1993, Foden et al., 2006).

Although outcrops of these Delamerian intrusions do occur sporadically crop out, for example in the Truro area, the Delamerian magmatic belt is largely covered by sediments of the Murray Basin Basin (Foden et al., 2002; Foden et al., 2020).

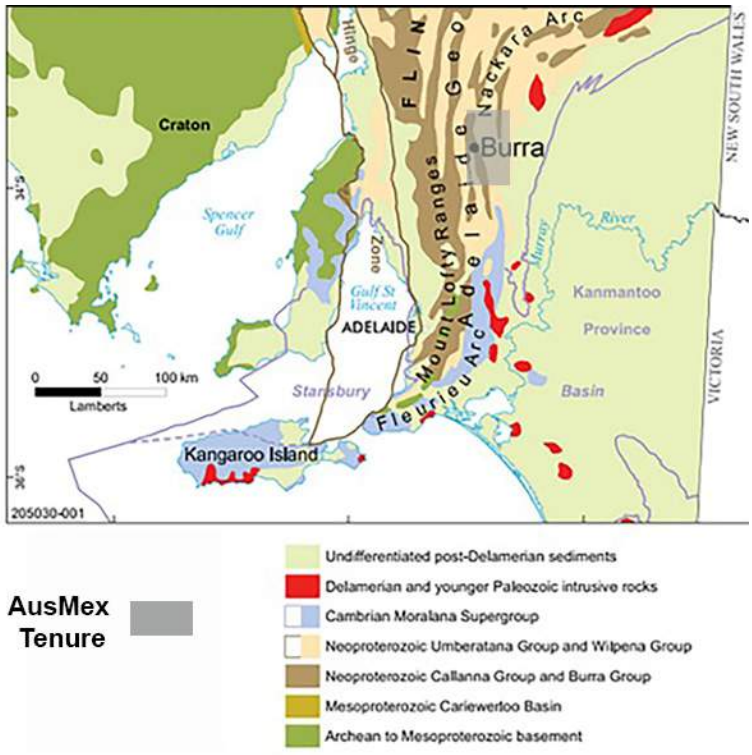

Figure 10: Location of AusMex Burra tenure in relation to major geological elements in South Australia. Image modified from Cowley (2020).

Foden et al. (2006) concluded that the orogen developed in a compressive regime that was initiated at 514 ± 3 Ma, and was terminated by rapid uplift and extensional magmatism at about 490 ± 3 Ma. Within the orogen there was a change from extensional margin back-arc rift volcanism and sedimentation in the Late Neoproterozoic to a Cambrian convergent regime that was associated with the onset of subduction-related magmatism (Foden et al. 2002). A similar change in volcanic regime also occurs in the northwest-trending, extension of the orogen into the Koonenberry Belt in northwest New South Wales reflected by the Neoproterozoic alkaline rift-related Mount Arrowsmith Volcanics and the Cambrian calc-alkaline Mount Wright Volcanics (Crawford et al. (1997).

The current review has identified chemistry K-rich alkaline lithologies such as absarokites, shoshonites and banakites as well as high-K calc alkaline compositions in the Delamerian magmatic belt (see below). These rare lithologies are highly fertile hosts for Cu-Au porphyries (e.g. Müller and Groves 2016).

As a result, this new information indicates that the entire length of the Delamerian magmatic belt has significant exploration potential for discovery of Cu-Au porphyry systems similar to the recent discovery by Staverly Minerals in western Victoria (Staverly Minerals ASX Announcement 2020).

The presence of bends termed salients and re-entrants) along the orogen, e.g. in the Fleurieu and Nackara arcs, are interpreted to indicate the presence of tears in the subducting oceanic lithosphere (e.g. Rosenbaum and Agostinetti 2015),. These fearures have implications for generation of shoshonite suite magmas and metallogenesis (Collerson et al., 2015). Slab tears also play an important role in localising mineral deposit formation (e.g., Fiorentini and Garvin, 2010; Holm et al., 2019). For example, in Papua New Guinea, one of the most prospective regions for intrusion-related mineral deposits in the World, because of the tectonic complexity and lack of comprehensive regional geological datasets, the link between mineralization and the regional-scale geodynamic framework has not been appreciated. However, In an important paper, White et al., (2014) showed that the locations of major gold and copper deposits in New Guinea are considered to be controlled by a series of transfer faults that strike N–S to NE– SW, perpendicular to the long axis of the island. This is because these faults dilate perpendicular to the regional stress field, forming conduits for metalliferous gases and fluids to drop out of solution.

Furthermore, these faults are the surface expression of even deeper tears that have been imaged using seismic tomography in the subducted oceanic slabs that underlie PNG. These tears are important, because they provide a conduit for plume transport of Au originating from the core (Collerson 2015). This explains the common association between ocean island basalt magmatism (plume) with shoshonite suite lithologies in magmatic arc terranes.

8. Geochemical Confirmation of Shoshonites

Shoshonite suite lithogies which includes absarokites, shoshonites and banakites are best identified using plots of K versus SiO_2, total alkalies Na_2O+K_2O versus SiO_2 (TAS). Shoshonites also have high Ba and Sr (~>800 to 1000 ppm). They are important hosts for Cu-Au porphyry mineralisation (Müller and Groves 2016) and thus their presence within geological record has considerable prospectivity implications. Figure 11 shows the typical variation in SiO_2 and K_2O in the Grasberg, Porgera, Lihir, Tavua- Emperor and Tuvatu Cu-Au porphyry deposits.

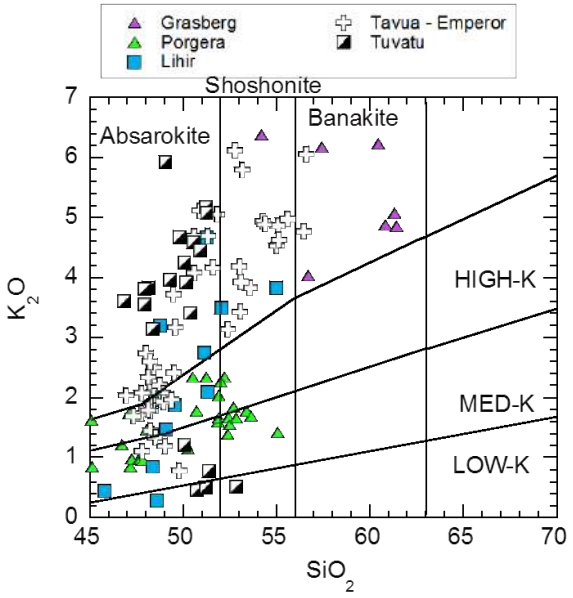

Figure 11: K_2O versus SiO_2 plot showing data for gold-bearing shoshonite suite samples from other locations in Tavua and Tuvatu Fiji, PNG and West Irian. Data source: Lihir data Muller et al. (2001), Porgera data (Richards, 1990), Grasberg data (MacDonald and Arnold, 1994).

Data for Truro alkaline basalts and Murray Basin alkaline lithologies from Foden et al., (2020) are shown in Figure 12. Both suites are clearly dominated by alkaline compositions (a) that range from Low-K to high-K and shoshonitic (absarokite) compositions. For comparison, Figure 12 c and d show data from the Koonenberry Arc from Greenfield et al, (2011). The Koonenberry arc lithologies are dominated by fractionated compositions (SiO_2) ranging from ~40 to 68 wt.% (basanite to trachyte). A substantial portion have shoshonitic compositions ranging from absarokite to banakite. The shoshonitic compositions identified in the Truro alkaline basalts, Murray Basin alkaline suite and the Koonenberry Arc are all significantly enriched in Sr and Ba.

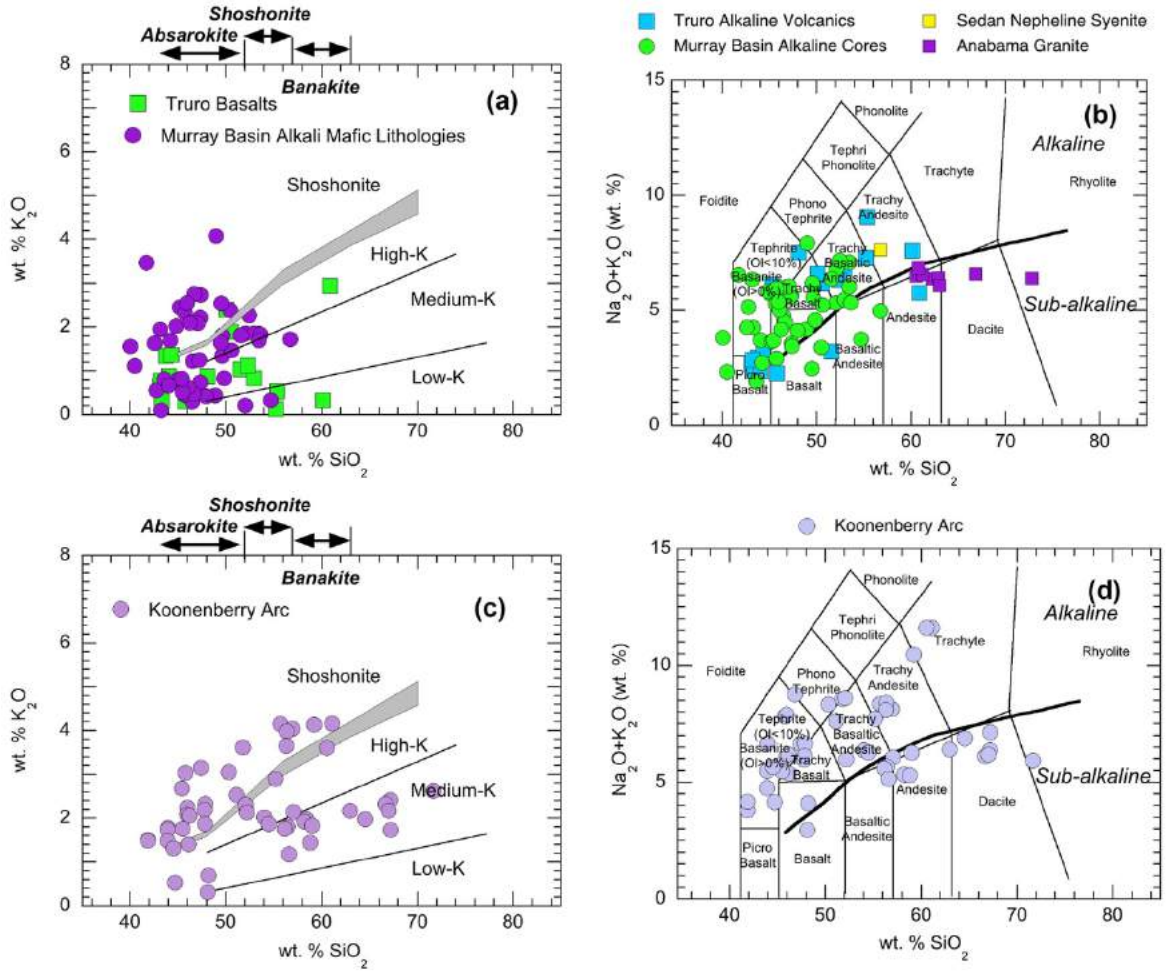

Figure 12: (a) K_2O versus SiO_2 projection of Peccerillo and Taylor (1976) showing data for Truro alkaline basalts and Murray Basin alkaline lithologies from Foden et al., (2020). (b) Truro alkaline basalts and Murray Basin alkaline lithologies plotted on TAS diagram with lithological classification after Le Maitre et al., (1989). Both suites are clearly dominated by alkaline compositions (a) that range from Low-K to high-K and shoshonitic (absarokite) compositions. (c) and (d) show data for the Koonenberry Arc from Greenfield et al, (2011). The Koonenberry arc lithologies are dominated by fractionated compositions (SiO_2) ranging from ~40 to 68 wt.% (basanite to trachyte). A substantial portion have shoshonitic compositions ranging from absarokite to banakite. The shoshonites in the Truro alkaline basalts and Murray Basin alkaline suite as well as the Koonenberry Arc are significantly enriched in Sr and Ba.

Figure 13 shows comparative data for the Neoproterozoic Boucault volcanics which yield an age of 788±6 Ma (Armistead et al., 2020). These bi-modal volcanics comprising a K-rich and a Na-rich suite are part of the Neoproterozoic Adelaide Rift and they lie at between the Burra Gp. and the underlying Callanna Gp.
By contrast the Staverly Arc in the Delamerian of Western Victoria which hosts the recently discovered

Staverly porphyry Cu-Au deposit is characterised by medium-K and low-K calc alkaline lithologies. Samples of Anabama granite a possible Delamerian porphyry system east of Burra are sub-alkaline in character (Figure 12b).

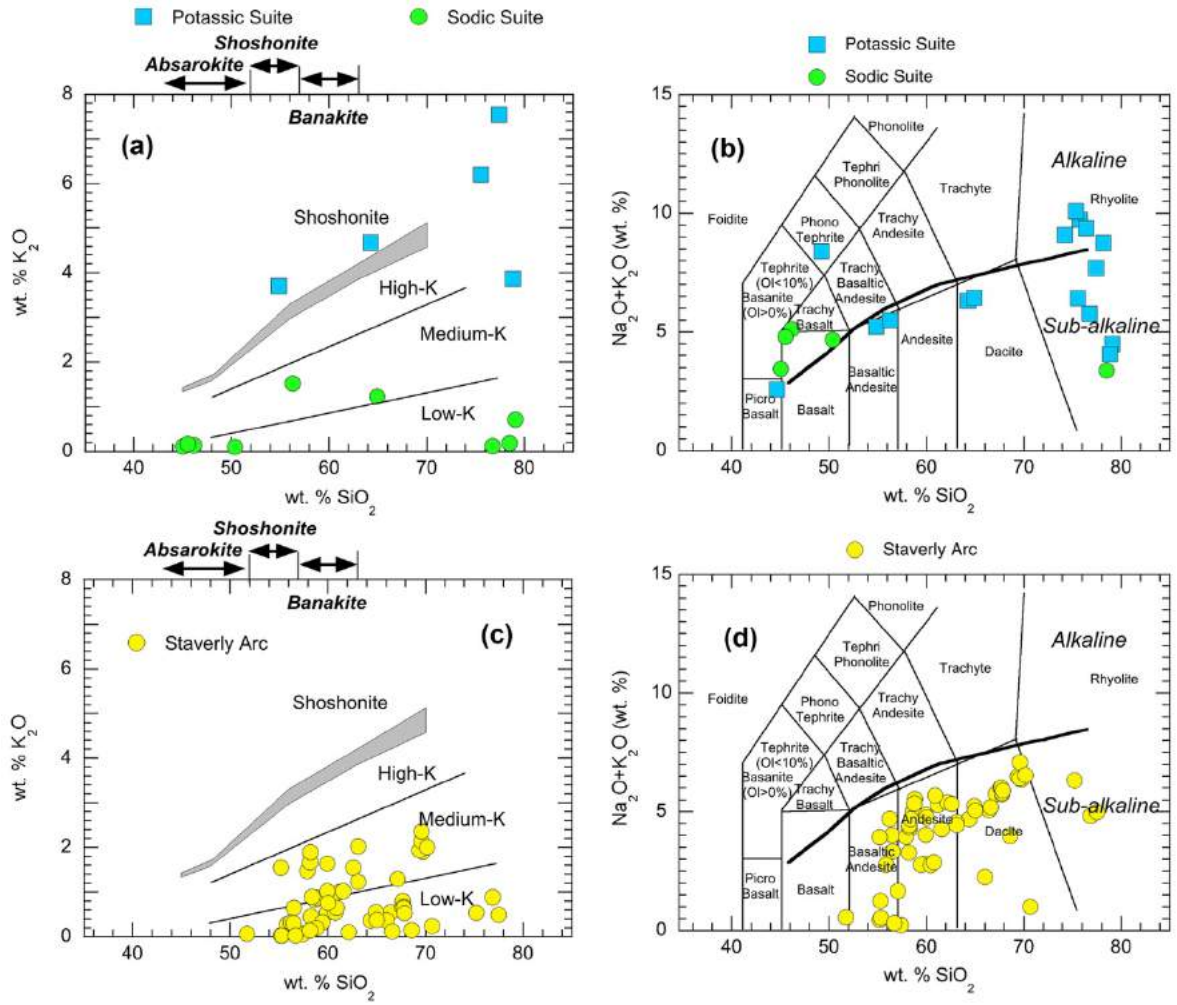

Figure 13: (a) K_2O versus SiO_2 projection of Peccerillo and Taylor (1976) showing data for Boucault volcanics from Armistead et al., (2020). (b) Data for Boucault lithologies plotted on TAS diagram with lithological classification after Le Maitre et al., (1989). Compositions define a potassic and a sodic suite. The potassic suite includes high-K and shoshonitic compositions. (c) and (d) shows data for the Staverly Arc from. This arc terrane is characterised by typical calc alkaline compositions.

Figure 14 and 15 show data for shoshonite suite lithologies from the Emperor gold mine in Fiji and the Macquarie Arc in N.S.W.. These compositional variations are very similar to those exhibited by the potassic lithologies (shoshonite suite samples) from the Delamerian Orogen. This confirms the conclusion that the buried Delamerian basement in South Australia has considerable potential for discovery of Tier One Cu-Au porphyry mineral systems. It appears that this fact has not previously been appreciated.

Geodynamic support for this conclusion is provided by the fact that the basement suite investigated by Foden et al., (2020) all fall within the postulated region of back-arc extension. This is the same tectonic environment that hosts shoshonite suites in Fiji (Collerson 2015).

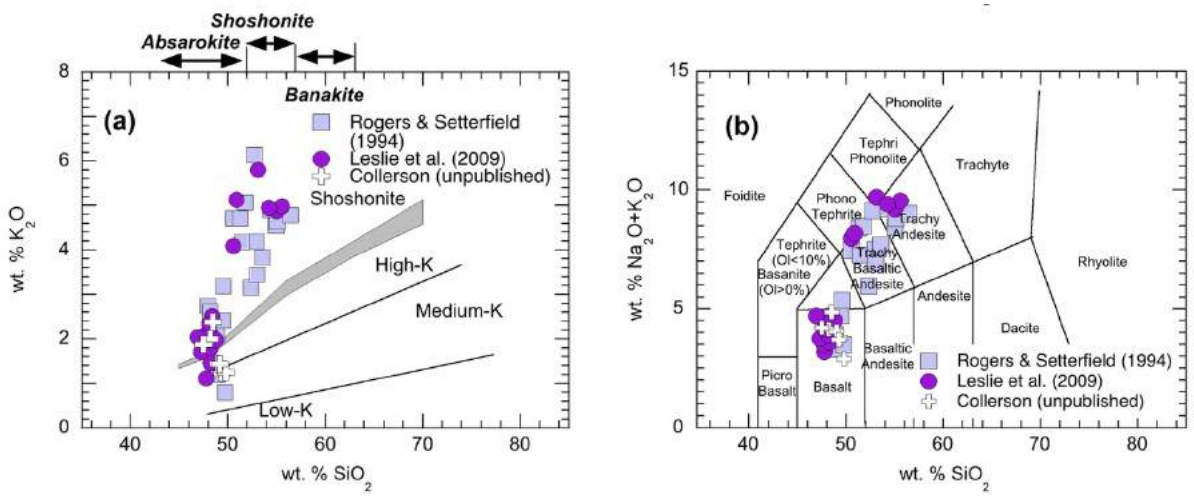

Figure 14: (a) K_2O versus SiO_2 projection of Peccerillo and Taylor (1976) and (b) TAS diagram showing data for shoshonite suite samples from Tavua (Emperor Gold Mine) Viti Levu in Fiji. Data source: Rogers and Setterfield (1994), and Leslie et al., (2009).

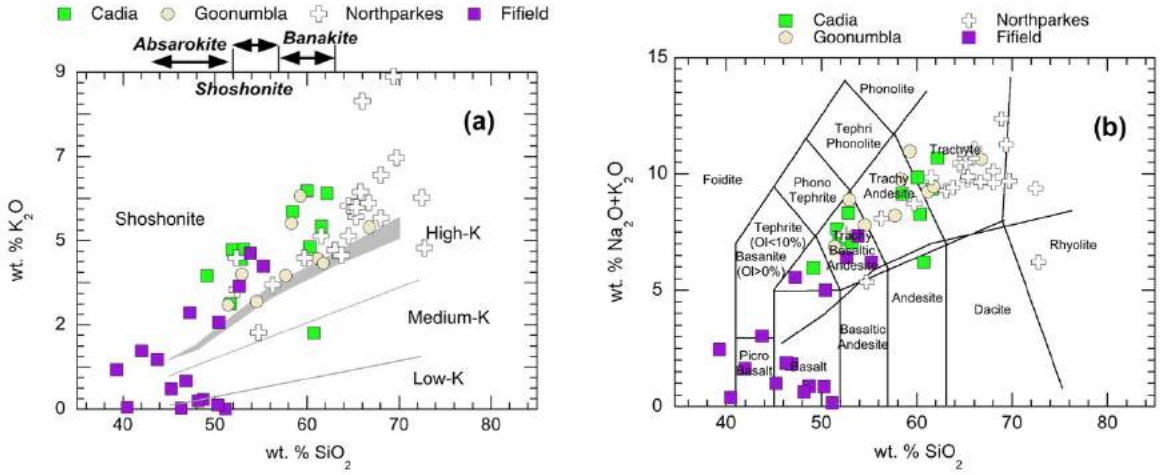

Figure 15: (a) K_2O versus SiO_2 projection of Peccerillo and Taylor (1976) and (b) TAS diagram showing data for shoshonite suite samples from Cu-Au porphyries in the Macquarie Arc NSW .

9. Chemical Geodynamic Constraints on the Delamerian Arc Magmatism

9.1 La/Nb - Nb Systematics

It is important to understand the geochemical geodynamic constraints that subducting slab structures have on the source of chemically different reservoirs and the metallogenic fertility in the mantle wedge (Rosenbaum et al., 2008 and Gianni et al., 2019). Variation between LREE/HFSE (La/Nb) ratios and Nb concentrations in basic and intermediate arc lithologies provide an assessment to be made regarding the role of mantle plume magmatism in the arc environment (Figure 16).

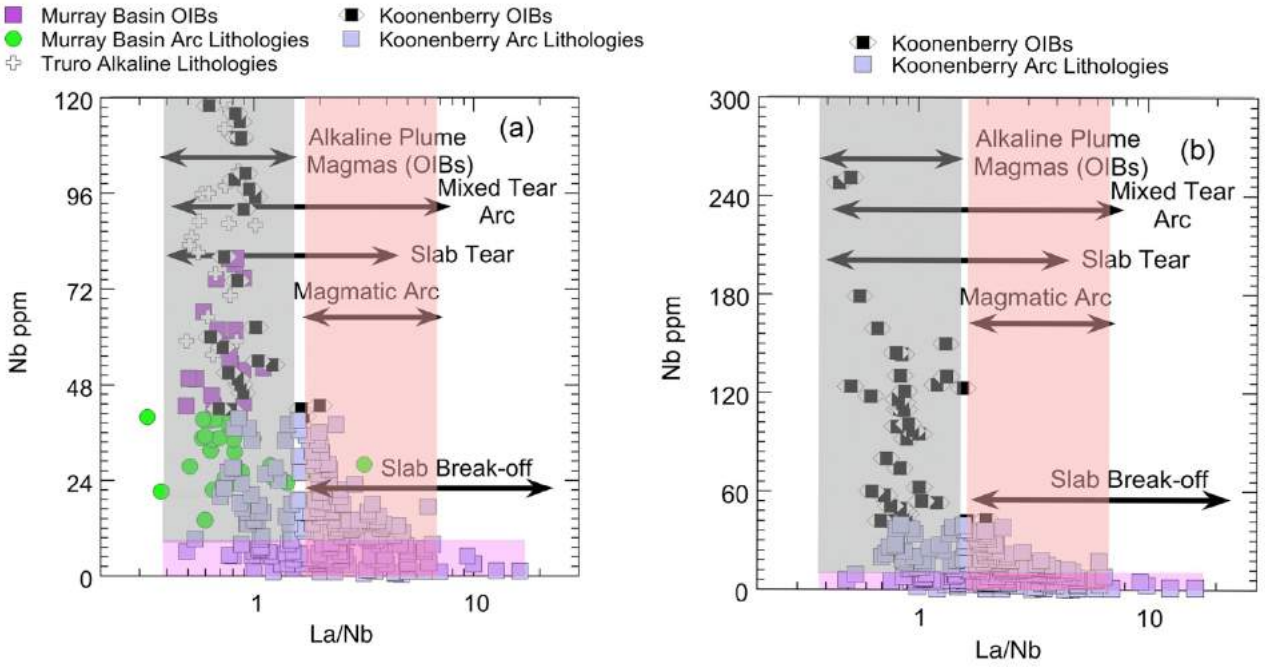

Figure 16: Covariation between Nb with La/Nb in Delamerian igneous suites from South Australian and western N.S.W. Nb-rich OIB - plume generated suites crop out at Truro and in the Koonenberry Arc. They also occur in the Murray Basin drill cores. Calc alkaline mafic arc magmatism suites also occur in the Koonenberry Arc and in the Murray Basin basement. Both the Koonenberry Arc and the Fleurieu Arc both contain shoshonitic compositions with high prospectivity potential for hosting porphyry Cu-Au mineralisation. Grey field - range of La/Nb and Nb concentrations (>16 ppm) of OIBs. Pink field - range of La/Nb and Nb concentration Arc Magmas generated in regions affected by slab break-off.

Figure 16 shows covariation between Nb with La/Nb in Delamerian igneous suites from South Australian and western N.S.W. As shown in Figure 16, these compositional variations in the source of arc magmas in the mantle wedge, are the result of slab tears that provide a conduit for rising thermochemical plumes to enter the magma genetic zone. This zone is also affected by metasomatic contributions due to dehydration of the underlying subducting plate. As a result, abundances of the lithophile elements such as K, Rb and Cs as well as the other transition elements especially Cu, are metasomatically transferred from the dehydrating slab. However, other elements such as the HFSE ratios (Zr, Nb, Ta, Hf) reflect the contribution of upwelling plume magmas through slab tears into the metasomatized mantle sources. Mantle plumes also provide heat that facilitates melting of the mantle wedge resulting in the formation of arc magmas. Thus two sources slab dehydration and mantle plumes both contribute to the metal enrichment seen in ultra-potassic arc magmatic suites such as porphyry Cu-Au deposits (Collerson et al., 2015).

The effect of mantle metasomatism is well illustrated by variations in LILE/HFSE (La/Nb) in mafic rocks (Rosenbaum et al., 2008). Low La/Nb indicate an asthenosphperic mantle source that was little affected by mantle metasomatism during slab subduction. For example, Nb enriched OIB-type magmas have characteristically low La/Nb (<2). Magmas derived from a subduction-metasomatized mantle by melting during slab break-off are characterized by high La/Nb (2 - 20). Continental arc-related magmatism is characterized by LILE/HFSE values (La/Nb > 2) in mafic-intermediate compositions and LREE/HREE ratios (La/Yb) of 20– 30.

Nb-rich OIB - plume generated suites crop out at Truro and in the Koonenberry Arc. Similar OIB compositions also occur in the Murray Basin drill cores. Some members of the Koonenberry suite are highly enriched in Nb, reflecting their strongly alkaline character.

The Koonenberry Arc and Murray Basin basement of the Fleurieu Arc also contain a suite of calc alkaline mafic arc lithologies some of which are clearly shoshonitic in character and thus have high prospectivity potential for hosting porphyry Cu-Au mineralisation

9.2 Plume Involvement in K-rich Delamerian Arc Magmatism

Figure 17a shows In primitive mantle normalised plots of Ta/U versus Nb/Th for data from the Koonenberry Arc segment of the Delamerian Orogen. This projection, from Niu and Batiza (1997) and Niu et al., (1999) shows that plume-derived magmas, formed by melting in lower mantle upwellings, plot close to unity. Whereas, magmas contamination by continental crust, crustal fluids, or fluids derived from subducted slabs, lie in the lower left-hand quadrant, with Ta/U_{PMN} of ~0.01 and Nb/Th_{PMN} of ~0.1.

The data set provided by Foden et al., (2020) lacked Ta abundances and so Ta/U_{PMN} ratios could not be calculated. However, Nb/Th_{PMN} ratios exhibited similar compositional ranges to the OIBs and shoshonite suite lithologies in the Koonenberry Belt.

Importantly, the compositional fields shown in Figure 17a are also broadly similar to the fields exhibited by shoshonite suite lithologies from Fiji (Figure 17b). The Koonenberry shoshonites have identical compositions to shoshonites from Fiji, Tavua and Monasavu which host or occur close to the Emperor epithermal gold mine on Viti Levu. Details of this Fijian association are discussed in Collerson et a., (2015)

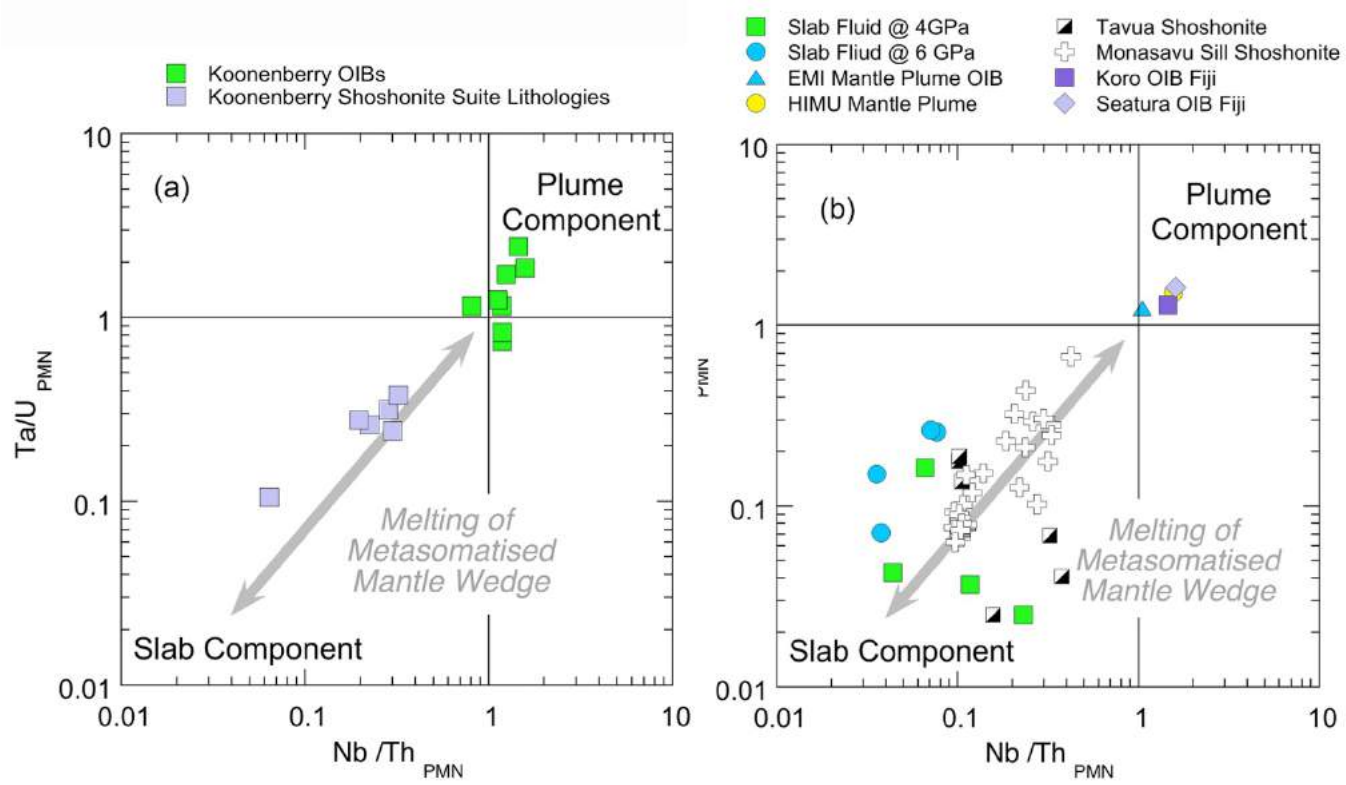

Figure 17: (a) Ta/U PMN versus Nb/Th PMN plots showing data for Koonenberry OIBs plotting in the lower mantle field while Koonenberry shoshonites plot in the field of metasomatised mantle wedge. The Koonenberry shoshonites have identical compositions to shoshonites from Fiji, Tavua and Monasavu which host or occur close to the Emperor epithermal gold mine on Viti Levu. Ta/U and Nb/Th ratios, calculated using primitive mantle values from McDonough and Sun (1995) and Lyubetskaya and Korenaga (2007),

Shoshonite suite lithologies are an important class of alkaline potassic igneous rocks that contain world class epithermal gold-silver and porphyry copper-gold deposits in many parts of the circum Pacific region (Sillitoe, 1997, 2002; Jensen and Barton, 2000). Significant gold deposits include the 2520 t Grasberg Mine in West Papua, the 1190 t Ladolam-Lihir deposit in Papua New Guinea, and the 100 t Emperor-Tavua and 14 t Tuvatu deposits in Fiji (e.g., MacDonald and Arnold, 1994; Pollard et al., 2005; Müller et al., 2001; Anderson and Eaton, 1990; Scherbarth and Spry, 2006). The giant (660 t) Porgera deposits in Papua New Guinea are also hosted by medium-to-high potassium-bearing gabbro and mafic porphyry with compositions that trend towards shoshonites (Richards, 1990; Richards and Kerrick, 1993). To understand the origin of shoshonite suite-hosted gold deposits and shoshonite magmatism in general, it is important to know the source of metals, the degree of partial melting of the sub-arc mantle, the role of element transfer into the mantle wedge during subduction and the timing of shoshonite magmatism during the life cycle of the subduction zone.

10. Regional MT, Gravity, Magnetics and Radiometrics

Images showing regional MT, magnetic, gravity, ternary radiometric, filtered elevation images for Ausmex Burra tenure are given in Figures 18 to 20, Figures 21 to 23, Figures 24 to 26, Figure 27 and Figure 28 respectively.

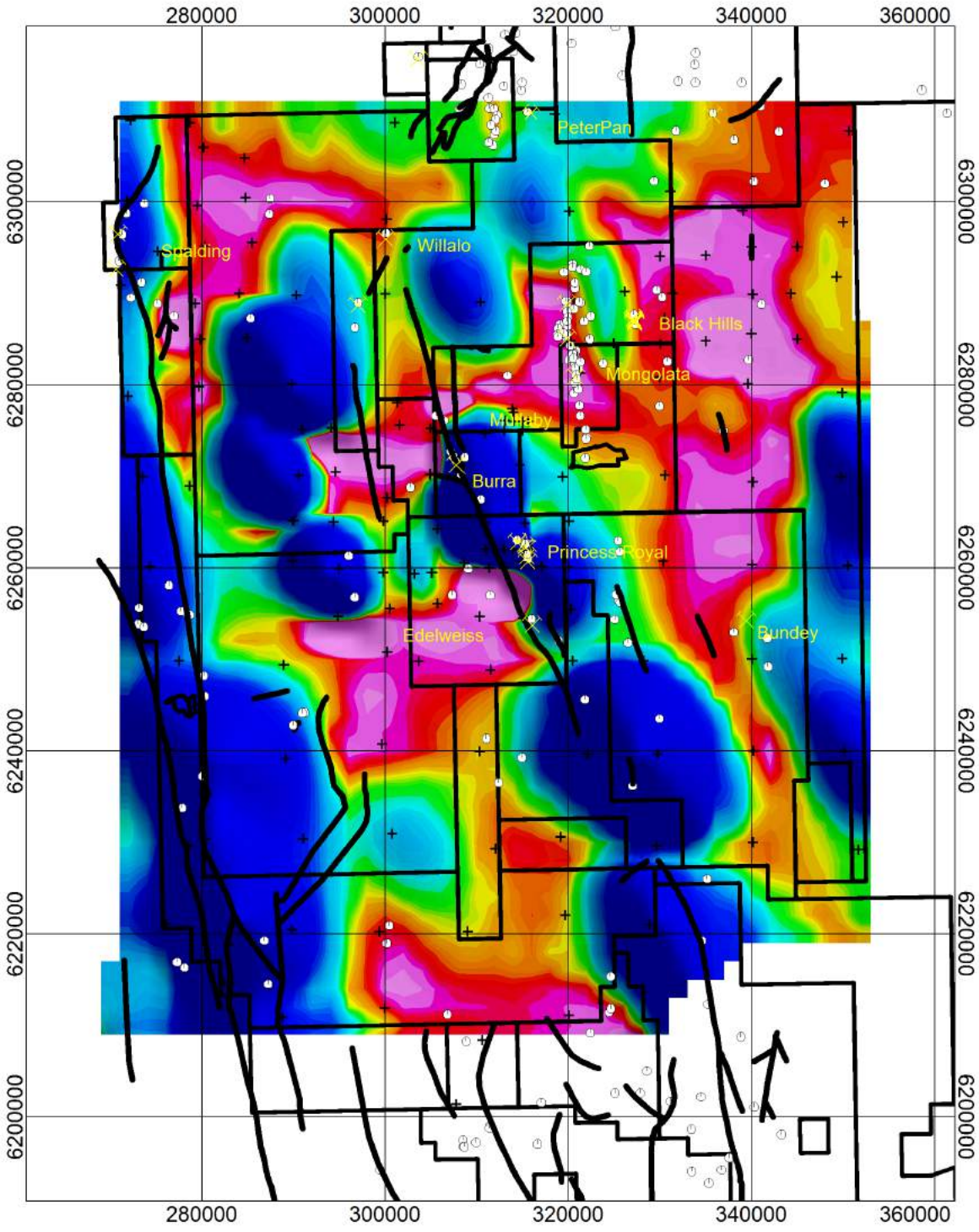

Figure 18: Regional MT Deep – Depth Slice through 3D grid at -6000m RL. Station locations shown with black crosses. Warm colours indicate higher conductivities. There is a broad region of higher conductivity in NE region with a general NW-SE trend evident. A potential crosscutting feature located to NW of Burra.

:

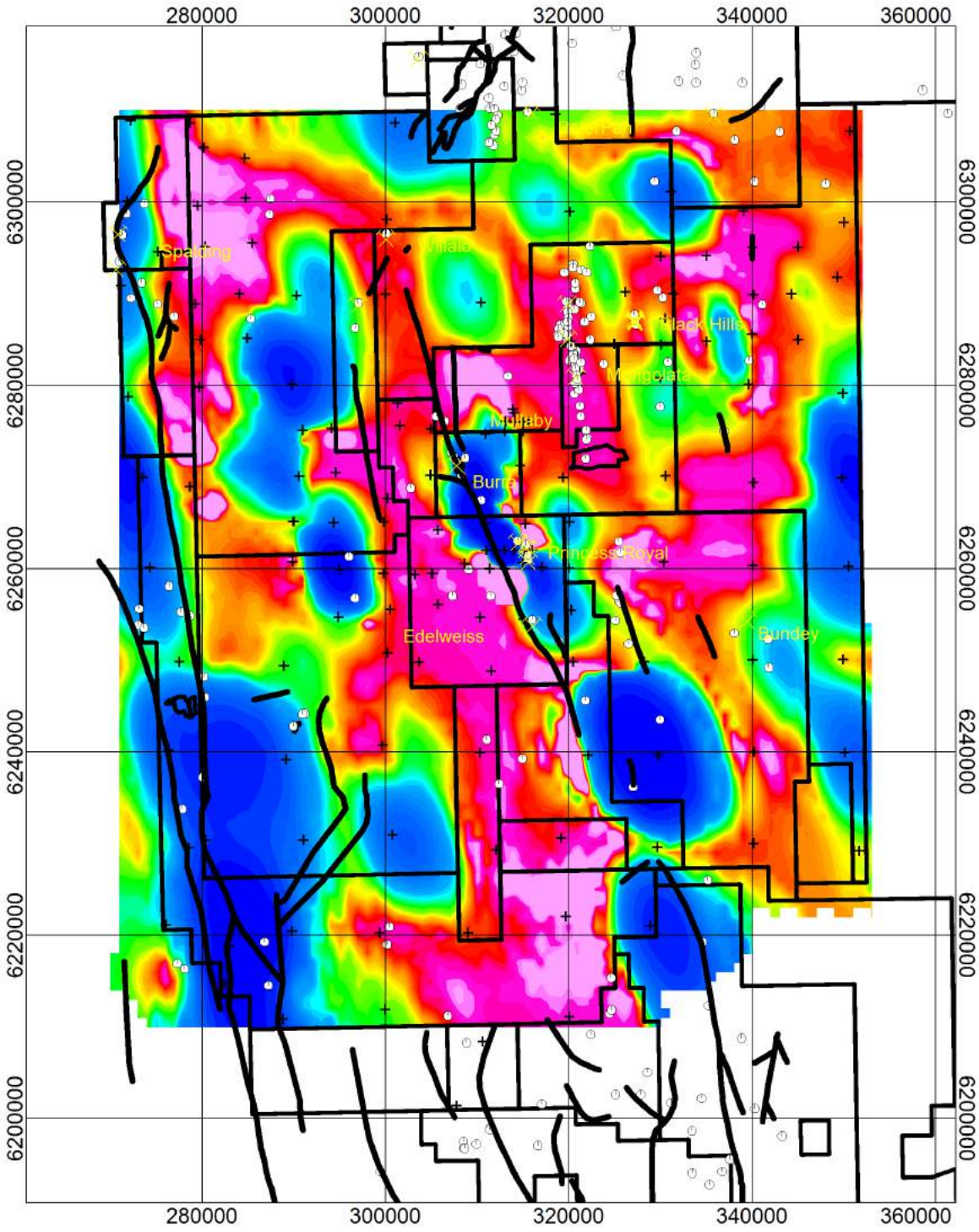

Figure 19: Regional MT - Depth Slice through 3D grid at -4000m RL. Station locations shown with black crosses. Warm colours indicate higher conductivities. The electrical structure at this depth broadly appears to reflect NW-SE trends (deep-seated faults?).

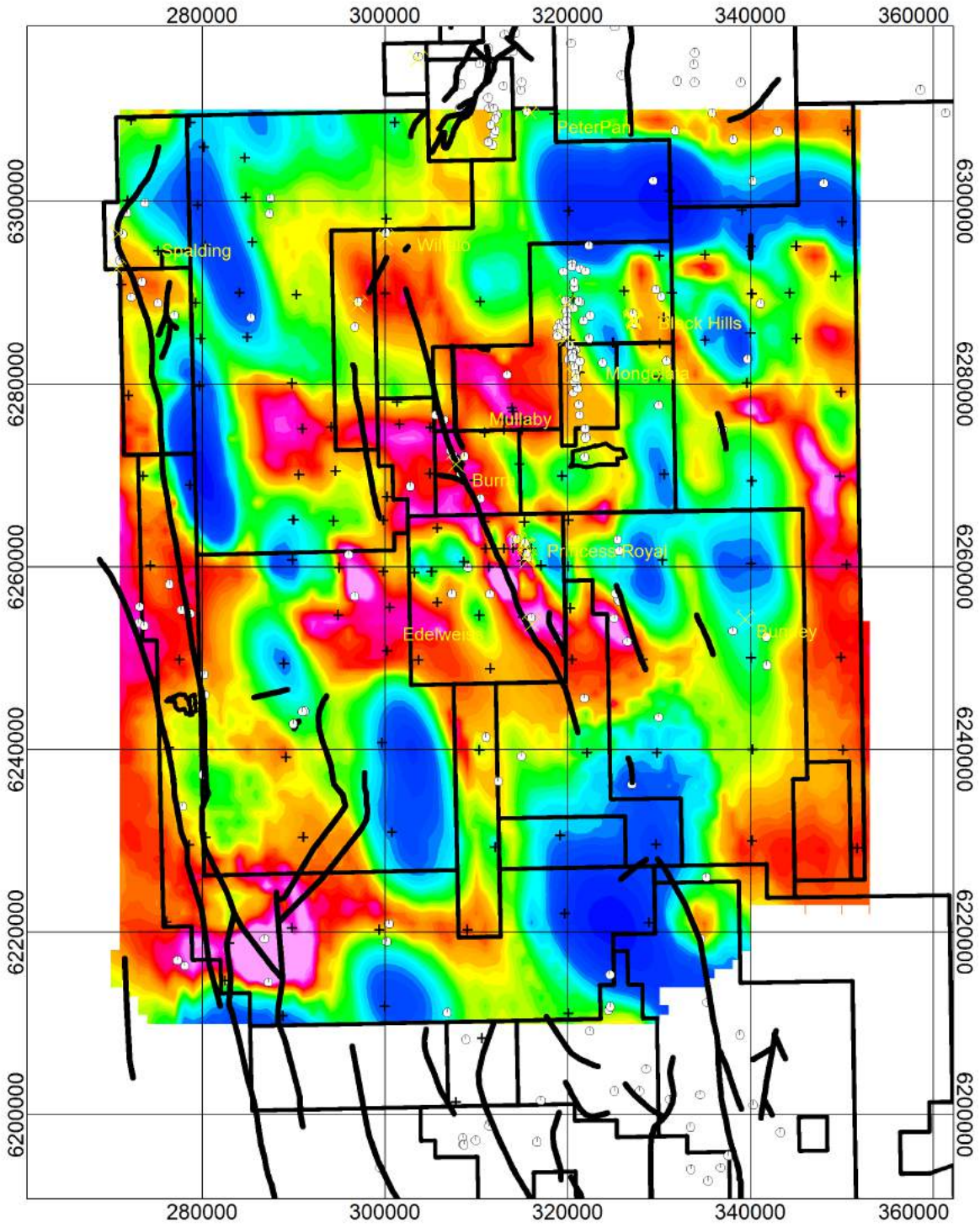

Figure 20: Regional MT Shallow – Depth Slice through 3D grid at 0m RL. Station locations shown with black crosses. Warm colours indicate higher conductivities. Regions of higher conductivity are more constrained – may reflect lithology / faults

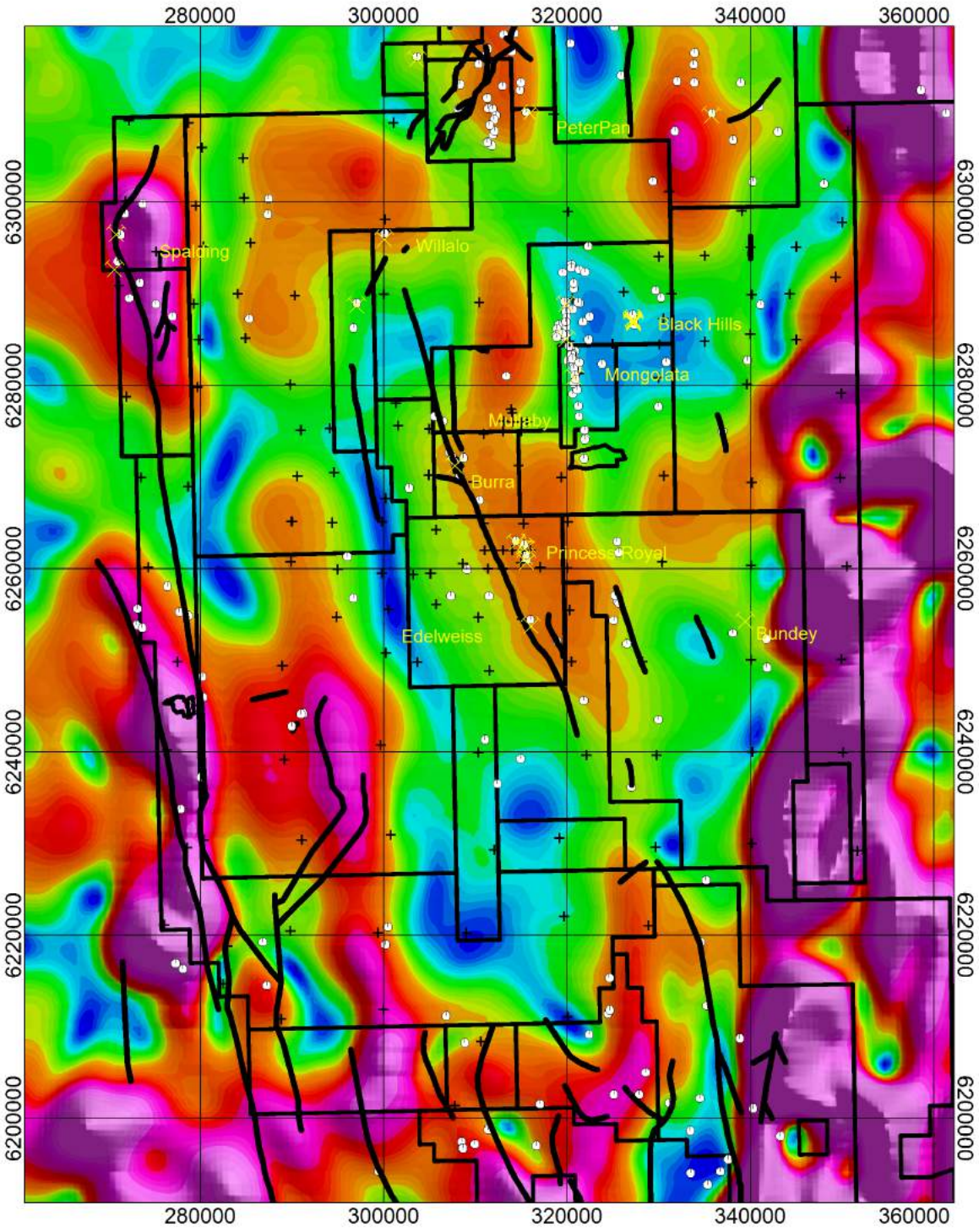

Figure 21: Depth Slice through 3D Magnetic MVI model at -4000mRL. The MVI model output reflects both induced magnetic field and remanence. Regions displaying magnetic response and coincident resistive response – possible granite / intrusions?

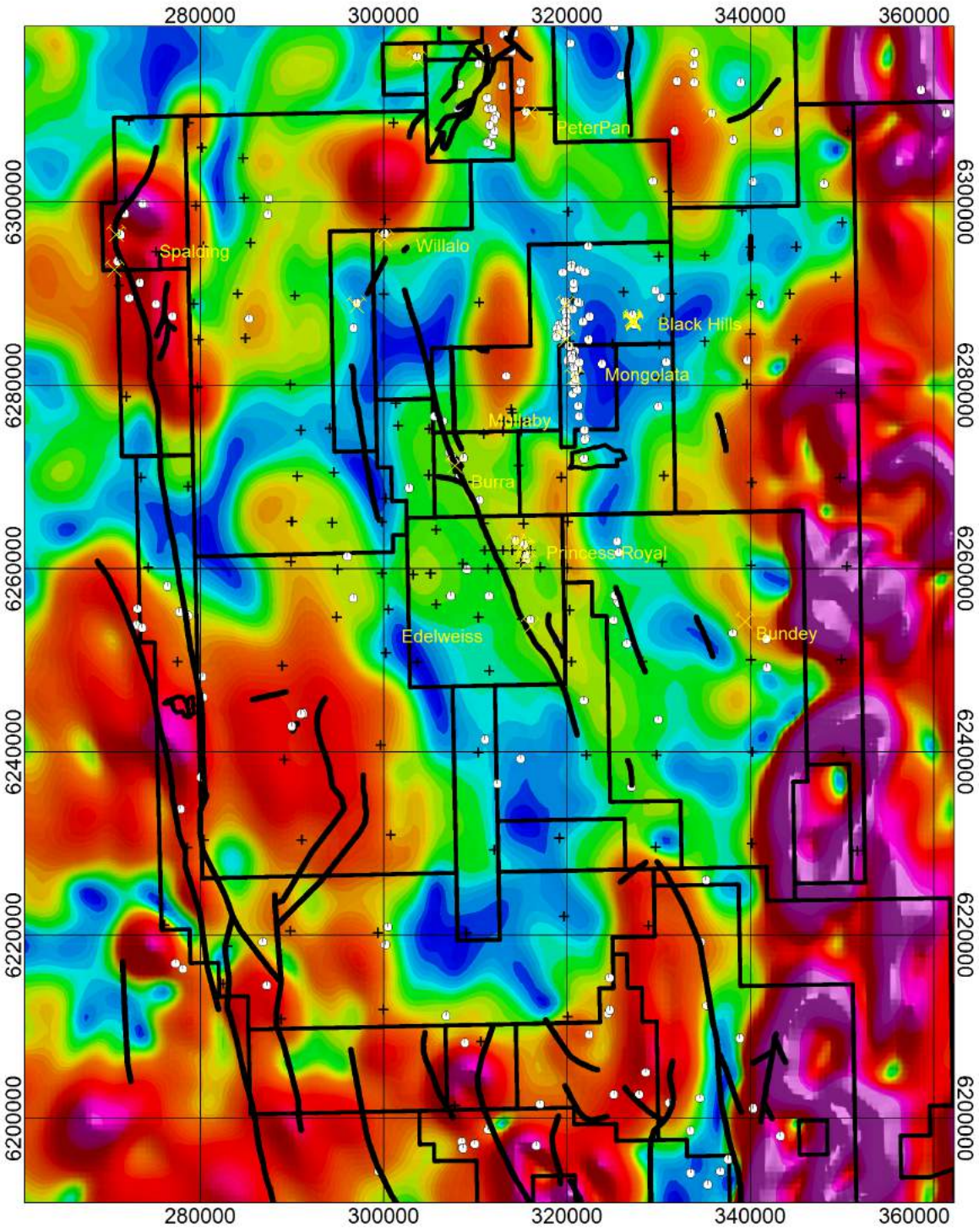

Figure 22: Depth Slice through 3D Magnetic MVI model at -2000mRL. The MVI model output reflects both induced magnetic field and remanence.

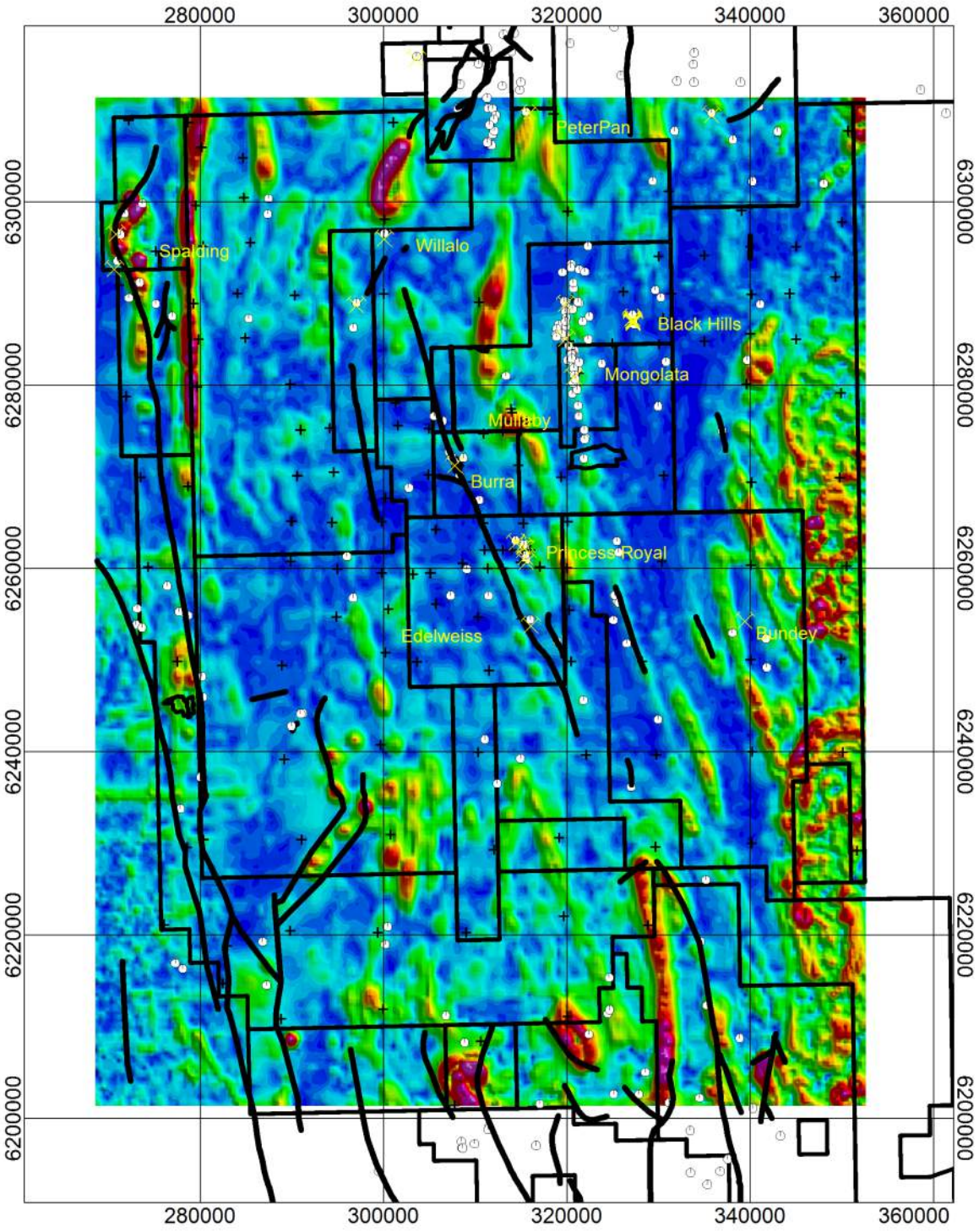

Figure 23: Depth Slice through 3D Magnetic MVI model at 0mRL. The MVI model output reflects both induced magnetic field and remanence.

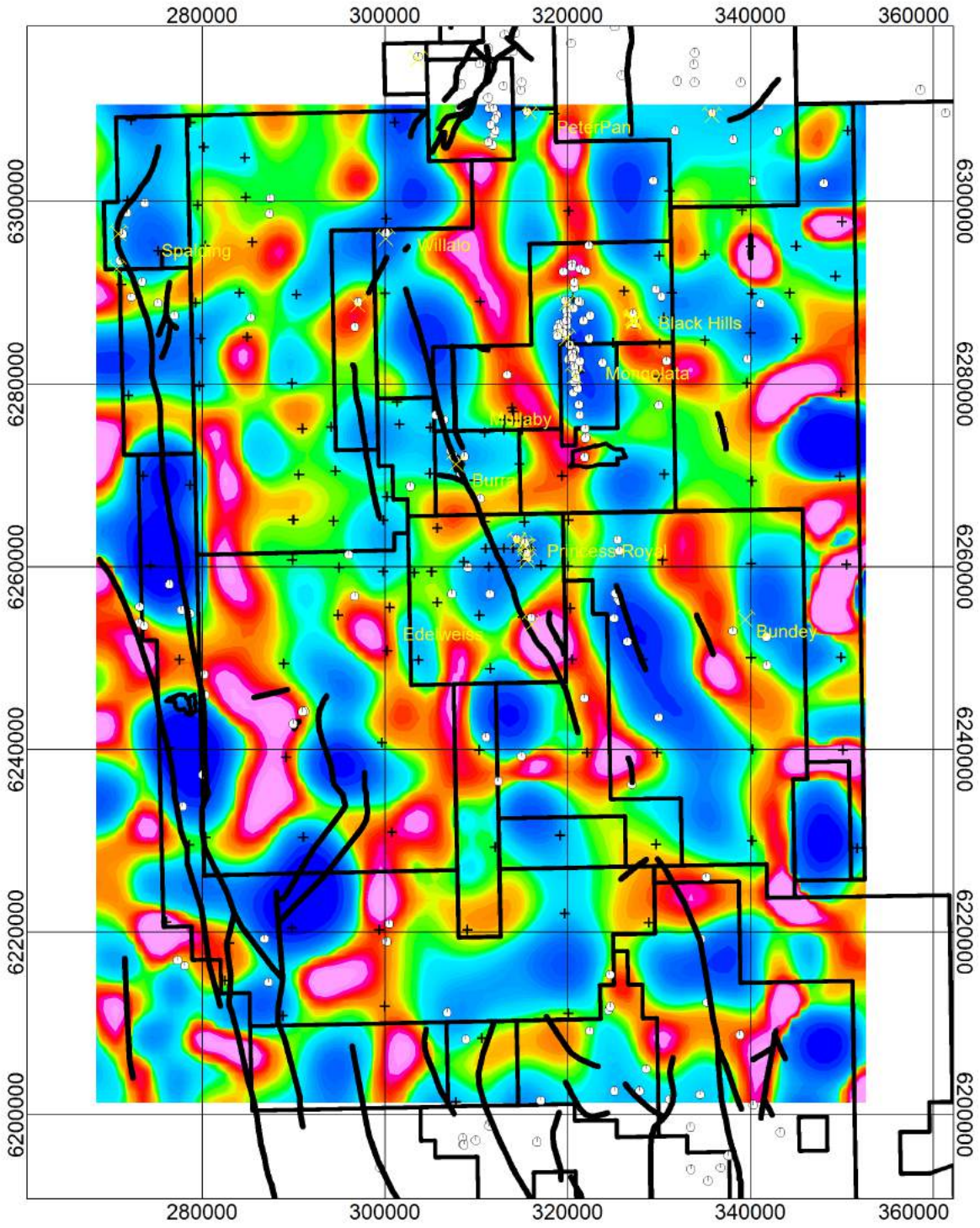

Figure 24: Depth Slice through 3D Gravity model at -4000mRL. Regional Gravity stations. Typically lower gravity responses may reflect granites / thicker sediments.

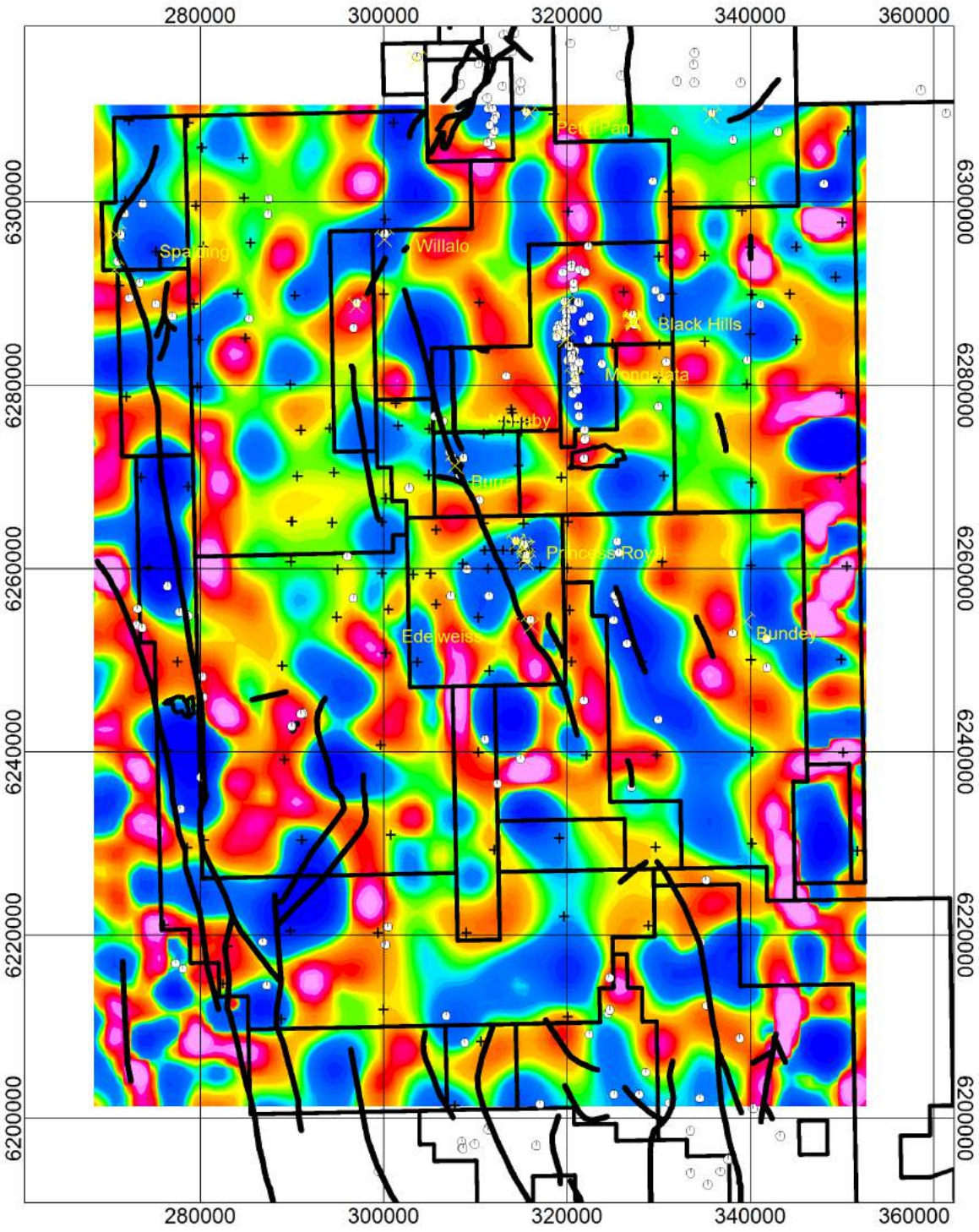

Figure 25: Depth Slice through 3D Gravity model at -2000mRL.

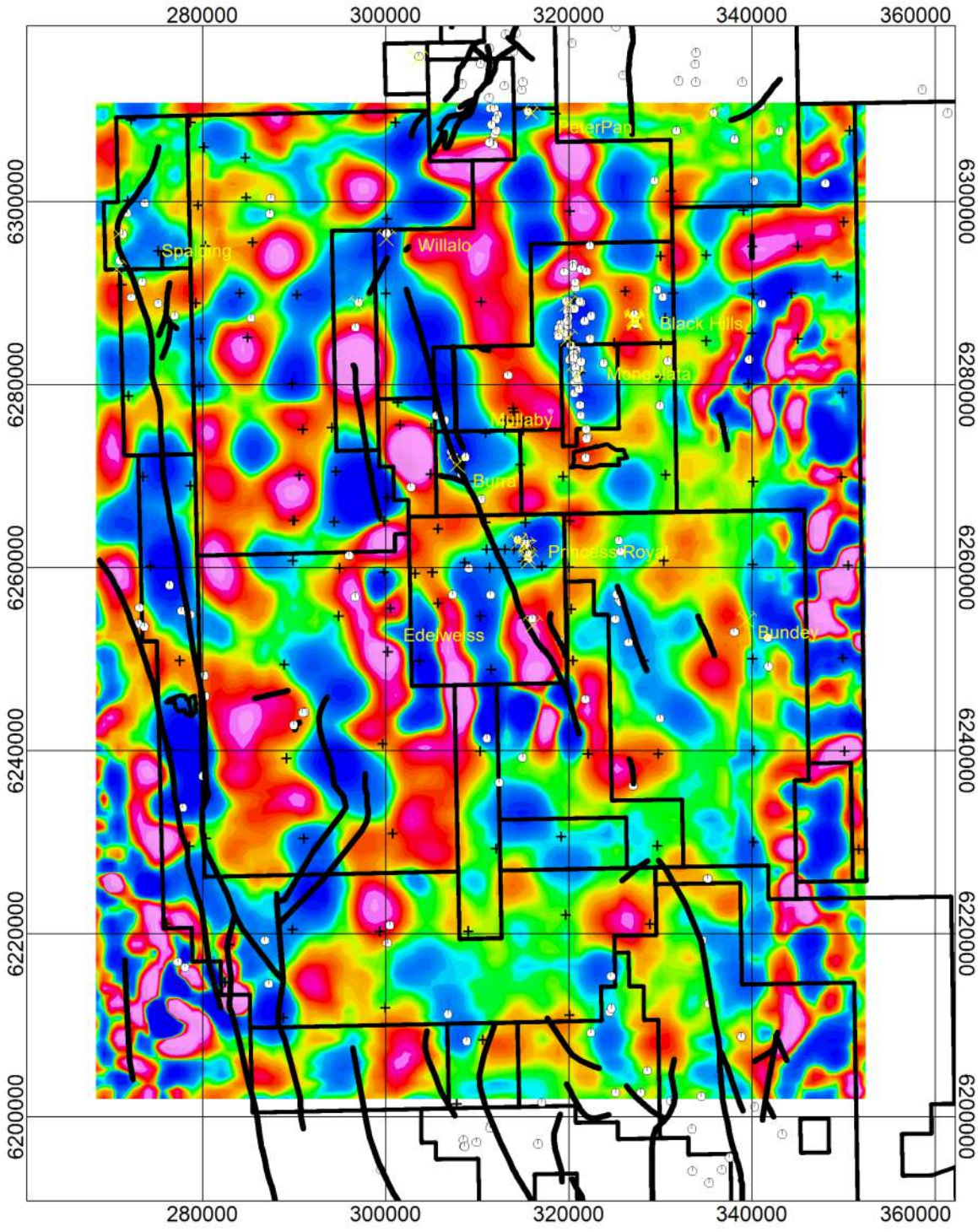

Figure 26: Depth Slice through 3D Gravity model at 0mRL.

Figure 27: Ternary Radiometrics

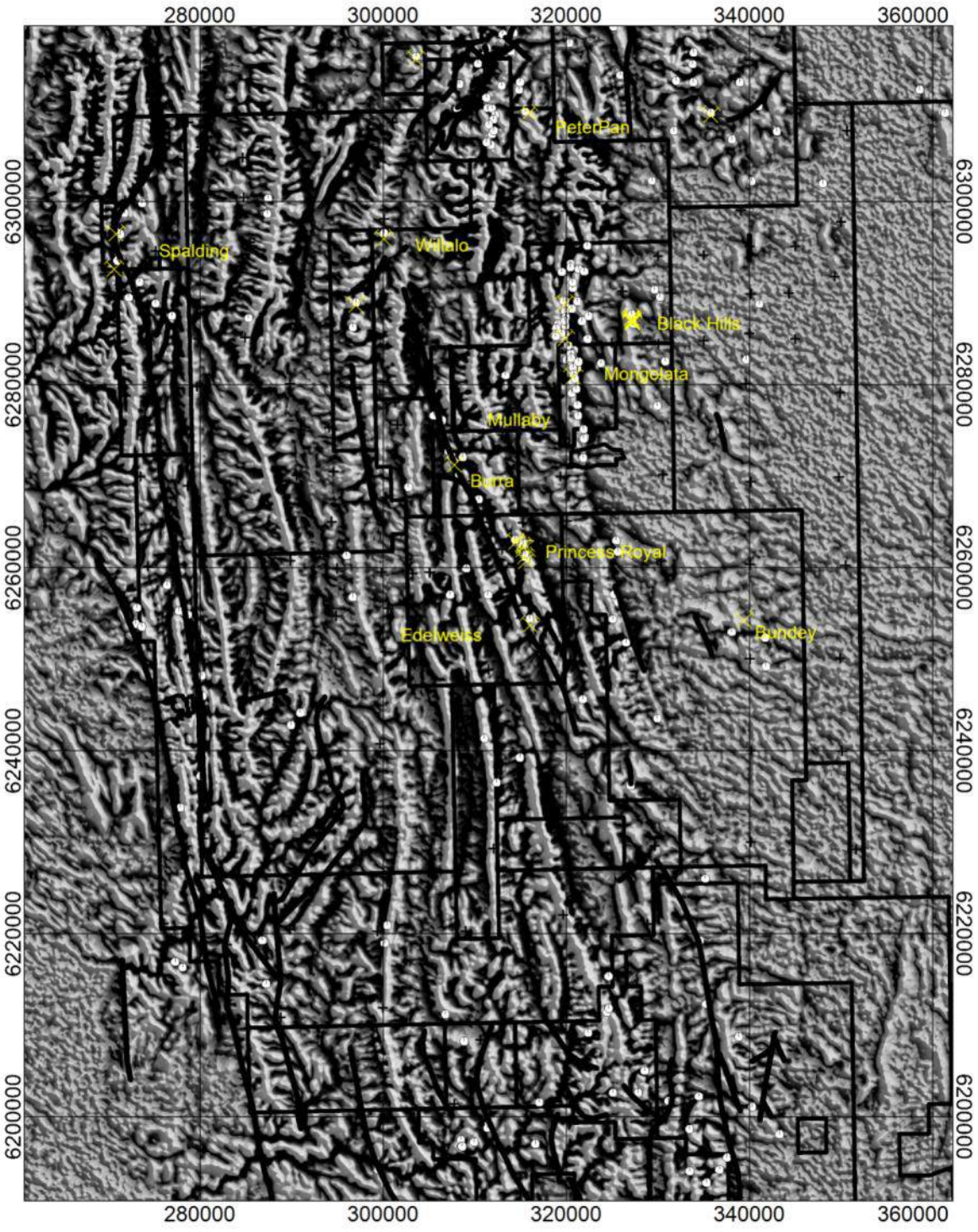

Figure 28: Filtered Elevation Product – showing that pronounced terrane contrast east of the Kingstone Fault near Princess Royal. This structureless region is underlain by Delamerian intrusions apparently surrounded by of epithermal alteration zones that extend as far as Mongolata and Black Hills.

11. Sampling Additional Basement Cores Close to AusMex Burra Tenements

Table 2 lists drill holes that intersected plutonic lithologies in the magmatic terrane that lies to the east of Tombola's tenure. A number of these intersected magnetic highs or demagnetised lows in the magmatic terrane. Locations of these drill holes are shown in Figures 29 to 32. Depths to basement range from 9 to 205 m.

It is recommended that samples from these drill holes are inspected and that litho-geochemical samples are collected for petrology and major and trace element analysis. The use of an Olympus Vanta p-xrf to document vector element abundances e.g., Cu, Zn, Y, Se, Bi, Ni etc would facilitate this exercise to identify the sweet spot. i.e. the shoshonite suite intrusions. This will provide information critical for vectoring to mineralisation, as well as providing a sound data set to allow better understanding of the prospectivity of each of the intrusions.

Table 2: Cores to basement east of Burra

DH Name	Hole ID	Long.	Lat.	Depth	From	To	Lithology
Bendigo							
81MBR 43	77550	139.4435	-33.3262	124.5	123.6	124.5	Silt, light red, clayey, & sand, coarse-granular, quartzose, angular; hard basement ?granite.
81MBR 42	77549	139.4752	-33.3374	101	94	101	Sand, green, fine-coarse, angular, over granite, green, micaceous, hard.
BM 72	77561	139.4505	-33.2328	79.25	30.48	79.25	Granite, completely weathered, white-yellow.
BM 76	77565	139.4652	-33.2308	28.35	7.62	28.35	Biotite-granite, completely weathered, white-yellow.
CRN 51	137127	139.4622	-33.2507	17	4	17	Granite, quartz-felspar-plagioclase-biotite-hornblende, mainly weathered to sand above 14m, becoming harder & fresher with depth.
CRN 100	137176	139.3994	-33.3769	106	102	106	Weathered granite; clay, light brown-yellow/brown, gritty with angular fragments of quartz, felspar, grey siltstone & weathered ?granite or ?gneiss.
CRN 115	137191	139.4914	-33.3568	90.5	59.8	90.5	Granite, green, medium grained quartz-pelspar-biotite+/-fine black mafic minerals, weathered upwards & mainly decomposed to whitish mottled gritty clay above 76m.
CRN 52	13712	139.437	-33.2454	55	28	55	Granite, mainly weathered, mainly weathered to clay above 44m, becoming fresher with depth.
CRN 52	13712	139.437	-33.2454	55	18	28	Clay, brown-olive green with biotite & occasional gravel of greisen fragments, ?weathered granite.
BM 77	77566	139.465	-33.2354	41.76	9.14	41.76	Biotite-granite, completely weathered, white-yellow.
MUR 15	137206	139.5228	-33.3589	127.5	47	127.5	Granite, weathered, fine grains of clear quartz, pink felspar, minor black mafics, becoming harder with depth, completely weathered to gritty off white-grey clay above 84m.
CRN 49	13712	139.4511	-33.2499	56.5	12	56.5	Clay, weathered granite, quartz grains & felspars, occasional opaques, becoming harder & fresher in bottom 4m.
CRN 50	137126	139.4561	-33.2511	73	48	73	Clay & weathered basement ?altered granite, grains of quartz, biotite, chloritised plagioclase; bottom 1m is fine grained quartz-muscovite-greisen.
CRN 50	13712	139.4561	-33.2511	73	16	48	Clay, mainly sandy with grains of quartz, felspar & biotite.
CRN 97	137173	139.4778	-33.2601	62.5	18	62.5	Granite, quartz-plagioclase-hornblende-biotite, highly weathered & mainly decomposed to clay above 48m, becoming fresher with depth, mylonitic & albitised 48-52m.
CRN 103	137179	139.4271	-33.3609	127	100	122	Clay, pale grey-white-buff, with remnant granitic texture & fragments of weathered or altered granite, botryoidal calc-silicate, & granite mylonite at 118m.
PAAC 9	18500	139.4954	-33.3363	131	130	131	Diorite, coarse grained, light grey.
PAAC 9	18500	139.4954	-33.3363	131	66	130	Saprolite, grading to saprock from 114m, dark red/brown-orange-grey.
KR 4	77606	139.4657	-33.2505	39.5	3	39.5	Granite, highly weathered to partly weathered at depth, fragments of fine-medium grained quartz-biotite granite in grey-white powdery clay matrix.
MUR 14	137205	139.528	-33.3591	91.5	60.5	91.5	Clay, gritty fine-medium quartz & fragments of ?sandstone or ?basic intrusive; towards bottom silicate rock, olive green ?basic intrusive.
KR 5	77607	139.4496	-33.2506	57	12	57	Granite, partly weathered at bottom, highly weathered towards top, with quartz, chloritised mica & biotite in clay matrix.
KR 15	77610	139.4498	-33.2914	87	53	87	Clay, powdery, pink/brown, containing fine-coarse broken quartz grains, with chloritised mica increasing with depth.
CRN 95	13717	139.4706	-33.2584	9	2	9	Granite, quartz-biotite-felspar, weathered, slightly gneissic & foliated.
KR 21	77603	139.4659	-33.2912	28	12	28	Granite, highly to partly weathered.
BM 70	77554	139.451	-33.2244	76.81	27.43	76.81	Biotite-granite, completely weathered, white-yellow.
KR 23	77604	139.4657	-33.2773	52.5	15	52.5	Completely to partly weathered biotite-granite; clay, whitish towards top, becoming green/grey with depth, containing fine-coarse quartz grains & chloritised biotite; white kaolin 18.25-30m.
KR 1	77609	139.4499	-33.2776	48	38	48	Completely to highly weathered granite.
KR 1	77609	139.4499	-33.2776	48	34.5	38	White clay, sparse green mottling, ?completely weathered granite.
KR 10	77615	139.434	-33.2779	49	19	49	Granite, highly weathered towards top, fine-medium quartz fragments in white-yellow powdery clay, becoming fresher with depth.

CRN 25	13710	139.4405	-33.3234	119.5	88	119.5	Weathered granite; clay, silty & sandy, in part shows relict interlocking grain structure & gneissic texture, pale grey-off white.
PAAC 11	185006	139.4971	-33.3351	110	109	110	Granite-monzogranite, fine grained, light grey-white, fresh.
PAAC 11	185006	139.4971	-33.3351	110	72	109	Saprolite, white-red-grey.
BM 74	77563	139.4599	-33.2196	28.35	5.49	28.35	Biotite-granite, weathered, white-yellow.
BM 73	77558	139.4488	-33.2367	51.51	13.72	51.51	Biotite-granite, completely weathered, white-yellow.
KR 20	77602	139.466	-33.3046	90.5	72	90.5	Weathered granite; olive-green powdery clay containing medium quartz fragments & greenish chloritised mica, fresh biotite at depth.
KR 20	77602	139.466	-33.3046	90.5	51	72	Clay, dark brown, containing fine-medium quartz fragments & minor fine opaques, ?highly weathered granite.
CRN 111	137187	139.4616	-33.3336	107.5	64	107.5	Granite, dark green/grey, medium grained, fresh & hard at bottom, intergrown felsic & mafic minerals, minor biotite, rare quartz, weathered upwards & mainly white-khaki clay above 98m.
CRN 113	137189	139.4803	-33.4002	111.5	78	111.5	Granite? or quartz-rich intrusive, fine-medium grained, quartz-weathered felspar-muscovite, trace black minerals, commonly weathered to gritty & felspathic clay, white, red/green mottled.
K 231	15672	139.423	-33.3433	132	98	132	?Highly weathered granite; quartz sand, red clay, some magnetite.
KR 11	77618	139.4172	-33.278	78	72	78	Clay, light grey-dark grey, abundant weathered micas & coarse rough-edged quartz grains; ?weathered granite.
BH 4	77466	139.4531	-33.2059	83.52	0	83.52	Biotite-granite, pale grey-pink, minor green sericite alteration, minor disseminated pyrite, rare chalcopyrite, rare quartz-limonite veins.
CRN 24	137100	139.4287	-33.322	117	76	117	Sand of quartz grains & muscovite, clayey towards top, grading down to granite, quartz-felspar-muscovite-biotite +/- hornblende, green fresh hard at botom.
CRN 87	13716	139.4482	-33.2109	36	16	36	Granite, quartz-felspar-biotite, weathered, occasional hematite & limonite, clayey above 24m.
PAAC 12	18500	139.4978	-33.3345	99	69	99	Saprolite, weathered felsic rock, white-light grey.
KR 9	77605	139.4656	-33.2638	27	1.5	27	Granite, weathered to partly weathered.
KR 14	77614	139.4342	-33.2916	47	18.5	47	Granite, highly to partly weathered.
CRN 53	13712	139.4283	-33.2447	73.5	34	73.5	Granite, quartz-plagioclase-biotite-hornblende, weathered throughout, mainly weathered to clay above 52m.
BM 78	77567	139.4648	-33.2407	32	12.19	32	Granite, completely weathered, white-yellow.
CRN 23	13709	139.4186	-33.3206	109	98	109	Sand of quartz grains & biotite, clayey towards top & grading downwards to fresh granite, quartz-felspar-biotite showing faint
KR 16	77620	139.4178	-33.3053	29.5	11	29.5	Biotite-granite, weathered to partly weathered.
CRN 48	13712	139.4409	-33.2468	78	68	78	Weathered granite, clayey, angular quartz & felspar, becoming fresher at bottom with plagioclase hornblende biotite epidote.
CRN 48	13712	139.4409	-33.2468	78	32	68	Clay, white-brown-pale olive, sandy with angular quartz & weathered felspars, occasional coarse dark grey metallic mineral.
PAAC 13	185008	139.5062	-33.3457	143	138	143	Diorite, biotite rich, grey-green, fresh.
PAAC 13	185008	139.5062	-33.3457	143	107	138	Saprolite, grading in part to felsic & mafic saprock, white-black-grey.
MUR 16	13720	139.5121	-33.3579	103.5	76.5	103.5	Clay, white-brown-yellow-grey-purple, common grit of quartz, mafic minerals, felspar, might be two distinc granitic lithologies.
BM 75	77564	139.4631	-33.2261	73.15	6.1	73.15	Biotite-granite, completely weathered, white-yellow.
KR 13	77619	139.4172	-33.2919	91.5	84	91.5	Clay, grey, powdery, containing numerous fine-medium quartz grains & minor mica; ?highly weathered granite.
PAAC 10	185005	139.4962	-33.3356	123	115	123	Diorite & felsic intrusive, grey-green-white.
PAAC 10	185005	139.4962	-33.3356	123	69	115	Saprolite, red-purple-grey-green.
BM 69	77553	139.4514	-33.2184	76.81	27.43	76.81	Biotite-granite, completely weathered, white-yellow.
KR 8	77608	139.4496	-33.264	71	56	71	Granite, highly weathered at top, fine-medium quartz & chloritised biotite in light grey clay matrix, becoming less weathered with depth.
K 236	15672	139.438	-33.2865	10	2	10	Hornblende-biotite-granite.
PAAC 8	18500	139.4946	-33.3368	111	87	111	Mafic intrusive, light grey/green.

PAAC 8	18500	139.4946	-33.3368	111	57	87	Saprolite, dark red/grey.
PAAC 15	18501 0	139.508	-33.3447	115	104	115	Mafic intrusive rock tending to monzodiorite, grey-green.
PAAC 15	18501 0	139.508	-33.3447	115	103	104	Saprolite, olive-grey.
PAAC 14	18500 9	139.5071	-33.3452	126	118	126	Mafic intrusive rock, dioritic, coarse grained, grey-black.
PAAC 14	18500 9	139.5071	-33.3452	126	110	118	Mafic saprolite, becoming harder with depth, olive-yellow-brown.
PAAC 6	18500	139.493	-33.3379	119	116	119	Gabbro, medium grained, weathered, chloritic alteration.
PAAC 6	18500	139.493	-33.3379	119	48	116	Mafic saprolite, brown-olive-pink-grey.
PAAC 20	18501	139.4428	-33.351	125	124.5	125	Gabbro, coarse grained, green-grey.
PAAC 7	18500	139.4937	-33.3373	90	48	90	Mafic saprolite, brown-red-pink.
82FN5RM	87125	139.5285	-33.3704	57.3	44	57.3	Gabbro, dark green, massive, medium-coarse grained, altered, 5-7% Ti-magnetite altered to leucoxene.
82FN5RM	87125	139.5285	-33.3704	57.3	28	44	Clay, green-brown, silty, very micaceous ?phlogopite, minor epidote; weathered mafic rock.
CRN 112	13718 8	139.4684	-33.3393	135	121	135	?Diorite, dark green, 70% weathered mafic minerals, 30% white-pale green weathered felspar, minor biotite & quartz, decomposed to gritty clay in top 1m, fresh & hard at bottom.
K 301	15672 6	139.406	-33.364	137	96	137	Diorite (or andesine gabbro), dark greey/green, fine grained, micaceous, minor carbonate & chlorite, mainly weathered to clay in top 6m.
East of Burra							
SR 3	77457	139.3691	-33.6791	117	116	117	Biotite granite, fresh-slightly weathered, green.
SR 6	77460	139.3559	-33.6699	159.25	132	159.25	Biotite-granite, weathered to partly weathered, mainly decomposed to pink clay with quartz grains & biotite above 142m.
SR 6	77460	139.3559	-33.6699	159.25	106	132	Medium-coarse quartz grains & opaques in a pink clay matrix; ?"granitic detritus".
SR 4	77458	139.3727	-33.6881	128.85	128	128.85	Granite, weathered to partly weathered, & clay.
TG 16	77451	139.3718	-33.7959	85.25	84	85.25	Hornblende diorite, dark green-black. (Petrology).
PADD 36	18502	139.3482	-33.8336	174.5	160.8	174.5	Gabbro, sericite-carbonate alteration, trace pyrite-chalcopyrite, grey-yellow-white.
PADD 36	18502	139.3482	-33.8336	174.5	154	160.8	Saprolite, ?weathered gabbro, grey-green.
East of							
83FS34R M 1	77125	139.4047	-34.1559	94.9	88	94.9	Diorite; plagioclase-biotite-hornblende+/-garnet-apatite-magnetite, trace disseminated sulphides; completely weathered to clay in top 6m.
83FS14R	77124	139.3394	-34.0122	69.7	67.7	69.7	Granite; quartz-orthoclase-plagioclase-biotite-magnetite, orange-white, fresh.
PADD 22	18502	139.4492	-33.9512	198.4	161.8	198.4	Mixed igneous intrusives: gabbro, undifferentiated mafics, granitoid, monzodiorite, griesen, some Kspar-chlorite alteration.
M117	77407	139.3554	-33.9708	121.5	103	121.5	Blebs of white soft clay with fragments of biotite-hornblende granite from 118m.
PADD 20	18621	139.3918	-34.0366	204.5	171.2	204.5	Variably layered felsic to mafic intrusives, mainly diorite/granodiorite, lesser gabbro, granite, several thin aplite dykes.
PADD 20	18621	139.3918	-34.0366	204.5	168	171.2	Saprolite, ?weathered gabbro, brown-grey.
PADD 17	18621	139.3234	-34.1348	150.7	116.25	150.7	Gabbro, plagioclase-biotite-amphibole-quartz, minor dolerite, trace pyrite/pyrrhotite, banded in part, grey, minor green.
PADD 17	18621	139.3234	-34.1348	150.7	108	116.25	Saprolite, weathered mafic rock, olive-brown-green.
82MP 1	86642	139.5613	-34.033	244	231	244	Gabbro, medium grained, green-dark green, altered, accessory magnetite, no sulphides, completely altered to chloritic clay in top 3m.
PADD 19	18621	139.3099	-34.1029	114.5	96.3	114.5	Gabbro/norite, plagioclase-pyroxene-hornblende-biotite.
PADD 19	18621	139.3099	-34.1029	114.5	93	96.3	Saprolite, weathered gabbro, green.

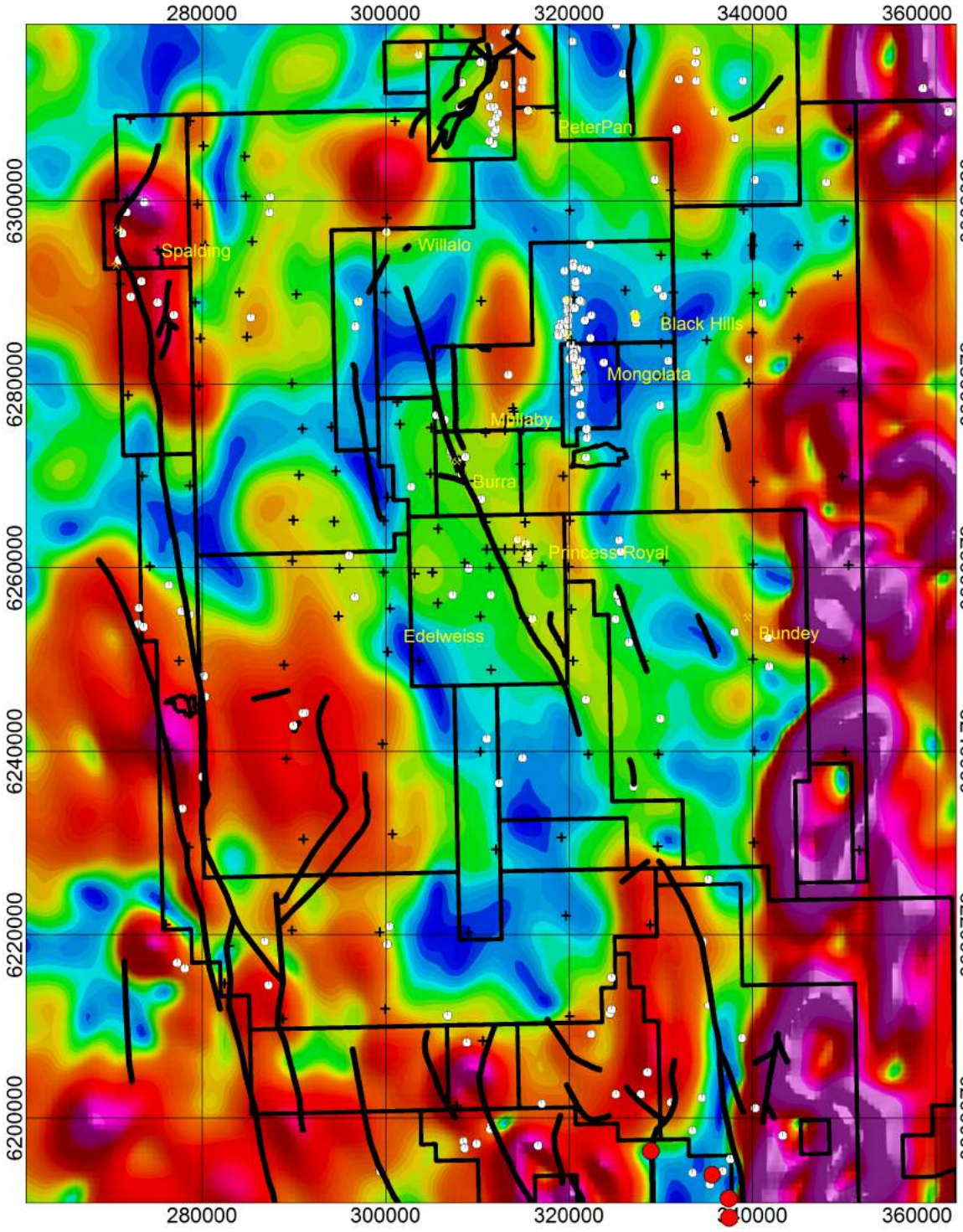

Figure 29: Depth slice through 3D Magnetic MVI model at -2000mRL. The MVI model output reflects both induced magnetic field and remanence. The red dots show the location of Truro Alkaline Suite samples reported by Foden et a., (2020)

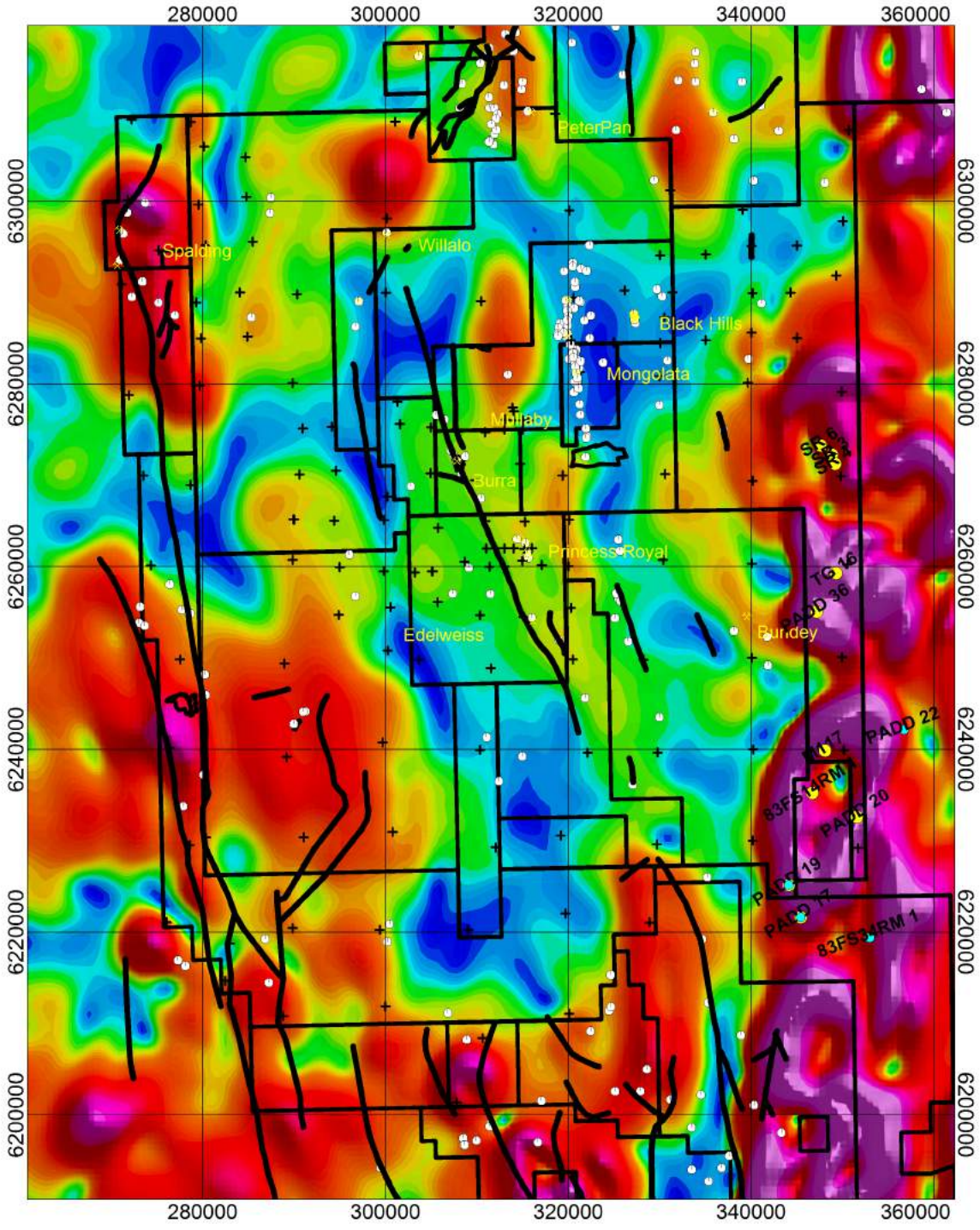

Figure 30: Depth slice through 3D Magnetic MVI model at -2000mRL. The MVI model output reflects both induced magnetic field and remanence. The yellow dots shows the location of gabbros, diorites, monzonites and granites identified in Table 2.

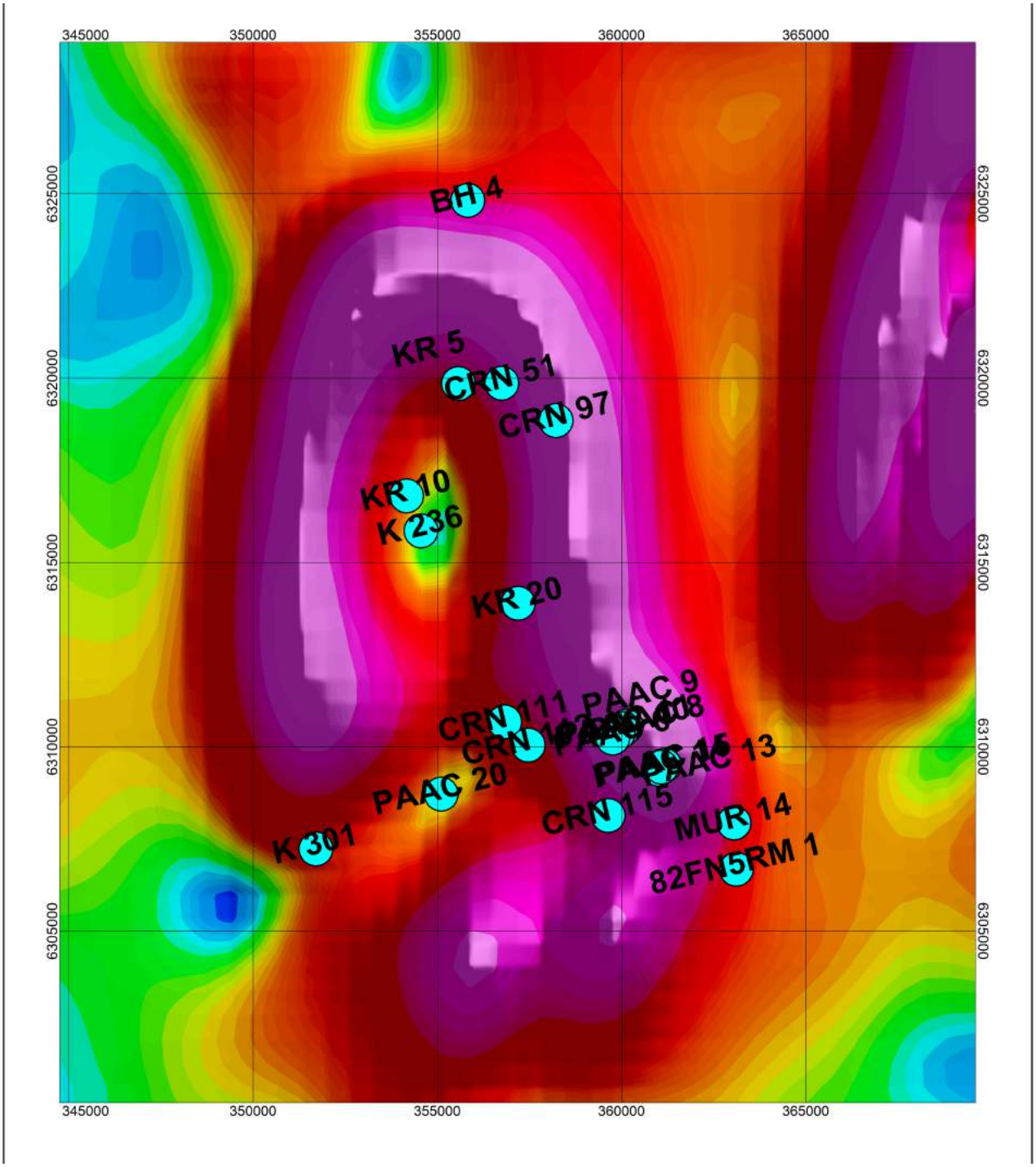

Figure 31: Depth slice through 3D Magnetic MVI model at -2000mRL. The MVI model output reflects both induced magnetic field and remanence. The yellow dots show the location of drill holes into a possible porphyry intrusion identified in Table 2

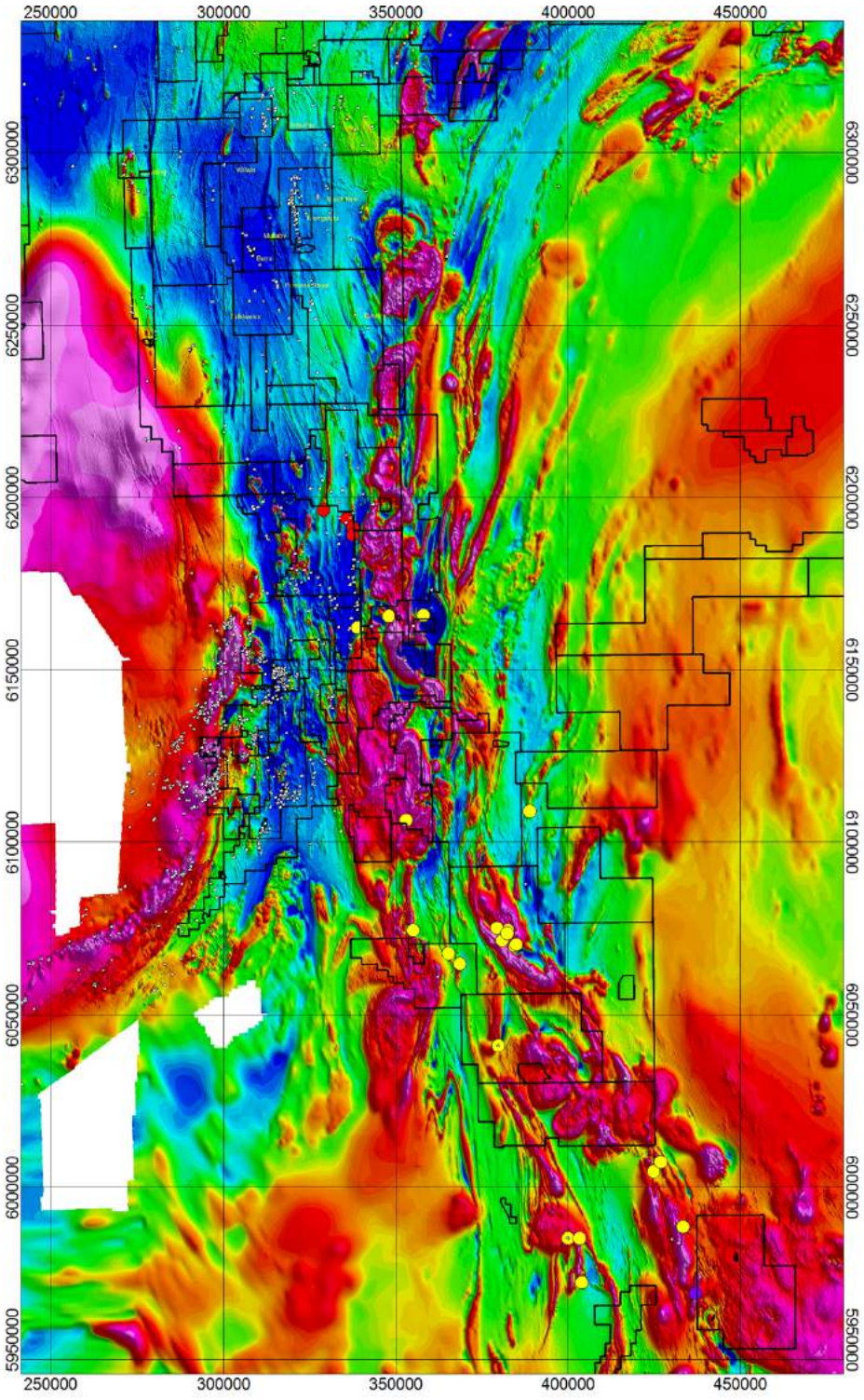

Figure 32: Basement cores from Foden et al. (2020) show on a magnetic image from the southern Mt Loft Ranges to north of Burra. Red dots - Truro Alkaline Suite. Yellow dots - shoshonite suite. Blue dot boninite

12. Cartarpo Cu-Co-HREE Opportunity

In 2018 Investigator Resources Limited announced the discovery of rare earth element (REE) mineralisation at the 19th century Cartarpo copper-cobalt mine within the Company's tenement EL 5999 (Figure 1a, 2 and 33).

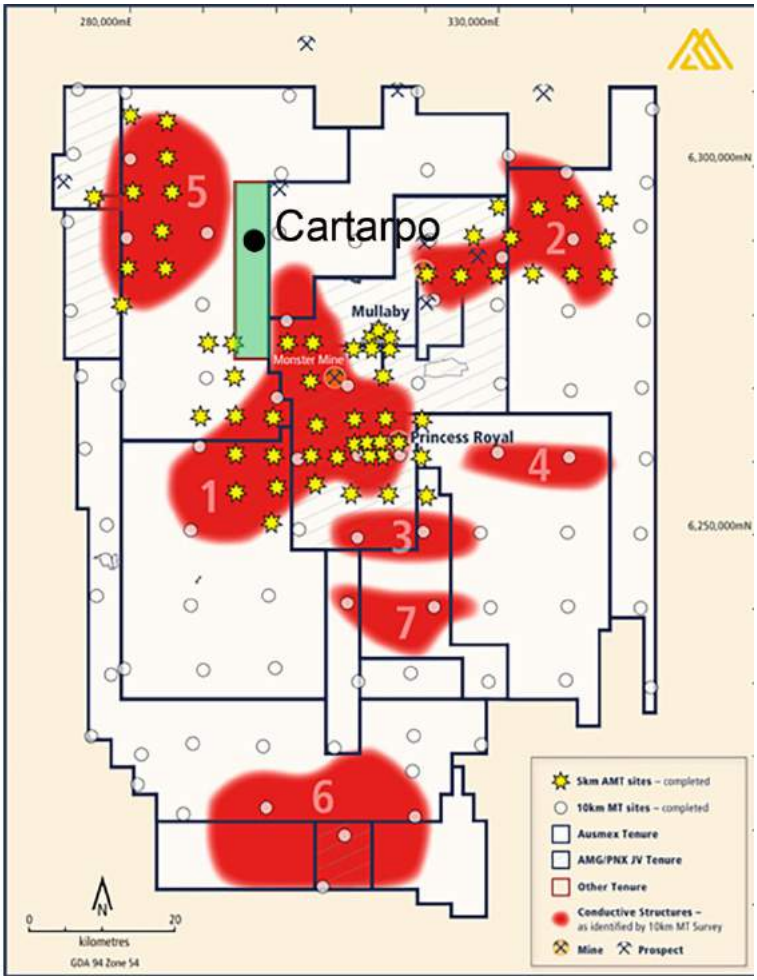

Figure 33: Relationship between Cartarpo and other Tombola's tenure in the Burra area

The Cartarpo mine comprises small largely infilled workings scattered along about 400m strike length (Figure 33). The mineralisation was recorded as cobaltite and malachite in quartz veins with iron and manganese oxides. About 6 tonnes of high-grade ore were reported to have been mined during 1867 - 1872 with one ore parcel estimated to grade 5% cobalt and 6% copper. The main shaft has been infilled, likely with mullock which is absent on the surface.

Investigator Resources conducted a field visit in November to verify the cobalt mineralisation and exploration potential. Sampling of the remaining gossan exposures 200m apart returned strong values of up to 1.78% cobalt and 1.1% combined REEs including heavy REEs, along with copper to 0.5%, nickel to 0.4% and lithium to 0.3% (Figure 34).

Unfortunately, according to Investigator Resources, the workings were not accessible to determine mined widths of mineralisation or the presence of alteration haloes.

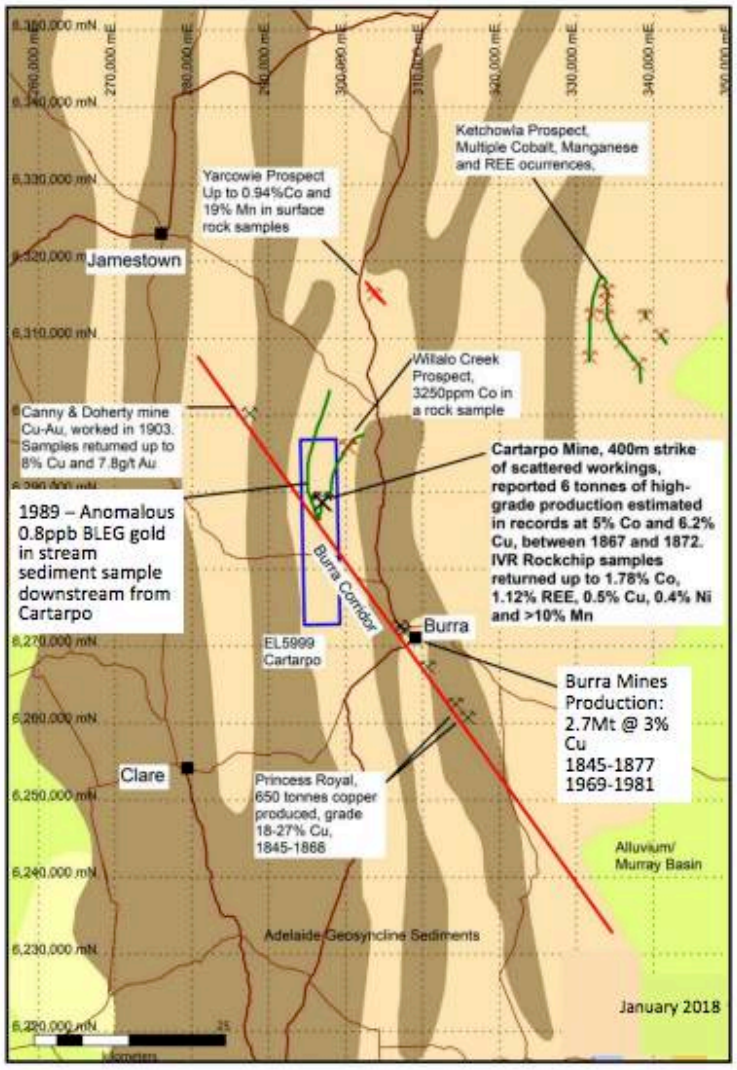

Figure 34: Location of Cartarpo Mine, NW of Burra and reported grades (Investigator Resources 2018)

Investigator interpreted the Cartarpo mine to be situated on a north-west corridor of substantial historic copper and gold mines extending from Burra. During the 1800's, Burra was the largest metals mine in Australia and current work has identified that the copper mineralisation is likely associated with intrusion alkaline magmas (Collerson 2018).

The Cartarpo mineral system was interpreted by Investigator to be a new deposit style in the Burra area that was similar to metals associated with alkalic or carbonatite/kimberlitic intrusions.

It appears the that early prospectors located the Cartarpo mineralisation where gullies incised the western side of the soil- and calcrete-covered ridge corresponding with the trend of the workings. The only effective prior exploration was a 1989 regional stream sediment survey that returned an anomalous gold sample of 0.8 ppb in the north-westerly drainage dispersing from Cartarpo. This implies further targets, as no gold was detected in the Cartarpo gossans. Results of a new soil geochemical sampling program undertaken on four 250m spaced traverses by Investigator Resources are shown in Figures 35 - 37.

These data defined several coherent mineralised zones containing elevated copper, cobalt, lithium, REE and nickel that extended away from and parallel to the historic workings. According to Investigator Resources, these anomalous geochemical zones extend 400m north of the workings and are open to further extension to the south.

Given the metal association there appears to be considerable potential for intrusive-related mineralisation under the ridge parallel to the 400m trend of workings. This and the surrounding 50km^2 area is interpreted to have a prospective combination of favourable faults and stratigraphy to source and host mineralisation.

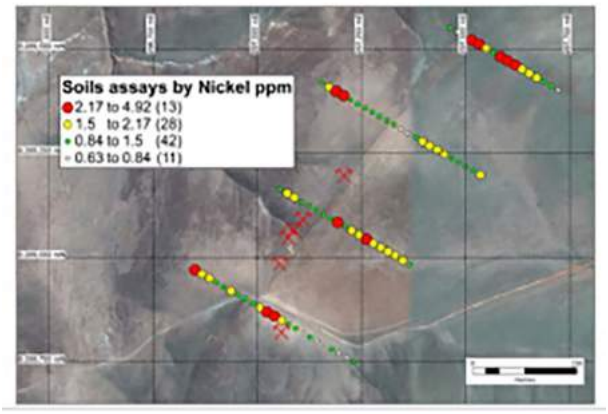

Figure 35: Ni (ppm) recorded in soil geochemistry in the vicinity of the Cartarpo Deposit

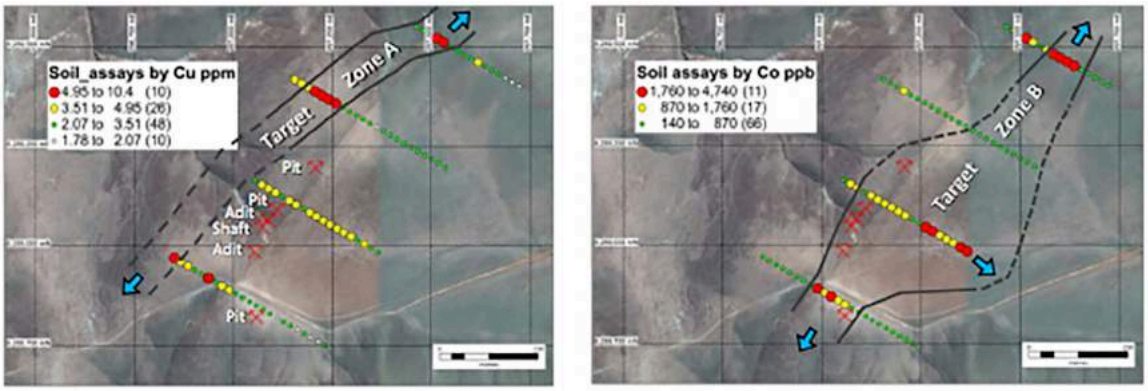

Figure 36: Cu and Co soil geochemistry in the vicinity of the Cartarpo Deposit

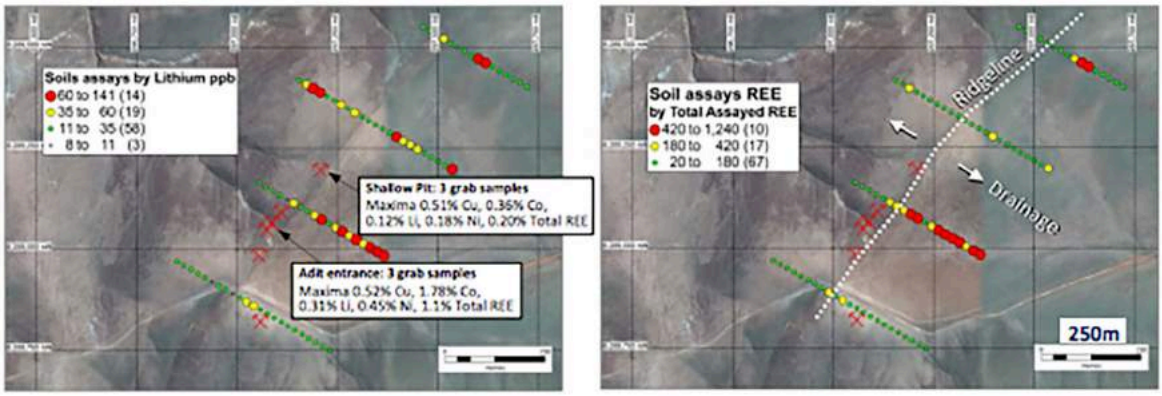

Figure 37: Li and REE soil geochemistry in the vicinity of the Cartarpo Deposit

Figure 38 shows discrete zones of elevated K in the tenement as well prominently zones of high Th relative to K. These differences may reflect presence of a concealed intrusion in the vicinity.

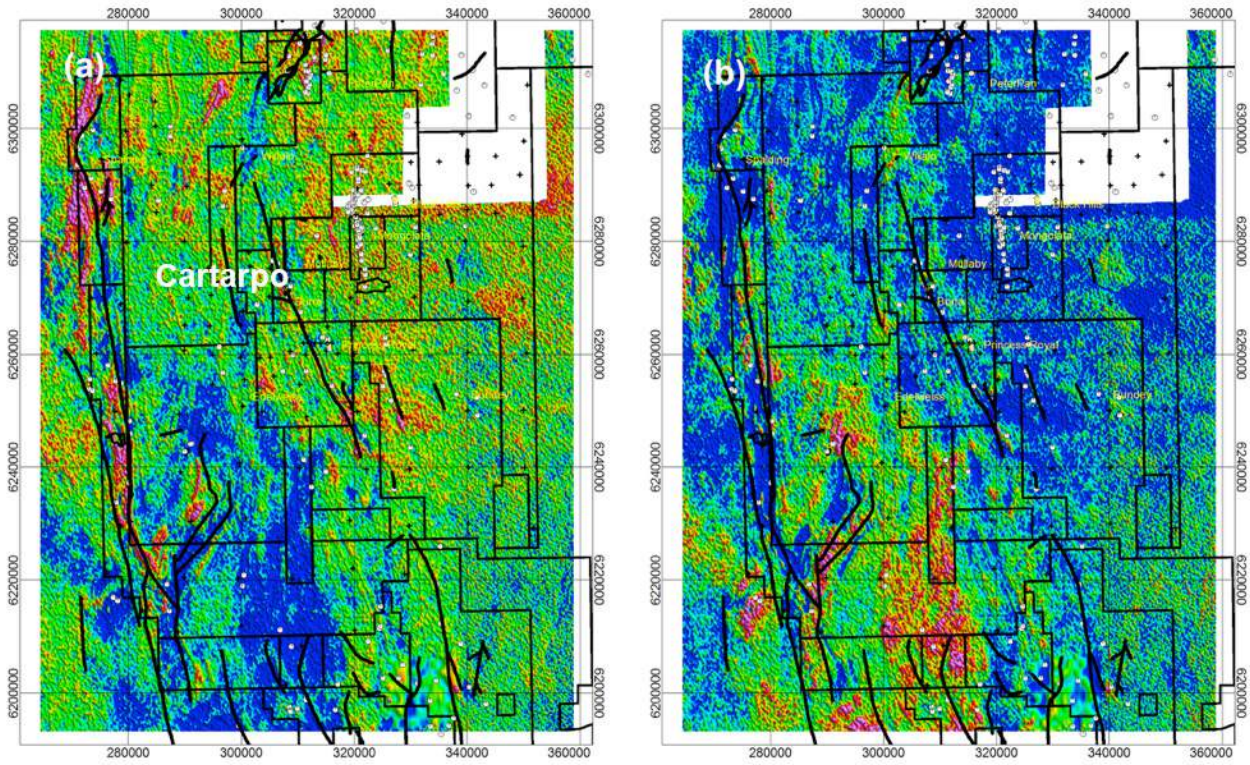

Figure 38: (a) Plot of K/Th and (b) Th/K showing data for the Cartarpo area. Radiometric compilation 2019 (available on Gadds) gridded at 80m cell size. (a) Shows discrete zones of elevated K in the tenement (b) Shows more prominently zones of high Th relative to K in the tenement.

Figure 18 and 19 show MT depth slices at -6000 mRL and -4000 mRL show the presence of an oval shaped region of high conductivity lying immediately east of the Cartarpo tenement. This conductive zone appears to underlie this tenement in the modelled MT at 0 mRL, suggesting the possible presence of a conductive phase like sulphides.

Depth slice through 3D Magnetic MVI model at -4000mRL are shown in Figure 21. The MVI model output which reflects both induced magnetic field and remanence shows the presence of a subtle demagnetised region underlying the Cartarpo tenement that lies between magnetic shoulders on the east near Mullaby and on the north near Willalo. These anomalies are even more pronounced in Figure 22 at -2000mRL and Figure 23 at 0m RL, and might reflect presence of an underlying intrusion. Thus, the demagnetised zone is interpreted to reflect hydrothermal alteration possibly caused by epithermal fluids.

Gravity images at -4000 mRL, -2000 mRL and 0 mRL shown in Figures 24 to 26 show a gravity low in the centre of this feature and a gravity high coinciding with the position of the magnetic rim of the putative intrusion.

12.1 Reconnaissance Rock Chip Assays

Reconnaissance rock chip assays from Cartarpo are given in Table 3. [1]

Table 3: Assay data (ppm) for rock chip samples from Investigator Resources Cartarpo tenement

	Ag	As	Ba	Bi	FeO wt.%	MnO wt%	Co	Ni	Cu	Zn	Ga
CART01	1.94	14.2	>10000	0.24	1.08	12.91	17800	4280	5150	3100	15.95
CART02	0.91	6.5	8680	0.04	1.08	12.91	6940	3740	2120	1900	7.52
CART03	1.75	29.3	>10000	0.18	0.85	12.91	11800	3540	2540	2140	56.7
CART04	0.37	8.1	3210	0.87	2.57	12.91	3640	1350	1035	1010	6.82
CART05	0.13	14.2	1800	0.05	3.53	11.00	3090	1780	1135	1020	6.42
CART06	26.3	17.4	1460	7.81	2.65	6.37	1330	990	5090	573	4.2
	Ge	Zr	Li	Y	La	Ce	Pr	Nd	Sm	Eu	Gd
CART01	1.06	33.2	3140	>500	110	742	55	284	85	26	166
CART02	0.58	36.8	2860	253	29	147	23	175	59	16	75
CART03	12.15	17.8	1980	>500	680	3990	815	>1000	880	216	1000
CART04	0.46	49.2	1160	286	50	153	23	135	44	12	62
CART05	1.69	14.7	1550	>500	63	194	59	482	177	45	173
CART06	0.69	19.4	77000	395	32	79	27	229	90	25	116
	Tb	Dy	Ho	Er	Tm	Yb	Lu	La/Yb	TREE	Ce/Ce*	HREY/TREY
CART01	30	186	44	119	16.4	101.0	18.8	1.09	1983	2.29	0.36
CART02	11	61	12	29	4	26	4	1.12	668	1.30	0.53
CART03	156	904	188	449	58	336.0	53.8	2.02	10725	1.12	0.31
CART04	10	55	12	30	4	26	4	1.95	619	1.08	0.55
CART05	26	128	25	61	9	55	9	1.14	1505	0.70	0.35
CART06	16	88	17	44	6	39	6	0.83	812	0.60	0.62
	La_2O_3	CeO_2	Pr_2O_3	Nd_2O_3	Sm_2O_3	Eu_2O_3	Gd_2O_3	Tb_2O_3	Dy_2O_3	Ho_2O_3	Er_2O_3
CART01	129.0	911.4	64.4	331.3	98.5	30.1	190.8	35.0	213.5	50.7	136.1
CART02	33.4	180.0	26.9	204.1	67.8	18.5	86.0	12.9	69.7	13.5	33.0
CART03	797.5	4901.2	953.8	1166.4	1020.5	250.1	1152.6	179.0	1037.5	214.8	513.4
CART04	58.6	187.3	26.9	157.5	50.7	13.9	71.7	11.3	63.0	13.3	34.1
CART05	73.9	237.7	69.0	562.2	205.3	51.9	198.8	29.4	146.9	28.9	70.0
CART06	37.5	96.9	31.6	267.1	104.8	28.4	133.7	18.2	100.5	18.9	50.0
	Tm2O3	Yb2O3	Lu2O3	Y2O3	TREO	TREO wt%					
CART01	135.9	18.6	114.8	>634.95	2460	0.25					
CART02	33.0	4.6	29.0	321.3	813	0.08					
CART03	512.8	66.2	382.1	>634.95	13148	1.31					
CART04	34.0	4.8	29.2	363.2	757	0.08					
CART05	69.9	10.4	63.0	>634.95	1818	0.18					
CART06	49.9	6.9	44.0	501.6	989	0.10					

Samples were analysed using Analytical Laboratory Services' (ALS) ME-MS61R method A prepared sample (0.25 g) is digested with perchloric, nitric, hydrofluoric and hydrochloric acids. The residue is topped up with dilute hydrochloric acid and analyzed by inductively coupled plasma atomic emission spectrometry. Following this analysis, the results are reviewed for high concentrations of bismuth, mercury, molybdenum, silver and tungsten and diluted accordingly. Samples meeting this criterion were then analyzed by inductively coupled plasma-mass spectrometry. Reported results were corrected for spectral inter-element interferences. Note: As 4 acid dissolution does not dissolve refractory REE-bearing phases, the REE concentrations reported in this table are minimum concentrations, particularly for the HREEs and Y.

Figure 39 shows covariation between (a) Ni and Co, (b) Ni and Cu, (c) Cu and Co, (d) Zn and Cu, (e) Zn and Ag and (f) Li and Zn comparing assay data from Cartarpo with data from Princess Royal, Peter Pan, Black Hills and Willalo. Ni and Co are strongly correlated in Figure 39a, suggesting igneous fractionation from an ultramafic to mafic parent magma. Ni and Cu are also broadly correlated except in samples from

[1] These results were published in an ASX Announcement released by Investigator Resources Limited on 22 January 2018.
The information in this Report that relates to Reconnaissance Rock Chip Assays in Item 12.1 above, is extracted from an ASX Announcement titled "High Cobalt and REEs Upgrade Potential at Historic Copper Mine in South Australia" released by Investigator Resources Limited (ASX | IVR) on 22 January 2018.
I am not aware of any new information or data that materially affects the information included in the Investigator Resources Limited ASX Announcement referred to above and that all material assumptions and technical parameters underpinning the estimates in this Report continue to apply and have not materially changed.

Princess Royal, where Cu concentrations are likely to have been decoupled from Ni, Co and Zn due to supergene enrichment (Figure 39 b-d). Ag and Zn are broadly correlated in samples from Princess Royal (Figure 39e).

The most surprising aspect of the data are the significant levels of enrichment in Li shown by Cartarpo, Princess Royal and some sample from Willalo. Li is well correlated with Zn in samples from Cartarpo, Willalo and Black Hills (Figure 39f). However, Li is decoupled from Zn in Peter Pan and Princess Royal samples.

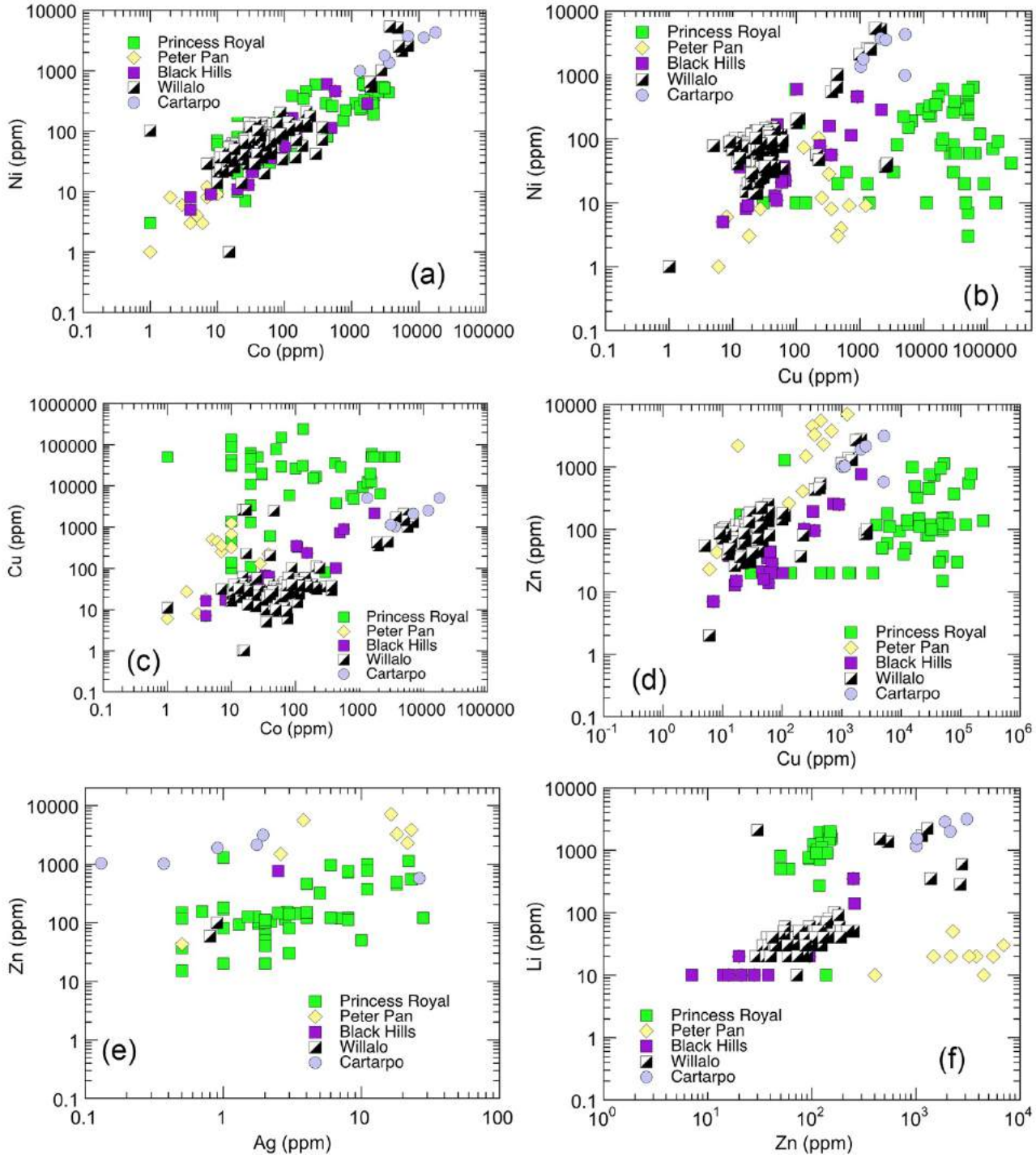

Figure 39: Covariation between (a) Ni and Co, (b) Ni and Cu, (c) Cu and Co, (d) Zn and Cu, (e) Zn and Ag and (f) Li and Zn.

The chondrite normalised REE patterns in Figure 40, show the effect of oxidation producing a +ive Eu anomaly. This is most likely the result fluid phase reaction, rather than weathering induced oxidation. The HREE enriched patterns reflect the presence of xenotime an Y and HREE phosphate. However, the elevated LREE abundances indicates that the xenotime is coexisting with a LREE-phase, resulting in mixed patterns. HREE abundances at Cartarpo are significantly higher than at Princess Royal.

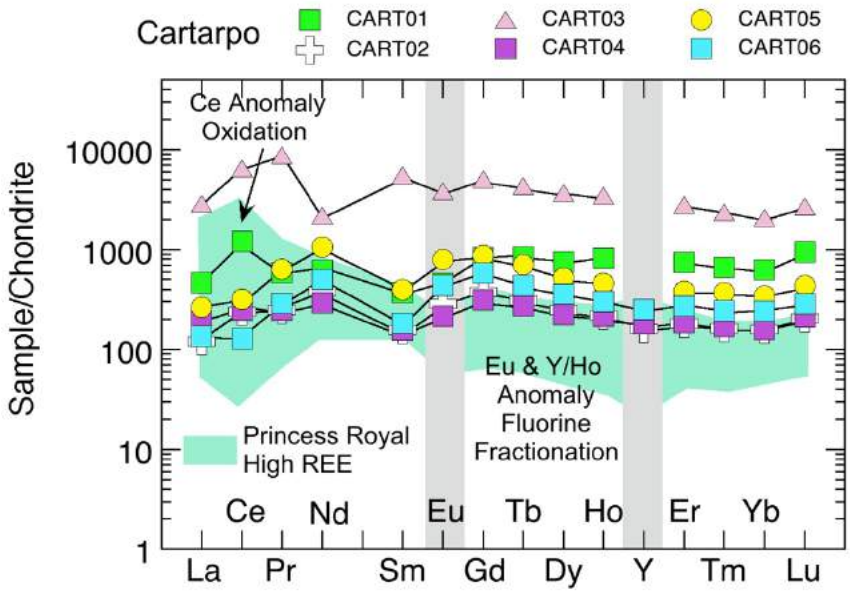

Figure 40:Chondrite normalised plot of Cartarpo REE data determined by 4 acid dissolution and ICPMS. REE data from Princess Royal differs from the Cartarpo profile which suggests that Princess Royal ha ssampled a different part of the alkaline source.

As refractory REE-bearing phases like xenotime are not fully dissolved using 4 acid dissolution, the HREE concentrations reported in Table 3 must be viewed as minimum concentrations, particularly for the HREEs and Y. Thus it is recommended that in future assays, Li borate fusion should be used as the digestion method. The HREE concentrations would then be expected to increase substantially.

Nevertheless even at these levels >100 x chondrites (Figure 40) the REEs in the Cartarpo rock chips are at a levels that is potentially economic.

La/Yb versus total REEs data for Cartarpo (Figure 41) are HREE enriched with low La/Yb ratios and significant enrichment in HREEs. This HREE enrichment is interpreted to reflect fractionation by carbo-thermal fluids. By comparison, samples from Princess Royal define two populations, one that is similar to Cartarpo reflecting carbo-thermal fluid fractionation, the other with La/Yb ratios that show LREE enrichment due to fractionation of a mafic - ultramafic alkaline magma.

Both Cartarpo and some Princess Royal samples are significantly enriched in HREEs, that are rare, and have high commercial value. Thus the HREEs are a previously unappreciated extremely valuable exploration target at Cartarpo, Princess Royal and in the entire Burra system.

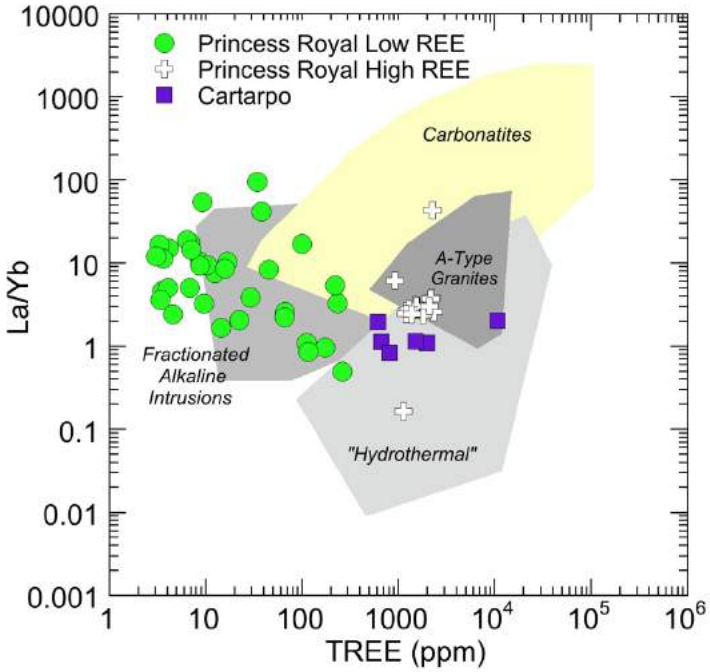

Figure 41: Plot of La/Yb versus Total REEs. Low La/Yb reflect enrichment in HREEs. High La/Yb ratios indicate LREE enrichment. Cartarpo and some PR samples are significantly enriched in HREE. These are rare and have high commercial value.

12.2 Soil Geochemical Results

Investigator Resources undertook a conventional multi-element soil assay program in 2018 on four 250m spaced traverses. A compilation of Au, and Cu data from this survey together with molar Cu/Au from this program is given in Table 4. These ratios are plotted in Figure . The mean molar Cu/Au ratio for 154 Cartarpo soils is 34,923 ± 27,145 this is typical of values for alkaline porphyry systems. A small population of samples (n = 12) have a mean the molar Cu/Au ratio 6529±1738 which which indicates fractionation of Ag:Au in an epithermal system.

Cu/Au ratios and bulk metal contents, specifically Au grades are controlled by magmatic chemistries (Sillitoe 1997, Halter et al., 2002; Heinrich, et al., 2005) and by fluid phases separation into brine and vapour . This process results in Cu-Au fractionation into vapour and possibly to partial separation of the two metals (Simon et al., 2005, 2007, Pokrovski et al., 2008). Final ore grades are however controlled by precipitation efficiency of Cu-sulphides and native Au during cooling (Ulrich et al., 2001). Molar Cu/Au ratios are thus believed to be controlled initially by magma source chemistries and subsequently by the physical-chemical evolution of the ore forming hydrothermal fluids.

The log normal distribution of Ag/Au ratios (Cole and Drummond, S.E. 1986) shown in Figure 42b provides further support for epithermal fluid activity at Cartarpo indicated by the magnetic destruction seen in Figures 21-23.

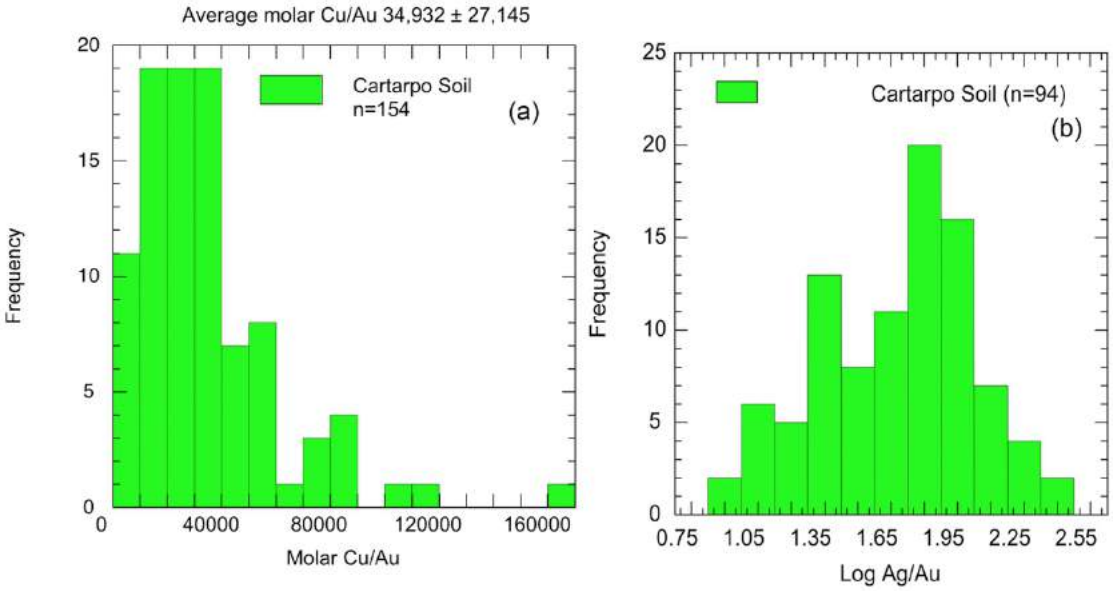

Figure 42 (a) Indicates alkaline epithermal and porphyry source (b) Log normal Ag/Au indicates epithermal processes.

Table 4: Molar Cu/Au ratios for Cartarpo soils assays Investigator Resources (2018)

Sample #	GDA94Z54	GDA94Z54	Cu	Au g/t	Cu/Au	Sample #	GDA94Z54	GDA94Z54	Cu	Au g/t	Cu/Au	Sample #	GDA94Z54	GDA94Z54	Cu	Au g/t	Cu/Au
	East	North			(molar ratio)		East	North			(molar ratio)		East	North			(molar ratio)
CART101	296850.00	6288970.00	6.34	0.0007	29773	CART133	297210.00	6289074.00	3.81	0.0001	84349	CART165	297536.00	6289198.00	3.40	0.0002	5464
CART102	296867.00	6288960.00	4.37	0.0004	36607	CART134	297227.00	6289064.00	3.67	0.0002	59868	CART166	297463.00	6289551.00	2.47	0.0002	47848
CART103	296885.00	6288950.00	3.72	0.0003	34939	CART135	297245.00	6289054.00	4.17	0.0002	71804	CART167	297480.00	6289541.00	2.26	0.0003	20602
CART104	296902.00	6288940.00	3.32	0.0003	34301	CART136	297262.00	6289044.00	3.93	0.0002	81206	CART168	297497.00	6289531.00	3.10	0.0003	385433
CART105	296919.00	6288930.00	2.72	0.0005	17205	CART137	297279.00	6289034.00	3.64	0.0001	86785	CART169	297515.00	6289521.00	7.40	0.0007	33240
CART106	296937.00	6288920.00	5.76	0.0005	38810	CART138	297297.00	6289024.00	3.86	0.0001	108762	CART170	297532.00	6289511.00	6.79	0.0008	25982
CART107	296954.00	6288910.00	3.20	0.0005	19074	CART139	297314.00	6289014.00	3.33	0.0001	79394	CART171	297549.00	6289501.00	2.99	0.0005	18171
CART108	296971.00	6288900.00	3.54	0.0008	14067	CART140	297331.00	6289004.00	4.77	0.0003	59137	CART172	297567.00	6289491.00	2.82	0.0004	24279
CART109	296989.00	6288890.00	3.53	0.0003	35294	CART141	297349.00	6288994.00	3.42	0.0002	58890	CART173	297584.00	6289481.00	2.97	0.0004	26301
CART110	297006.00	6288880.00	2.53	0.0002	32673	CART142	297366.00	6288984.00	3.46	0.0001	119157	CART174	297601.00	6289471.00	3.13	0.0008	11831
CART111	297023.00	6288870.00	2.94	0.0011	8437	CART143	297155.00	6289418.00	3.56	0.0003	39407	CART175	297619.00	6289461.00	3.87	0.0005	25521
CART112	297041.00	6288860.00	2.93	0.0008	11949	CART144	297172.00	6289408.00	4.14	0.0003	42772	CART176	297636.00	6289451.00	3.50	0.0003	32873
CART113	297058.00	6288850.00	3.33	0.0002	54322	CART145	297189.00	6289398.00	4.92	0.0006	25415	CART177	297653.00	6289441.00	3.20	0.0004	28338
CART114	297075.00	6288840.00	3.36	0.0001	80109	CART146	297207.00	6289388.00	5.63	0.0005	35612	CART178	297671.00	6289431.00	2.73	0.0003	30220
CART115	297092.00	6288830.00	2.84	0.0003	32602	CART147	297224.00	6289378.00	5.03	0.0005	34645	CART179	297688.00	6289421.00	2.06	0.0003	19953
CART116	297110.00	6288820.00	1.95	0.0002	35553	CART148	297241.00	6289368.00	10.40	0.0005	61989	CART180	297705.00	6289411.00	1.96	0.0003	24300
CART117	297127.00	6288810.00	2.14	0.0004	17007	CART149	297259.00	6289358.00	8.70	0.0002	168533	CART181	297723.00	6289401.00	2.05	0.0003	23533
CART118	297144.00	6288800.00	2.15	0.0001	51260	CART150	297276.00	6289348.00	3.18	0.0002	51875	CART182	296331.00	6293354.00	3.13	0.0007	14925
CART119	297162.00	6288790.00	1.92	0.0001	74387	CART151	297293.00	6289338.00	3.06	0.0002	49917	CART183	296350.00	6293365.00	1.85	0.0012	4901
CART120	297179.00	6288780.00	2.26	0.0003	25017	CART152	297311.00	6289328.00	3.45	0.0002	44555	CART184	296368.00	6293371.00	1.78	0.0012	4485
CART121	297196.00	6288770.00	2.04	0.0002	33278	CART153	297328.00	6289318.00	2.91	0.0002	47471	CART185	296387.00	6293378.00	2.39	0.0011	6988
CART122	297214.00	6288760.00	1.88	0.0002	24279	CART154	297345.00	6289308.00	2.09	0.0003	25911	CART186	296407.00	6293385.00	2.22	0.0012	5983
CART123	297231.00	6288750.00	2.38	0.0003	24589	CART155	297362.00	6289298.00	1.92	0.0003	23804	CART187	296426.00	6293390.00	3.53	0.0014	7651
CART124	297054.00	6289164.00	3.26	0.0007	14859	CART156	297380.00	6289288.00	2.46	0.0003	30499	CART188	296443.00	6293398.00	3.96	0.0012	9898
CART125	297072.00	6289154.00	4.51	0.0008	17473	CART157	297397.00	6289278.00	2.64	0.0004	21533	CART189	296464.00	6293403.00	4.18	0.0022	5970
CART126	297089.00	6289144.00	3.75	0.0007	15707	CART158	297414.00	6289268.00	3.07	0.0006	16128	CART190	296481.00	6293402.00	3.96	0.0010	12653
CART127	297106.00	6289134.00	3.53	0.0008	13025	CART159	297432.00	6289258.00	2.99	0.0004	22603	CART191	296499.00	6293400.00	5.70	0.0034	5136
CART128	297124.00	6289124.00	2.52	0.0002	35503	CART160	297449.00	6289248.00	3.15	0.0007	15020	CART192	296517.00	6293398.00	3.12	0.0020	4959
CART129	297141.00	6289114.00	4.34	0.0011	12572	CART161	297466.00	6289238.00	2.69	0.0003	32067	CART193	296536.00	6293399.00	4.79	0.0007	20063
CART130	297158.00	6289104.00	4.10	0.0015	8472	CART162	297484.00	6289228.00	2.82	0.0006	14097	CART194	296558.00	6293402.00	5.97	0.0007	27617
CART131	297176.00	6289094.00	3.13	0.0007	14925	CART163	297501.00	6289218.00	2.70	0.0002	49227					Mean	34932
CART132	297193.00	6289084.00	4.08	0.0002	57481	CART164	297518.00	6289208.00	2.91	0.0002	47471					SD	27145

13. New Assays for Eagle Prospect IP Targets

During a search for IP data for the Burra area as part of the current study it was discovered that Phoenix Copper (2012) drilled a number of holes at the Eagle Prospect, to test a number of IP targets. The Eagle Prospect is located 800 m north-west of the Monster Mine (Figure 43).

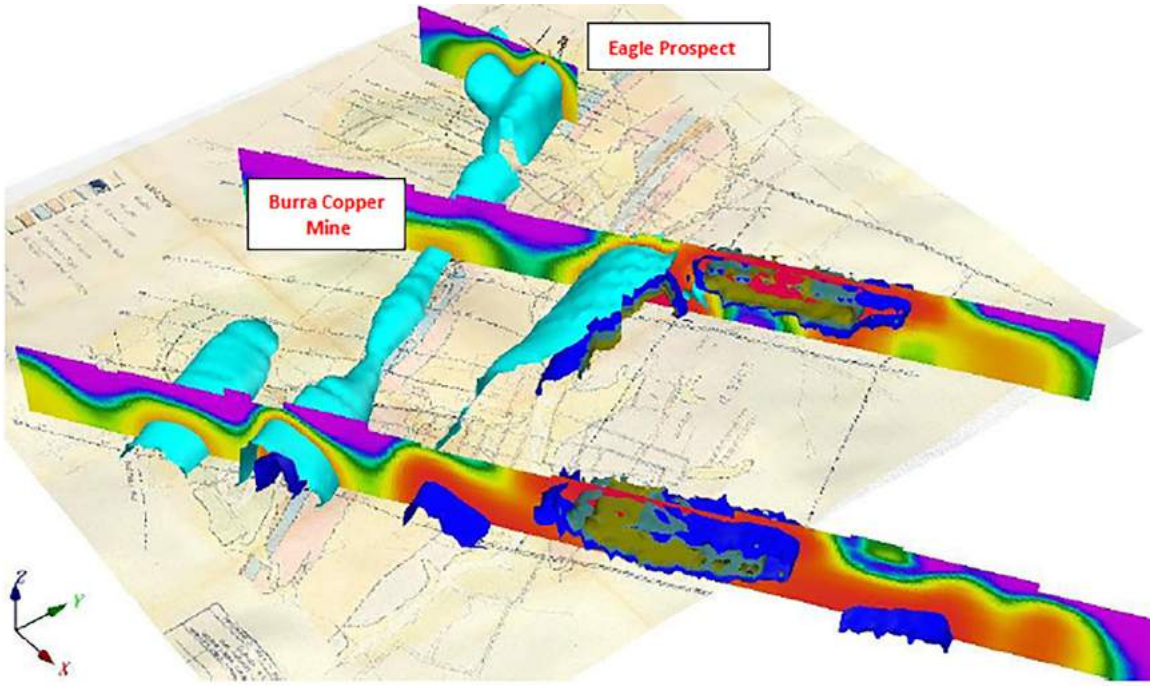

Figure 43: 3D Image viewed from the southeast to the northwest with IP response displayed (from Phoenix Copper ASX Announcement 12th Dec. 2012)

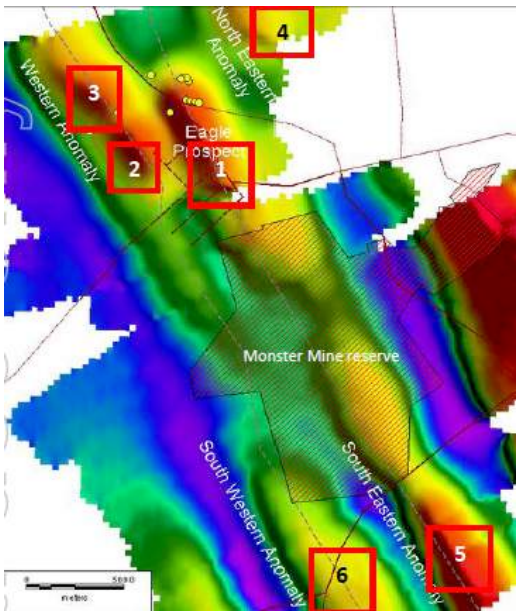

Figure 44: IP Targets at the Eagle Prospect (from Phoenix Copper ASX Announcement 12th Dec. 2012)

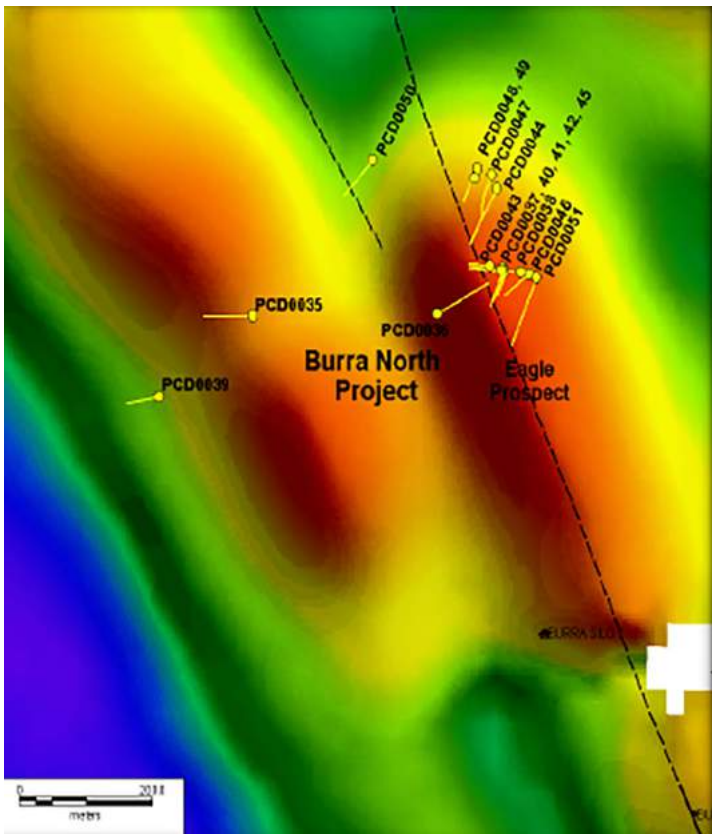

Figure 45: Drill hole traces over IP targets at the Eagle Prospect.

As only partial analytical results were reported (Table 5)in order to better understand the prospectivity of the mineral system in the Burra area it is recommended that a litho-geochemical study be undertaken of 50 selected samples of these cores. Suggested sample intervals are given in Table 6.

Table 5: Summary data for drill holes and Cu grades

Hole ID	Northing	Easting	Azimuth	Dip	Down hole depth m	RL	From m	To m	Width m	Grade %
PCD0035	6272610	306832	276	-60	205.3	466	-	-	-	NSI
PCD0036	6272623	307106	61	-50	177.5	468	-	-	-	did not reach target depth
PCD0037	6272682	307204	0	-90	46.0	469	-	-	-	NSI
PCD0038	6272680	307234	280	-60	121.0	468	94.9	117.4	22.5	0.81% Cu
including							102.6	110.7	8.1	**1.46% Cu**
PCD0039	6272500	306700	266	-60	144.7	467	-	-	-	missed target
PCD0040	6272682	307203	281	-60	77.0	469	50.7	77	26.3	**2.86% Cu**
including							61.1	74.8	13.7	**5.23% Cu**
PCD0041	6272682	307204	200	-60	87.0	469	54.1	70.8	16.7	0.63% Cu
including							64.7	70.8	6.1	0.95% Cu
PCD0042	6272682	307204	200	-47	73.0	469	47	58.9	11.9	0.48% Cu
PCD0043	6272687	307184	201	-60	52.9	469	31	36	5	0.44% Cu
PCD0044A	6272787	307193	215	-60	144.0	496	-	-	-	NSI
PCD0045	6272683	307203	202	-74	98.7	469	69.2	82.5	13.3	**1.22% Cu**
including							69.3	75.3	6	**1.61% Cu**

It is recommended that samples are selected during a site visit by KDC to Burra. Assays to be undertaken by Intertek Genalysis in Perth. Data for Au, Pt and Pd will be by (FA25/MS). 4 acid dissolution will be

used to analyse 48 elements by Triple Quad MS (4A/MSQ48) and Li borate fusion (FP6/OM) will be used for REEs and the HFSEs.

Table 6: Details of drill holes at the Eagle Prospect for lithogeochemical sampling

Hole ID	Northing	Easting	Azimuth	Dip	Depth DH	RL	From M	To M	Width m	Cu wt.%	Samples for Assay
PCD0038	6272680	307234	280	-60	121	468	94.9	117.4	22.5	0.81	10
PCD0038	6272680	307234	280	-60	121	468	102.6	110.7	8.1	1.46	4
PCD0040	6272682	307203	281	-60	77	469	50.7	77	26.3	2.86	12
PCD0040	6272682	307203	281	-60	77	469	61.1	74.8	13.7	5.23	10
PCD0041	6272682	307204	200	-60	87	469	54.1	70.8	16.7	0.63	12
PCD0041	6272682	307204	200	-60	87	469	64.7	70.8	6.1	0.95	5
PCD0042	6272682	307204	200	-47	73	469	47	58.9	11.9	0.48	10
PCD0043	6272687	307184	201	-60	52.9	469	31	36	5	0.44	4
PCD0045	6272683	307203	202	-74	98.7	469	69.2	82.5	13.3	1.22	10
							69.3	75.3	6	1.61	5
PCD0036	6272610	307106	61	-50	177.5	468	170 to 177	7		Did not reach target	4
									Total		**50**

14. Drilling Targets

Following a meeting with Kate Nelson at GeoDiscovery the following targets were identified for deeper RC and diamond drilling at Princess Royal. Potential drill targets based on IP, MT conductivity and Magnetics are shown in Figures 46-48.

General observations made by Geo Discovery are as follows:

- IP Chargeability (yellow) – response dominated by the presence of near surface shales - however could potentially map near surface mineralisation
- MT Conductivity – appears to be mapping shales and faults. Potentially mapping conductive mineralisation if present (and / or resistive silicification zones).
- Mag MVI – appears to map weak concentrations of magnetic minerals (iron??) – potentially associated with Cu mineralisation
- Near surface gravity highs appear to map faults (silicification?) lows may reflect more cavernous / fractured dolomite / limestone (ground water).

14.1 Details of Specific Targets

Target 1

Mapped cover (geology unknown Nds?), discrete weak magnetic high and near coincident MT conductive zone (within top 250m of surface), Gravity low / transition indicative of fault. Located on an inferred NW trending structure which may also be associated with known mineralisation / workings. No historical IP in this region.

Target 2

To NW of hole 14 and historical hole BU1. Mapped Dolomite/ Chert at surface, MT conductive zone extending to depth, coincident weak magnetic response, gravity low (cavernous limestone?). Also located on NW trending faults (similar to 10). Depth around 250m+.

Target 3

Located beneath Hole BU1 (Cu vein noted in hole). Weak conductive trend extending to depth. Edge Weak magnetic response, gravity transition zone (fault?). Depth 300m+. Lower priority.

Target 4

Mapped dol. Deep (400m+) MT conductive zone associated with edge of weak magnetic response and gravity transition zone (fault?).

Target 5

Weak conductive zone adjacent to strong conductive zone (Fault?) at ~300m depth located to west of historical hole BU2. Proximal to contact between shales and Dolomite. Northern extent of historical workings. Weak magnetic response, gravity low.

Target 6

Weak conductive zone at around 250m depth. Mapped dolomite at surface, gossan also noted in historical mapping, proximal to historical workings. Gravity transition zone (fault) and weak magnetic response.

Target 7

Mapped dol. Weak MT response associated with edge of magnetic response (cross-cutting fault?). No gravity data. Lower Priority.

Target 8

Gravity linear and coincident MT conductive linear (possibly fault zone) extending near surface (recommend surface reconnaissance) . Weak magnetics zone at greater depth. Lower Priority

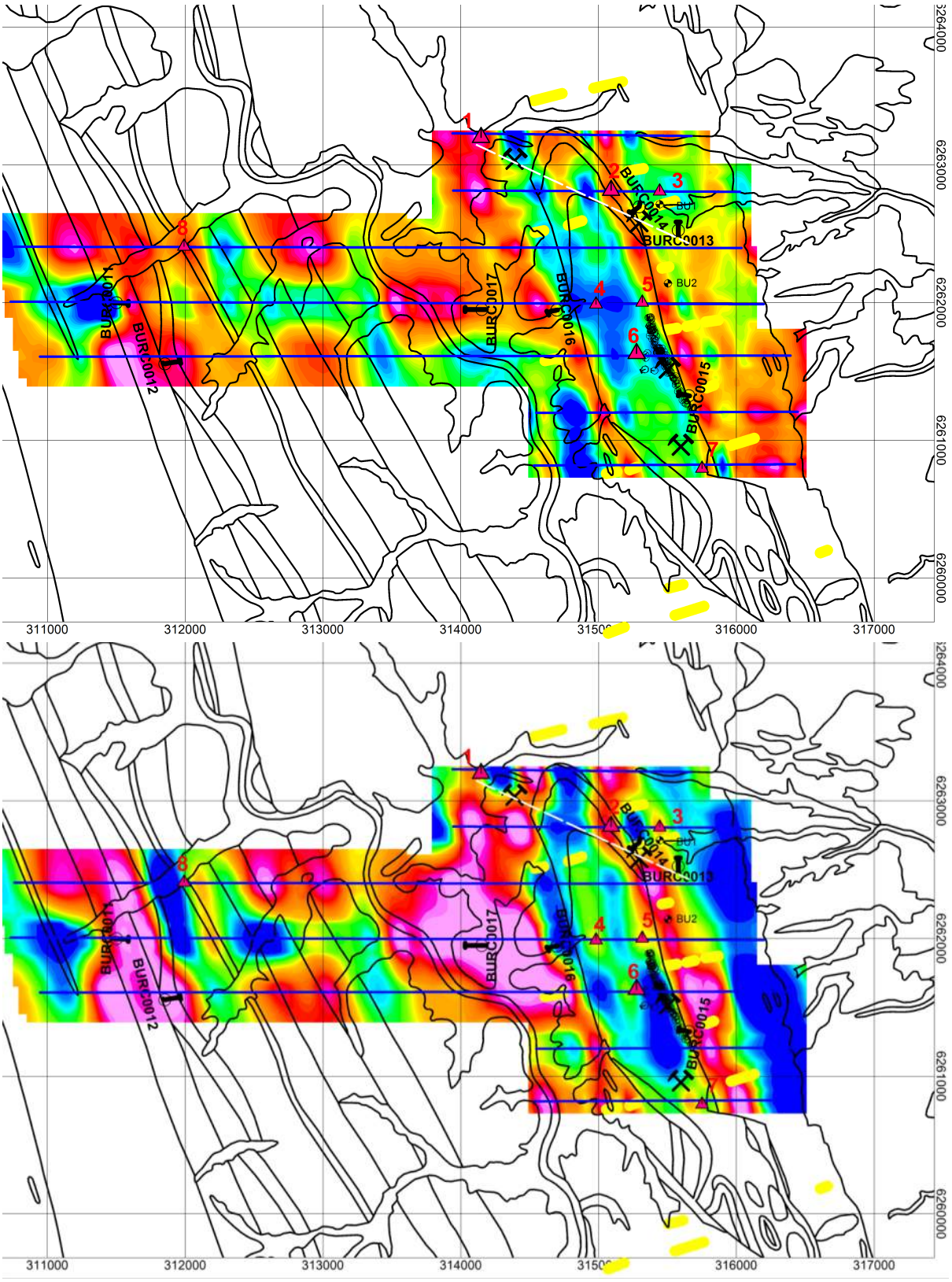

Figure 46: MT conductivity Depth Slices wrt potential target zones (red triangles). Yellow indicates near surface chargeable response.

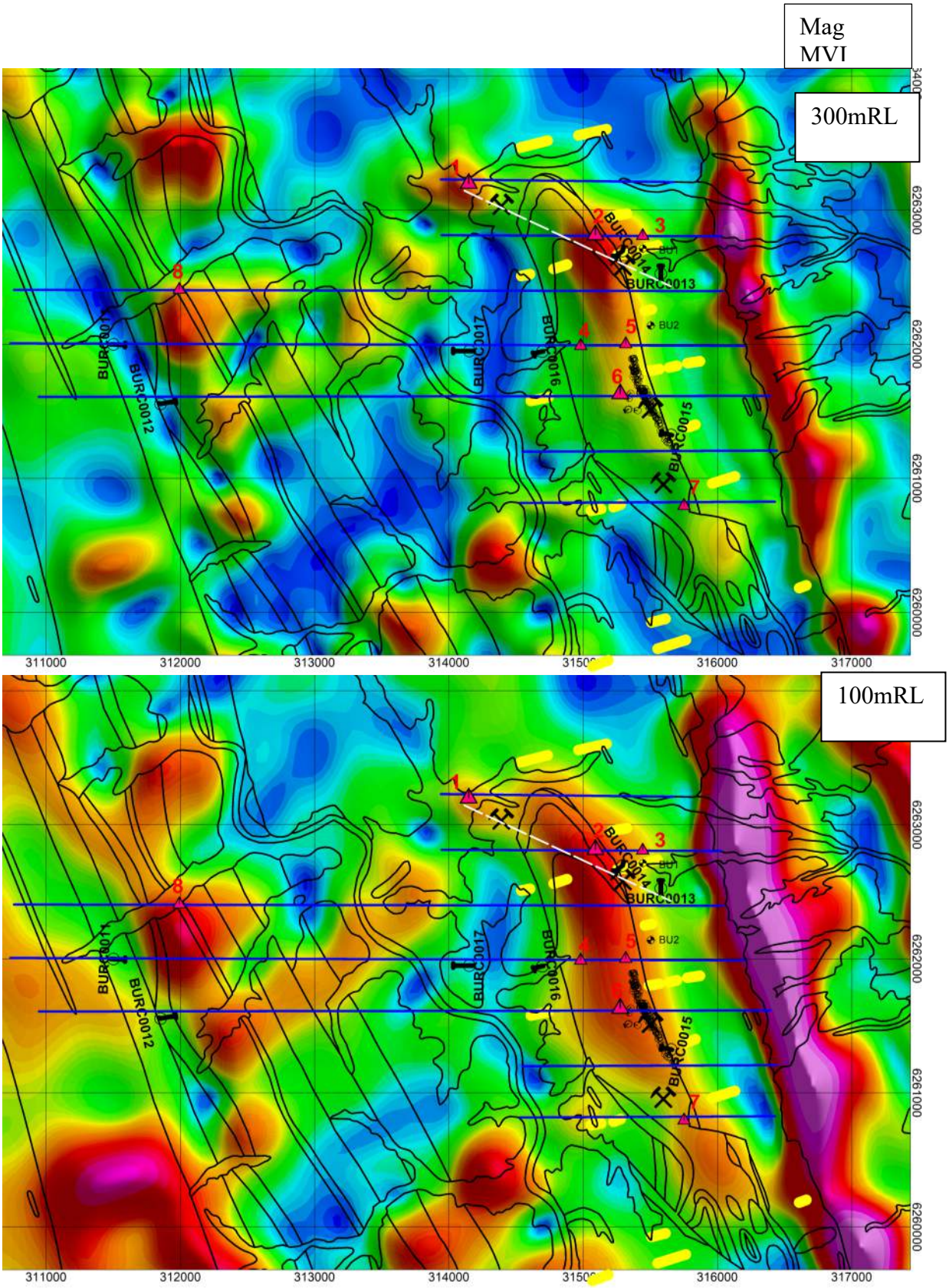

Figure 47: Magnetic MVI Depth Slices wrt potential target zones (red triangles). Yellow indicates near surface chargeable response

.

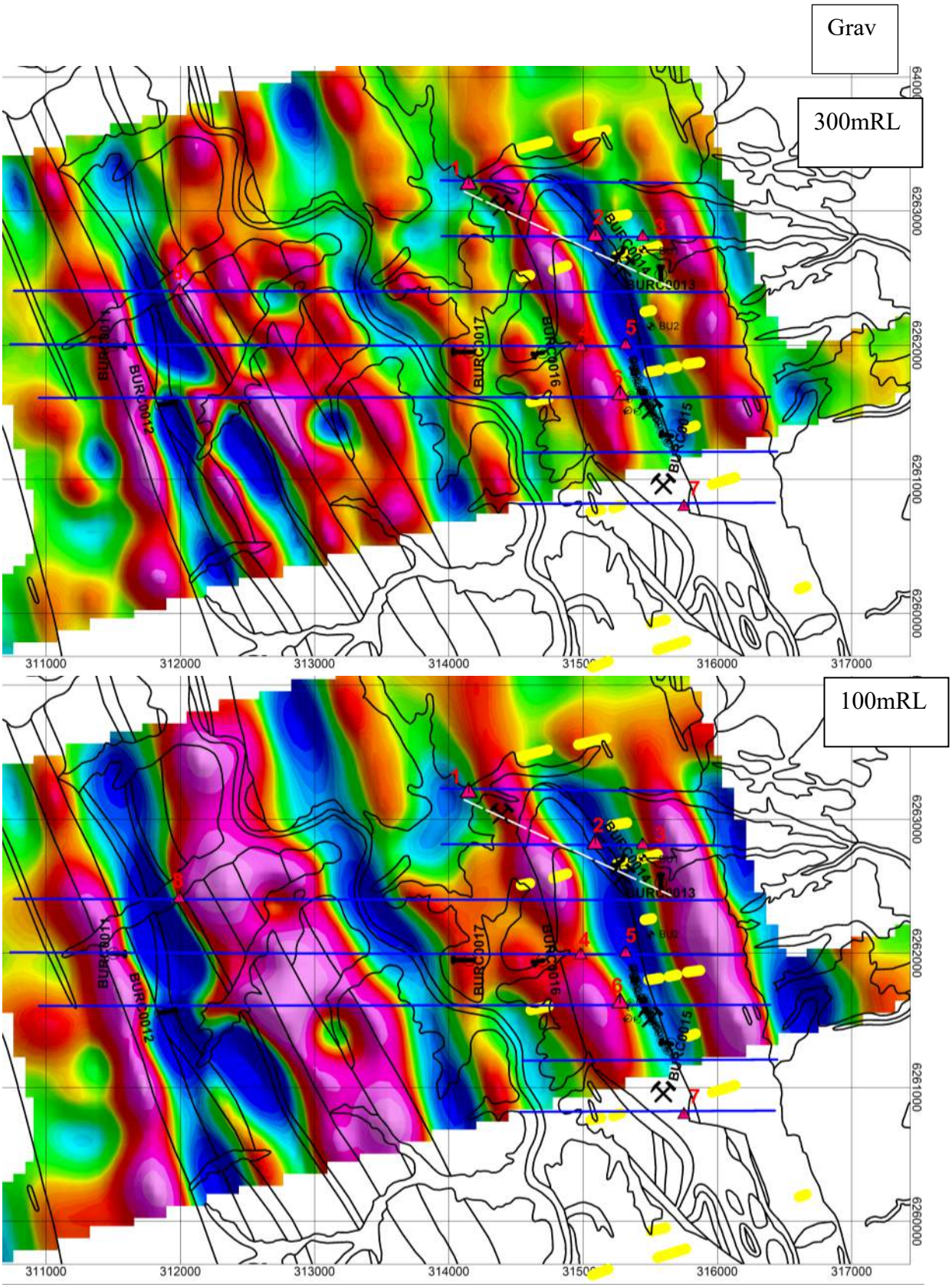

Figure 48: Density Depth Slices wrt potential target zones (red triangles). Yellow indicates near surface chargeable response

15. Recommndations

- The Mongolata - Black Hills area should be explored using an epithermal model.
- Soil geochemistry assays should be undertaken using the ultra-fine sampling strategy developed by CSIRO and Lab West.
- In areas where calcrete development obscures gold anomalism, depth profile assay techniques should be undertaken to improve resolution of basement Au anomalism.
- IP or SAM geophysical surveys should be undertaken to improve target delineation.
- A multi-element assay study should be undertaken on the poorly assayed cores that were drilled by Phoenix Copper at the IP defined Angel prospect at Burra.
- Consideration should be given to deep drilling of targets at Princess Royal identified in this study.

16. Summary

This report commissioned by Tombola Gold Limited, reviews historic exploration data including field observations, assay data and geophysical models obtained by AusMex and by Phoenix Copper Ltd. and other explorers in the Burra area.

The review was commissioned to provide constraints on the origin of Cu-Au-Ni-Co-REE mineralisation in the district.

In addition, regional context of projected boundary of the Delamerian Orogen is also discussed to provide information regarding the geochemical affinity of drill holes to basement.

Data reviewed includes geophysical, as well lithological and geochemical constraints for the following:
The region immediately east of Tombola's Burra tenure which contains numerous Delamerian mafic to granitic intrusions:

- The basement east of the Fleurieu Arc, east of the southern Mount Lofty Ranges that is obscured by a venieer Murray Basin sediments.
- The Konnenberry Arc which represents the northern extension of the Delamerian Orogen that flanks the Curnamona Craton

It is concluded that mineralisation in the Burra area evolved in two stages.

The first metallogenic event occurred during break-up of the Neoproterozoic supercontinent Rodinia. This allowed formation the Cu-Au-REE-Co mineralisation at Burra e.g., the Princess Royal Deposit.

Based on Cu-Ni-Co-HREE systematics, the metal source is interpreted to be associated with plume generated mafic to ultramafic intrusions. Geophysical data MT, magnetics, gravity and radiometric data indicate that such an intrusion possibly underlies the Cartarpo - Willalo- Mullaby area.

The second metallogenic event occurred in the early Palaeozoic, in response to Delamerian magmatism. The gold mineralisation at Mongolata, characterised by elevated Se, Te, Bi and Hg as well as by a log normal distribution of Ag/Au, is clearly epithermal in character. Radiometric data indicate that the source of the Mongolata system lies to the east, in the magmatic zone that flanks the western side of the Delamerian Orogen.

There is comparatively little known about the composition of the buried Delamerian intrusive suite east of Burra where, although outcrops of Bendigo granite have been mapped, no geochemical data is available ,although earlier studies based on alteration style suggested this granite could host a Cu-Au-Mo porphyry system.

A review of available chemical data for these Delamerian intrusions in the Fleurieu Arc east of the southern Mount Lofty Ranges and outcropping volcanics in the Konnenberry Arc shows that they contain potassic alkaline suites that chemically resemble members of the shoshonite suite, as well as plume generated ocean island basaltic compositions.

This is an important observation, because shoshonite suite lithologies are an important class of alkaline potassic igneous rocks that contain world class epithermal gold-silver and porphyry copper-gold deposits in many parts of the circum Pacific region e.g., gold deposits such as the 2520 t Grasberg Mine in West Papua and the 1190 t Ladolam-Lihir deposit in Papua New Guinea. The giant (660 t) Porgera deposit in Papua New Guinea is also hosted by medium-to-high potassium-bearing gabbro and mafic porphyry with compositions that trend towards shoshonites.

In view of the evidence for potassic alkaline magmatism in the Delamerian Orogen, it is recommended that basement cores be sampled for lithogeochemical study to establish if these potassic alkaline lithologies extend north from Truro north into the Burra area.

The area clearly has high potential for discovery of alkaline hosted Cu-Au porphyry style systems similar to the Cu-Au porphyry mineralisation recently discovered in western Victoria by Staverly Minerals (Staverly Minerals ASX Announcement Nov. 2, 2020). It possibly represents some of the most prospective, yet least explored, tenure in Australia.

17. References

Anderson, WB, and Eaton, PC, 1990. Gold mineralization at the Emperor Mine, Vatukoula, Fiji, Journal of Geochemical Exploration, 36:267-296.

Armistead , S.E., Collins. A.S., , Buckman, S., Atkins, R. (2020): Age and geochemistry of the proterozoic Adelaide Rift Complex, South Australia, Australian Journal of Earth Sciences, DOI: 10.1080/08120099.2021.1840435"

Brett, P.R., (1956) The geology of an area immediately south of Burra, with particular reference to mineralisation. BSc Hons Thesis School of Earth and Environmental Sciences, Geology & Geophysics, University of Adelaide. http://hdl.handle.net/2440/84478

Cole, D.R. Drummond, S.E. (1986) The effect of transport and boiling on Ag/Au ratios in hydrothermal solutions: A preliminary assessment and possible implications for the formation of epithermal precious-metal ore deposits. Journal of Geochemical Exploration, 25: 45-79.

Collerson, K.D. (2018) Rare Earth Element-Cobalt-Copper-Gold Mineral System at Burra, S.A: Significance of the AusLAMP Magnetotelluric Anomaly. Report for Ausmex, October 2, 2018, 43pp.

Collerson, K.D., Lal, J., Williams, Q., Rost, S. (2015) Cracking the metallogenic code for Fijian epithermal gold mineralisation. AusIMM Pacrim Conference Ext. Abstract March 2015, 219-226.

Crawford, A.J., Stevens, B.P.J., Fanning, M., 1997. Geochemistry and tectonic setting of some Neoproterozoic and Early Cambrian volcanics in western New South Wales. Australian Journal of Earth Sciences 44 (6), 831–852.

Crawford, A.J., Keays, R.R., 1978. Cambrian greenstone belts in Victoria: marginal sea-crust slices in the Lachlan Fold Belt of southeastern Australia. Earth and Planetary Science Letters 41, 197–208.

Dickinson, S. B., 1942. The structural control of ore deposition in some South Australian copper fields. South Australia. Geological Survey. Bulletin 20, 66-78.

Direen, N.G., Crawford, A.J., 2003a. Tasman Line: where is it, and is it Australia's Rodinian break-up boundary? Australian Journal of Earth Sciences 50 (4), 491–502.

Direen, N.G., Crawford, A.J., 2003b. Fossil seaward dipping reflector sequences preserved in southeastern Australia—a 600 Ma volcanic passive margin in eastern Gondwanaland. Journal of the Geological Society, Geological Society of London 160, 985–990.

Drexel, J. F., 2008. Review of the Burra Mine project, 1980–2008 — a progress report, Report Book 2008/16. Department of Primary Industries and Resources South Australia, Adelaide.

Drexel, J. F., McCallum, W. S., 1986. Origin and age of the Burra copper orebody. South Australia. Geological Survey. Quarterly Geological Notes 98.

Elliott HAL, Broom-Fendley S, Wall F, Sga (2019) Utilizing alteration (fenite) surrounding carbonatite intrusions as a REE and Nb exploration indicator. Life with Ore Deposits on Earth, Proceedings of the 15th Sga Biennial Meeting, 2019, Vols 1-4, 1756-1759.

Elliott HAL, Wall F, Chakhmouradian AR, Siegfried PR, Dahlgren S, Weatherly S, Finch AA, Marks MAW, Dowman E, Deady E (2018) Fenites associated with carbonatite complexes: A review. Ore Geology Reviews 93:38-59 doi:10.1016/j.oregeorev.2017.12.003

Elliott, P. J., Simpson, C. A., Plimer, I. R., Besley, R. E., Busuttil, S., Blampain, P. A., 2003. Burra Creek and Lagoon Hill, Els 2161 and 2217. Progress and annual reports for the period 24/4/1996 to 9/9/2003, for Elliott Geophysics Pty Ltd, Redfire Resources NL, Mount Isa Mines Ltd and Consolidated Broken Hill Ltd. South Australia. Department of Primary Industries and Resources. Open file Envelope, 9191 (unpublished)."

Fiorentini ML, Garwin SL (2010) Evidence of a mantle contribution in the genesis of magmatic rocks from the Neogene Batu Hijau district in the Sunda Arc, South Western Sumbawa, Indonesia. Contributions to Mineralogy and Petrology 159(6):819-837 doi:10.1007/s00410-009-0457-7

Flöttmann, T., Gibson, G.M., Kleinschmidt, G., 1993. Structural continuity of the Ross andDelamerian orogens of Antarctica and Australia along the margin of the paleo- Pacific. Geology 21, 319 - 322.

Foden, J., Elburg, M., Dougherty-Page, J., Burtt, A., 2006. The timing and duration of the Delamerian Orogeny: correlation with the Ross Orogen and implications for Gondwana assembly. Journal of Geology 114, 189–210.

Foden JD, Elburg MA, Turner SP, Sandiford M, O'Callaghan J, Mitchell S (2002) Granite production in the Delamerian Orogen, South Australia. Journal of the Geological Society 159:557-575 doi:10.1144/0016-764901-099

Foden J, Elburg M, Turner S, Clark C, Blades ML, Cox G, Collins AS, Wolff K, George C (2020) Cambro-Ordovician magmatism in the Delamerian orogeny: Implications for tectonic development of the southern Gondwanan margin. Gondwana Research 81:490-521 doi:10.1016/j.gr.2019.12.006

George, L. (2017) Geology and Exploration History of the Burra area, Confidential Report for Ausmex Mining Limited 21st July 2017, 91pp.

Gill JB (1970) Geochemistry of Viti Levu, Fiji,and its evolution as an island arc. Contributions to Mineralogy and Petrology 27:179-203.

Gill J, Whelan P (1989) Postsubduction ocean island alkali basalts in Fiji. Journal of Geophysical Research-Solid Earth and Planets 94:4579-4588.

Greenfield JE, Musgrave RJ, Bruce MC, Gilmore PJ, Mills KJ (2011) The Mount Wright Arc: A Cambrian subduction system developed on the continental margin of East Gondwana, Koonenberry Belt, eastern Australia. Gondwana Research 19(3):650-669 doi:10.1016/j.gr.2010.11.017

Griessmann, M (2011) Gold mineralisation in the Adelaide Fold Belt. PhD Thesis University of Adelaide (un published).

Halter, W.E., Pettke, T., & Heinrich CA (2002) The origin of Cu/Au ratios in porphyry-type ore deposits. *Science*, 296: 1844 -1846.

Heinrich, C.A., Halter, W.E., Landtwing, M.R., Pettke, T. (2005) The formation of economic porphyry copper (- gold) deposits: constraints from microanalysis of fluid and melt inclusions. *Geol. Soc. Lond. Spec. Publ.* 248: 247 - 263.

Holm RJ, Tapster S, Jelsma HA, Rosenbaum G, Mark DF (2019) Tectonic evolution and copper-gold metallogenesis of the Papua New Guinea and Solomon Islands region. Ore Geology Reviews 104:208-226 doi:10.1016/j.oregeorev.2018.11.007

Holwell DA, Fiorentini M, McDonald I, Lu YJ, Giuliani A, Smith DJ, Keith M, Locmelis M (2019) A metasomatized lithospheric mantle control on the metallogenic signature of post-subduction magmatism. Nature Communications 10 doi:10.1038/s41467-019-11065-4

Jensen, EP, and Barton, MD, 2000. Gold deposits related to alkaline magmatism, *Reviews of Economic Geology,* 13:279-314.

Johnson, W., 1965. Copper and lead ore deposits of South Australia, in McAndrew, J., ed., Geology of Australian ore deposits. Melbourne, Australasian Inst. Mining Metallurgy, 285-297.

Jones A,P., Genge, M., Carmody, L. (2103) Carbonate melts and carbonatites. Reviews in Mineralogy & Geochemistry. 75: 289-322.

Kamber BS, Greig A, Collerson KD (2005) A new estimate for the composition of weathered young upper continental crust from alluvial sediments, Queensland, Australia. Geochimica Et Cosmochimica Acta 69(4):1041-1058 doi:10.1016/j.gca.2004.08.020

Kwan, K., Prikhodko, A., Legault, J.M., Plastow, C., Kapetas, J., Druecker, M. (2016) "TEM airborne EM, aeromagnetic and gamma-ray spectrometric data over the Cerro Quema Panama, Exploration Geophysics, 47:3, 179-190, DOI: 10.1071/EG15080.

Lambert, I.B., Knutson, J., Donnally, T.H., Etminan, H., 1987. Stuart Shelf-Adelaide Geosyncline copper province, South Australia, Econ. Geol. 82, 108-123.

Langsford N.R. (1972) The investigation of the Bendigo copper and molybdenite project, report 3. S. Aust. Dept. Mines and Ener. Rept. Bk. 72/1 (unpublished).

Le Maitre, R. W., Bateman, P., Dudek, A., Keller, J., Lameyre, J., Le Bas, M. J., Sabine,P.A.,Schmid, R., Sørensen, H., Streckeisen, A., Woolley, A. R., and Zanettin, B.,(1989) A Classification of Igneous Rocks and Glossary of Terms, Oxford, Blackwell, p. 191

Leslie RAJ, Danyushevsky LV, Crawford AJ, Verbeeten AC (2009) Primitive shoshonites from Fiji: Geochemistry and source components. Geochemistry Geophysics Geosystems 10 doi:10.1029/2008gc002326.

Lyubetskaya, T., Korenaga, J., 2007. Chemical composition of the Earth's primitive mantle and its variance. *J. Geophys. Res*. 112, B03211, doi:10.1029/2005JB004223.

MacDonald, GD, and Arnold, LC, 1994. Geological and geochemical zoning of the Grasberg Igneous Complex, Irian Jaya, Indonesia, *Journal of Geochemical Exploration,* 50:143-178.

McDonough, W. F., Sun S.-S., 1995. The composition of the Earth, *Chem. Geol*., 120, 223–253.

Morrison, R.S. (1989) Igneous intrusive rocks of the Peake and Denison Ranges within the Adelaide Geosyncline. PhD Thesis (unpublished) The University of Adelaide. 289 pp.

Müller, D., Groves, D.I. (2016) Potassic Igneous Rocks and Associated Gold-Copper Mineralization, Mineral Resource Review, Springer Verlag, Heidelberg, New York Dordrecht, London, 311pp. ISBN 978-3-319-23050-4

Müller D, Heithersay PS, Groves DI (1994) The shoshonite porphyry Cu-Au association in the Goonumbla District, NSW, Australia. Mineralogy and Petrology 51:299-321.

Müller D, Rock NMS, Groves DI (1992) Geochemical discrimination between shoshonitic and potassic volcanic-rocks in different tectonic settings - a pilot-study. Mineralogy and Petrology 46:259-289.

Müller, D, Franz, L, Herzig, PM, and Hunt, S, 2001. Potassic igneous rocs from the vicinity of epithermal gold mineralization, Lihir Island, Papua New Guinea, *Lithos,* 57:163-186.

Niu, Y., Batiza, R. 1997. Trace element evidence from seamounts for recycled oceanic crust in the Eastern Pacific mantle. Earth Planet. Sci. Lett. 148, 471-483.

Niu, Y., Collerson, K.D., Batiza, R., Wendt, I. & Regelous, M. 1999. Origin of enriched-type mid-ocean-ridge basalt at ridges far from mantle plumes: The East Pacific Rise at 11°20'N. J. Geophys. Res. 104, 7067-7087.

Nixon, L. G. B., Townend, R., 1966. The occurrence and petrology of syenite porphyry at the Burra Copper Mine. South Australia. Geological Survey. Quarterly Geological Notes 17, 1-5.

Nixon, L. G., Fairburn, W. A., Warne, K. R., 1965. Progress report No. 1, Burra Mine investigation. South Australia. Department of Mines. Report Book, 61/47.

Peccerillo A, Taylor SR (1976) Geochemistry of Eocene calk-alkaline volcanic rocks from the Kastamonu area, northern Turkey. Contributions to Mineralogy and Petrology, 58:63-81.

Plimer, I 1997 The Mongalata Goldfield, South Australia, Redfire Resources N.L. internal report.

Pokrovski, G.S., Anastassia, Yu., Borisova, A.Y., Harrichoury, J-C. (2008) The effect of sulfur on vapour - liquid fractionation of metals in hydrothermal systems. *Earth Planet. Sci. Lett.* 266:345 -362.

Pollard, PJ, Taylor, RG, and Peters, L, 2005. Ages of intrusion, alteration and mineralization at the Grasberg Cu-Au deposit, Papua, Indonesia, *Economic Geology,* 100:1005-1020.

Preiss, W. V., 2002. Burra, South Australia 1:50 000 Geological Atlas Series Map, sheet 6630-I. Geological Survey of South Australia, Adelaide."

Preiss, W. V., Drexel, J. F., Reid, A. J., 2009. Definition and age of the Kooringa Member of the Skillogalee Dolomite: host for Neoproterozoic (c. 790 Ma) porphyry related copper mineralisation at Burra. MESA J. 55, 19-33. Investigator Resources (2018) High Cobalt and REEs upgrade potential at Historic Copper Mine in South Australia. ASX Announcement 22 January 2018.

Richards, JP, 1990. Petrology and geochemistry of alkali intrusives at the Porgera gold deposit, Papua New Guinea, *Journal of Geochemical Exploration,* 35:141-199.

Richards, JP, and Kerrick, R,1993. The Porgera gold mine, Papua New Guinea: magmatic-hydrothermal to epithermal evolution of an alkali-type precious metal deposit, *Economic Geology,* 88:1017-1052

Rogers NW, Setterfield TN (1994) Potassium and incompatible-element enrichment in shoshonitic lavas from the Tavua Volcano, Fiji. Chemical Geology 118:43-62.

Rosenbaum, G., Gasparon, M., Lucente, F. P., Peccerillo, A. & Miller, M. S. Kinematics of slab tear faults during subduction segmentation and implications for Italian magmatism. Tectonics 27 (2008).

Rosenbaum G, Agostinetti NP (2015) Crustal and upper mantle responses to lithospheric segmentation in the northern Apennines. Tectonics 34(4):648-661 doi:10.1002/2013tc003498

Scherbarth, NL, and Spry, PG, 2006. Mineralogical, petrological, stable isotope, and fluid inclusion characteristics of the Tuvatu gold-silver-telluride deposit, Fiji: Comparisons with the Emperor Deposit, *Economic Geology,* 101:135-158.

Schindler, C., Hagemann, S.G., Banks, D., Mernagh, T. and Harris, A.C., 2016 - Magmatic Hydrothermal Fluids at the Sedimentary Rock-Hosted, Intrusion-Related Telfer Gold-Copper Deposit, Paterson Orogen, Western Australia: Pressure-Temperature-Composition Constraints on the Ore-Forming Fluids: in Econ. Geol. v.111, pp. 1099-1126.

Sillitoe, RH, 1997, Characteristics and controls of the largest porphyry copper-gold and epithermal gold deposits in the circum-Pacific region, *Australian Journal of Earth Sciences,* 44:373-388.

Sillitoe, RH, 2002. Some metallogenic features of gold and copper deposits related to alkaline rocks and consequences for exploration, *Mineralium Deposita,* 37:4-13.

Simon, A.C., Pettke, T., Candela, P.A., Piccoli, P.M., Heinrich, CA (2005) Gold partitioning in melt - vapour - brine systems. *Geochim. Cosmochim. Acta,* 69:3321- 3335.

Simon, AC, Pettke T, Candela PA, Piccoli PM, Heinrich, C.A. (2007) The partitioning behavior of As and Au in S-free and S-bearing magmatic assemblages. *Geochim. Cosmochim. Acta*, 71:1764 - 1782.

Simpson, C.A. 1997 Redfire Resources Burra EL2217 and 2161 Annual Report to 25 October 1997.

Staverly Minerals (2020) Thursday's Gossan Copper Gold Project - Diamond Drilling Update. Exceptional High Grade Gold in Cayley Lode with best ever intercept of 48 m at 1.39% Cu and 6.33 g/t Au. ASX Announcement 2 November 2020.

Scheibner, E., 1992. Influence of detachment-related passive margin geometry on subsequent active margin dynamics: Applied to the Tasman Fold Belt System. Tectonophysics 214, 401–416.

Scherbarth NL, Spry PG (2006) Mineralogical, petrological, stable isotope, and fluid inclusion characteristics of the Tuvatu gold-silver telluride deposit, Fiji: Comparisons with the emperor deposit. Economic Geology 101:135-158.

Ulrich T, Günther D, Heinrich CA (2001) The evolution of a porphyry Cu–Au deposit, based on LA-ICP-MS analysis of fluid inclusions: Bajo de la Alumbrera, Argentina. *Econ. Geol.* 96:1743–1774.

White LT, Morse MP, Lister GS (2014) Lithospheric-scale structures in New Guinea and their control on the location of gold and copper deposits. Solid Earth 5(1):163-179 doi:10.5194/se-5-163-2014

Whittle, A. W. G., 1973. Rock samples, Burra open cut. Poseidon Ltd Report 22 - 24 (unpublished).

Williams, H.A., Stewart, J.R., Betts, P.G., 2009. Imposition of a Proterozoic salient on a Palaeozoic orogen at the eastern margin of Gondwana. Gondwana Research 16, 669–686.

Wright, R. G., 1975. Burra copper deposit, South Australia, in Knight, C. L., ed., Economic geology of Australia and Papua New Guinea. Melbourne, Australasian Inst. Mining Metallurgy, 1039-1044.

18. Certificate of Qualified Person

I, Emeritus Professor Kenneth D. Collerson, am the Principal of KDC Consulting (KDC^2) 33 Cramond St, Wilston, 4051 Queensland, Australia.

This certificate applies to this technical report titled:

Review of Exploration Data from Burra, S.A. to Improve Targeting Copper, Copper-Gold, and REE Mineralisation

that has an effective date of 18th February, 2022.

I am a Fellow of the Australasian Institute of Mining and Metallurgy (#100125). I graduated in 1993 as Doctor of Philosophy (Geology) from the University of Adelaide, South Australia and also have a Bachelor of Science degree with 1st Class Honors from University of New England, N.S.W., Australia (awarded in 1997). Emeritus Professorial status at the University of Queensland acknowledges of my contribution to research, management and teaching in the University sector.

I have practiced my profession as a Principal Consultant with Salva Resources, HDR Salva and Caracle Creek (Toronto) and as a self-employed consultant for more than 35 years. As a Principal Consultant in mineral exploration I have an excellent record of discovery. I have worked on a variety of multi-commodity metals exploration projects through high-level consulting activities in more than 15 countries.

In a consultancy for Geological Survey of Queensland (2014-2016) using spinifex grass as a biogeochemical exploration medium in the Simpson Desert, in 2014 I discovered a Devonian age alkaline metallogenic province, (Diamantina Province). Importantly, I showed that the Diamantina Province is part of a much larger belt (a plume track) of ~ 440 Ma to 365 Ma igneous activity that extends more than 2000 km from central NSW to the Northern Territory. The entire belt is prospective for a range of metals including scandium, cobalt, PGEs, copper, and gold, as well as for diamond.

Recent industry and Government consultancies include:

- AusMex Ltd February 2020 Target Vectoring in the Burra Mineral System, South Australia.
- Transition Resources 2019 to present Targeting Cu-Co-Au-HREE-Sc mineral systems in the Cloncurry area.
- Havilah Resources February 2020 - Technical Review of Havilah Resources Rare Earth Element Data from the Curnamona Craton, SA.
- Chinova Resources February 2020 - Targeting New Economy Minerals in the Sc-REE- Cu-Co-Ni-Au PGE Bearing Mount Cobalt - New Hope Mineral System
- Mayur Resources January 2020 - Prospectivity Assessment PNG Basilaki
- Chinova Resources December 2019 Lithochemical Characterisation and Exploration Vectoring - Mt Hope/Mt Cobalt Mineral System, south Cloncurry region, Northern Queensland
- Mayur Resources Sept. 2019 Prospectivity assessment of porphyry and epithermal Feni Konos, Rambutyo, Basilaki and Sidea Projects, PNG
- Mayur Resources July to August. 2019 Prospectivity assessment of Hardie Pacific assets in PNG viz., (1) Epithermal (Au) Gameta (EL2546) and Oredi Creek (EL2572) - Fergusson Island
- Qld. DNRM December 2018 - Cobalt and HREE Mineral Systems in the Mount Isa Block
- AusMex Ltd September 2018 - Rare Earth Element - Cobalt-Copper-Gold Mineral System at Burra, S.A: Significance of the AusLAMP Magnetotelluric Anomaly"
- Hammer Metals August 2018 - U-Pb Titanite Geochronological Constraints on Origin and Age of the Mount Philip Breccia
- Northern Cobalt June 2018 - Review of Wollogorang Project Chemistry: Mineral System and Exploration Vectors.

- Longford Resources Feb. 2018 - present. Targeting Co and PGE mineralisation in the Goodsprings area, Nevada.
- Hammer Metals Feb. 2018 - present. Identification of key mineralisation geochemical vectors, as well as mineralisation and alteration styles in the Mary Kathleen Belt
- Encounter Resources May 2017 - present. Spinifex biogeochemistry proof of concept survey over gold and Co anomalies in the Telfer area, WA
- Laconia Resources Ltd May 2017 - present. Au-Ni-PGE target generation in the Kraaipan Greenstone Belt, Botswana
- Caracle Creek International 2016 - present. Associate Pegmatite Specialist Providing field geological, petrological and geochemical advice for international clients on exploration for LCT pegmatites
- Tyranna Resources June 2016 - present. Improved understanding of calcrete gold geochemistry in the western Gawler Craton that allowed discrimination between true and false calcrete Au anomalies with great success.
- Macarthur Lithium 2016. Provided field geological, petrological and geochemical advice to the MD on lithium exploration in the Pilbara and Yilgarn Cratons. Developed a technique using trace elements in K-feldspar to identify the Li content of the source pegmatite. This IP has global application.
- Impact Minerals Ltd 2015 - present. Petrology and geochemistry of outcrop and drill core samples from Red Hill and Mulga Springs-Moorkaie Intrusions at Broken Hill. Decoded the geochemistry and petrology of PGE-Au-Cu-Ni-Zn mineralisation at Broken Hill, resulting in enhanced understanding of the entire mineral system at Broken Hill, one of Earth's largest accumulations of metals.
- Providence Natural Resources 2012 - present. LCT pegmatite exploration for lithium at Järkvissle in Central Sweden. Currently contracted to find a JV Partner for a JORC Li resource.
- Exco/Copper Chem 2014. Preparation of a geological briefing paper for the Mary Kathleen rare earth Government tender bid.
- Exco 2014. Preparation of a prospectivity assessment for the White Dam area, South Australia, specifically identifying geochemical vectors that allowed improved understanding of the style of mineralisation.
- Chinalco Yunnan Copper Resources Limited 2013 - April 2014.Reviewed and reinterpreted drill core at Elaine and Blue Caesar and developed new model for Cu-Au- Co-REE-U mineralisation in the Mary Kathleen Belt, NW Queensland. I identified the alkaline igneous source of metals in the terrane and demonstrated that these ~1526 Ma alkaline intrusions were emplaced at a shallow crustal depth and produced epithermal mineralisation. As well as improving knowledge of Mary Kathleen Belt mineral systems, this discovery also explains Cloncurry Belt IOCG mineralisation.
- Viti Mining Pty Ltd. 2013 April - Present. Confirmed the existence of world-class very high-grade Mn mineralisation (DSO) at a number of locations on Viti Levu, Fiji. Showed that mineralisation was hydrothermal and occurred as part of an epithermal alteration system above Au-Ag-Cu bearing shoshonite intrusions
- Golden Island Resources Pty Ltd. 2013 April - Present. Undertook a literature review and discovered "lost" reports showing very widely distributed high grade Au and Ag assays (up to 35 g/t) on Waya and Wayasewa. Showed that these islands formed an extension of the shoshonite – gold trend west of Viti Levu and following recovery of excellent panned concentrate results the islands are now being investigated using soil geochemistry to delineate drill targets.
- Golden Island Resources Pty Ltd. 2013 April - Present. I reprocessed magnetic and gravity data for Viti Levu and discovered a previously unknown ~40 km diameter Au-bearing shoshonite caldera south of Tavua caldera that has never been drilled. The Tavua caldera is host for the >1MOz epithermal Au-Ag Emperor goldmine on Viti Levu.

- Waratah Resources 2012 December. Prospectivity assessment of Gabon and the Republic of the Congo. Reviewed the geochemistry of BIFs in Waratah Resources tenements in Gabon and the Republic of the Congo to facilitate regional exploration and resource estimation.
- ASERA Iron Project 2012. December Geochemical evaluation of Lake Vättern orthomagmatic Fe-Ti-V project, Southern Sweden. Concluded that mineralisation is hosted by an anorogenic anorthosite intrusion not IOCG as previously believed.
- Triton Gold 2012 – August to December. Geochemical interpretation, Au and Mn target assessment on Viti Levu.
- Pacific Wildcat Resources 2011 – July to October. Fieldwork in Kenya and interpretation of DD core from Mrima Hill carbonatite and outcrops of nepheline syenite in a nearby intrusion. Showed that carbonatites and syenites were genetically related forming part of a >10 km diameter intrusion. Discovered an untested mineral system and identified zones of rare earth mineralisation for a subsequent RC and DD drilling program.

I am responsible for all sections of this report and am independent of Tombola Gold Ltd.,
I am confident that this report has been prepared in compliance with the JORC 2012 Code and with the instrument NI 43-101.

As of the effective date of the technical report, to the best of my knowledge, information and interpretation in the report contains all scientific and technical details that are required to be disclosed.

Dated 18th February, 2022

Professor Kenneth D. Collerson

Ph.D., FAusIMM

19. Glossary of Technical Terms

Absarokite	A K-rich basalt composed of olivine and augite phenocrysts in a groundmass of labradorite with alkali feldspar rims, olivine, augite, a small amount of leucite, and some dark-coloured glass. Absarokites grade into shoshonites. Absarokites are defined chemically by < 52 wt% SiO_2 and > 1.6 wt% K_2O. All members of the shoshonite suite are enriched in Ba, Sr and LREEs.
Alkaline lithology	Igneous rocks in which the chemical content of the alkalis (potassium oxide and sodium oxide) is great enough for alkaline minerals to form. Such minerals may be unusually sodium rich, with a relatively high ratio of alkalies to silica (SiO_2), as in the feldspathoids. Other alkaline minerals have a high ratio of alkalies to alumina (Al_2O_3), as in aegirine pyroxene and the sodic amphibole riebeckite. Alkaline rocks contain some of the world's largest deposits of REEs
Banakite	A trachyandesite rock containing phenocrysts of augite and sometimes olivine in a groundmass of sanidine mantling labradorite andesine, augite, biotite, analcime and opaques. It is similar to absarokite but contains less olivine and augite. Related to absarokite and shoshonite. Defined chemically by > 57 wt% SiO_2 and > 4.2 wt% K_2O. Enriched in Ba, Sr and LREEs.
Basanite	A term originally used for a porphyritic basalt containing pyroxene phenocrysts, but later used as a group name for rocks composed of clinopyroxene, plagioclase, feldspathoids and olivine.
Boninite	A high magnesia, low alkali, andesitic rock consisting of phenocrysts of protoenstatite (which inverts to clinoenstatite), orthopyroxene, clinopyroxene and olivine in a glassy base full of crystallites. The rock exhibits textures characteristic of rapid growth.
Calc alkaline basalt	A basalt not defined by its mineralogy but by its association with rocks of the basalt–andesite–dacite suite of the orogenic belts and island arcs.
Carbonatite	A collective term for an igneous rocks in which the modal amount of primary carbonate minerals > 50%. Associated with mantle plume magmatism and rifting.
Chondrite normalised plot	The customary practice for displaying REE abundances is to normalize them to chondritic abundances and then to plot these normalized abundances in order of atomic number. It avoids the Oddo-Harkin effect where REE elements with even atomic numbers are more abundant than REEs with odd atomic numbers, resulting in smooth patterns on log plots.
Delamerian Orogeny	Delamerian Orogeny occurred possibly between about 514 million years ago and 500 million years ago.
Diorite	A plutonic rock consisting of intermediate plagioclase, commonly with hornblende and often with biotite or augite.
Early Palaeozoic	Time period from ~500 to 541 Ma
Epithermal deposit	Mineral deposit formed when boiling hydrothermal solution flows through an open fissure and deposits its dissolved load. Commonly gold and silver rich. A great many veins occur close to bodies of intrusive igneous rocks because the igneous rocks serve as heat sources that create convectively driven flows in hydrothermal solutions. Precipitation of the minerals is usually caused by cooling of the hydrothermal solution, by boiling, or by chemical reactions between the solution and rocks lining the fissure.
HREE	Heavy rare earth elements; Gd, Tb, Dy, Ho, Er, Tm, Yb
Hydrothermal deposits	**Hydrothermal** mineral **deposits** are accumulations of valuable minerals which formed from hot waters circulating in Earth's crust through fractures.

Gabbro	A coarse-grained plutonic rock of basaltic composition composed essentially of calcic plagioclase, pyroxene and iron oxides. If olivine is an essential constituent it is olivine gabbro.
IOCG	Iron oxide - Copper - Gold Deposit
K-metasomatism	**K-metasomatism** is characterized by pervasive replacement of diverse rock types by K-feldspar (adularia) + hematite ± quartz ± illite
Kimberlite	An ultramafic rock consisting of major amounts of serpentinized olivine with variable amounts of phlogopite, orthopyroxene, clinopyroxene, carbonate and chromite. Characteristic accessory minerals include pyrope garnet, monticellite, rutile and perovskite. Associated with mantle plumes.
Magmatic arc	Where an oceanic plate is subducted beneath a less dense continental plate at a subduction zone. A region of raised elevation between the fore-arc and back-arc basins. Characterised by a chain of volcanoes formed above a subducting plate. Common along the edge of continental crustal plates.
Mantle plume	A themochemical upwelling originating from the core-mantle boundary. Associated with plume magmatism. Mantle plumes rising below supercontinents cause rifting and continental dispersal.
Mantle Wedge	A triangular shaped piece of mantle that lies above a subducting tectonic plate and below the overriding plate. Mantle wedge becomes hydrated and due to fluids derived from the underlying subducting slab. This induces melting and formation of island arc magmas.
Metallogenesis	The origin of ore deposits and of the interdependence in time and space of this process with other geologic processes such as tectonics
Metasomatism	Change in the composition of a rock as a result of the introduction or removal of chemical constituents.
Monzonite	Plutonic rock intermediate in composition between diorite and syenite. containing subequal portions of K feldspar and plagioclase (An_{30}-An_{50}), less than 5% quartz. Quartz-free monzonites can contain feldspathoids. May contain minor amounts of hornblende and biotite.
Neoprotrozoic	Time period from 1000 to 541 Ma
Oceanic lithosphere	Consists mainly of basaltic crust and underlying ultramafic mantle (peridotite) and is denser than continental **lithosphere**. Young oceanic lithosphere, occurs at mid-ocean ridges, and thickens as it becomes older s and moves away from the mid-ocean ridge.
Ocean Island Basalt	Ocean island basalt (OIB) is a volcanic rock, usually basaltic in composition, erupted in oceans away from tectonic plate boundaries. OIB magmas mainly erupt as basalt lava, but can differentiate to produce a range of other volcanic rock types, e.g., rhyolite, phonolite and trachyte. Unlike mid-ocean ridge basalts (MORBs), which erupt at spreading centres (divergent plate boundaries), and volcanic arc lavas, which erupt at subduction zones (convergent plate boundaries), ocean island basalts are the result of intraplate volcanism and form seamounts.
Orogen	An orogen or orogenic belt develops when a continental plate crumples and is uplifted to form one or more mountain ranges; this involves a series of geological processes collectively called orogenesis.
Palaeozoic	The Palaeozoic (or Paleozoic) era is the earliest of the three eras of the Phanerozoic. Its name means early life. It lasted from about 541 to 252 million years ago (mya), and ended with the greatest extinction event, the Permian–Triassic extinction event.
Pluton	A body of intrusive igneous rock
Porphyry Cu-Au Deposit	**Porphyry copper-*gold* deposits** are Cu and Au **ore** bodies that are formed from hydrothermal fluids that originate from a voluminous magma chamber several kilometers below the **deposit** itself. Predating or

	associated with those fluids are vertical dikes of **porphyritic** intrusive rocks from which this **deposit** type derives its name.
Porphyry	Textural term for an igneous rock consisting of large-grained crystals such as feldspar or quartz dispersed in a fine-grained silicate rich, generally aphanitic matrix or groundmass.
REE	Rare earth element or lanthanide; La, Ce, Pr, Nd, Sm and Eu are termed the light REEs and Gd, Tb, Dy, Ho, Er, Tm, Yb are known as the HREEs
Rodinia	Neoproterozoic supercontinent that assembled 1.1–0.9 billion years ago and broke up 750–633 million years ago
Salients and re-entrants in orogenic belts	Salients (or promontories) and re-entrants (or recesses) occur along the strike of bent orogenic belts. They form by a variety of geodynamic mechanisms such as changes in stratigraphic thickness across an orogen, rheological contrasts that occur across detachment surfaces, the presence of a rigid indenter in the foreland of a convergent orogen, or the crustal expression of tears in subducted oceanic lithosphere (slab tears).
Slab Tears	Slab tears reflect vertical or horizontal rupture in subducting plates. Horizontal slab-tearing occurs in convergent settings that undergo non-uniform slab retreat, or in zones at the edges of active margins accommodating back arc rifting. Vertical tearing occurs where aseismic ridges or oceanic fracture zones interact with active margins. Slab tears provide windows that allow penetration of hot mantle plumes into the mantle wedge above subduction zones. These facilitate melting and formation of shoshonite suite lithologies that host porphyry deposits. Slab tears accommodate formation of salients and re-entrants in orogenic belts.
Sub-arc mantle	The wedge of convecting upper mantle lying above subduction zones.
Shoshonite	A K-rich trachyandesite composed of olivine and augite phenocrysts in a groundmass of labradorite with alkali feldspar rims, olivine, augite, a small amount of leucite, and some dark-coloured glass. Defined chemically by SiO_2 between 52 and 57 wt% and 2 and 3.4 wt% K_2O. Enriched in Ba, Sr and LREEs.
Subduction Zone	Subduction zones are where the cold oceanic lithosphere sinks back into the mantle and is recycled. They are found at convergent plate boundaries and are overlain by chains of island arc volcanoes.
Syenite	A plutonic rock consisting mainly of alkali feldspar with subordinate sodic plagioclase, biotite, pyroxene, amphibole and occasional fayalite. Minor quartz or nepheline may also be present.